

Modelling and flexibility assessment for operational studies of future active distribution networks

Mónica Yus Santana

Technische Universiteit Delft

Modelling and flexibility assessment for operational studies of future active distribution networks

by

Mónica Yus Santana

to obtain the degree of Master of Science

Sustainable Energy Technology

at the Delft University of Technology,

to be defended publicly on Monday March 29, 2021 at 15:00 PM.

Student number: 4906381

Thesis committee:	W. van Buijtenen,	Phase to Phase BV	Company supervisor
	Dr. ir. J. Rueda Torres,	TU Delft, ESE - IEPG	TU Delft supervisor
	Prof. Dr. P. Palensky,	TU Delft, ESE - IEPG	Internal committee member
	Dr. L. Ramírez Elizondo,	TU Delft, ESE - DCE&E	External committee member

Front cover retrieved from:

<http://www.businessgoing.digital/artificial-intelligence-in-smart-cities/>

Abstract

At present, the energy transition is increasingly being driven by the integration of renewable energy into the grid. However, this weather-dependent energy generation imposes challenges to the system operators since the deviations between the forecasted and the actual generation keep increasing due to this intermittent generation. Moreover, new consumption patterns and the emergence of new types of loads in the distribution grids, such as heat pumps and electric vehicles, increase the dynamics and complexity of the power system. Therefore, distribution grids need to become more active, being able to monitor the real-time changes and controlling the different network elements.

In this context, operational flexibility is seen by the DSOs as a suitable solution for keeping the power balance of the system during a specific time period, coping with fluctuations and responding to variations of electricity supply and demand. For this purpose, the impact of the integration of different flexibility sources in the distribution grid has to be assessed by the DSO in order to overcome the operational challenges that it is currently facing.

In order to assess the performance of flexibility in a network, this thesis proposes how to model an active distribution network based on the Dutch standards. Taking as a reference a distribution grid built on the software Vision Network Analysis, a converter was developed in order to export the network data to the input data needed in the data matrices of the open-source tool Matpower. The second step was centred upon the development of controls that simulated the action of different flexibility sources, applied to the Matpower network. For this research, flexibility from the PV distributed generation, flexible loads with demand response and short-term flexible storage have been considered.

With the aim of performing a comparative assessment of the impact of these flexibility sources, the operating limits of the test network have been simulated under three different demand levels for a complete day. The base line scenario keeps the demand levels already set for the network, while the under-scaled scenario assumes a 40% lower demand for the complete day. Additionally, an over-scaled scenario has been proposed, which considers the expected demand increase for 2030 with the corresponding integration of heat pumps and electric vehicles. In general, higher demand rates imposed longer undervoltage peaks. Then, the effect of the flexibility sources was assessed by means of the 1-hour resolution controls. It was found that the voltage regulation performed by the droop control applied to distributed generators was minimum and not useful for this type of study. On the other hand, the combination of demand response and flexible storage can deal with all the voltage deviations beyond the allowed limits. The analysis for each case will depend on the limit set for the power curtailment by demand response and the size of the necessary flexible storage system to reach a complete voltage regulation along the network.

This analysis demonstrates the influence of reactive power in voltage control, as well as the influence of active power in the loading levels of the network branches. Based on these factors and in order to provide the DSO with operational indicators for the quantification of short-term flexibility, four indicators have been proposed in order to compare the needs of flexibility between networks and the performance of flexibility sources in terms of voltage regulation and loadings of the branches.

Acknowledgements

This thesis marks the end of my Masters and, therefore, of my student period. These 2 years and a half in the Netherlands have been truly exciting and enriching: new country, inspiring international friends, academic challenges and a huge personal growth. It must be said that it has not been an easy journey, with a global pandemic in between.

I have really enjoyed getting to know more about this topic, crucial for adapting our current infrastructure to the needs of the energy transition. The idea for this research started after an improvised chat at an event in Paris; thanks Wilbert Prinssen for giving me the opportunity of carrying out this project. I must also thank my TU Delft supervisor José Rueda for his patience and guidance. From Phase to Phase and Technolution, Walter van Buijtenen, Winifred Roggekamp and Anton Ishchenko, thanks for our weekly meetings and willingness to help and learn side by side with me. Also, many thanks to Peter Palensky and Laura Ramírez for accepting being part of my graduation committee.

Of course, I have survived this roller coaster thanks to the amazing people that surrounded me. Thanks Bertram, Eva, José and the Delft S.E.A. family among others. Thanks to the Originals group for making projects and life funnier: Patrycja, Megan, Chaturika, Damiano, Julian and Jop. Thanks Patrycja for your advice, help and talks every time we needed them. I cannot forget about my Spanish friends, specially Samantha and Cristina. Thanks for our daily conversations and for being so close, even though we all live in different countries.

My family always believed in me and I cannot be more grateful for their distance-support all these years. I would have also loved to discuss this project with my electrical engineer grandfather, who passed away during my student journey. Last but not least, thank you Josu for your constant support all these months, for your ever-lasting patience and all the Matlab sessions, you are the best.

Now, a new phase starts and I am sure it will bring more learning and life-changing experiences. I am excited about the future, how the energy transition will move forward and how I will contribute to it.

Mónica Yus Santana
Delft, March 2021

Contents

Abstract	iii
Acknowledgements	v
List of Acronyms	ix
List of Figures	xi
List of Tables	xv
1 Introduction	1
1.1 Motivation	1
1.2 Literature review	3
1.2.1 Flexibility quantification	3
1.2.2 Research gaps	7
1.3 Research objectives	8
1.4 Methodology	8
1.5 Scientific contributions of this thesis	9
1.6 Report outline	10
2 Modelling of steady-state power flow	11
2.1 Power flow calculations	11
2.1.1 Newton-Raphson method	13
2.1.2 Power flow through a line and line losses	16
2.2 Voltage control and reactive power support in steady-state	17
2.2.1 Droop control	18
3 Development of an open test model of an active distribution network	21
3.1 Power flow calculations in the tools Vision and Matpower	21
3.1.1 Vision Network Analysis	22
3.1.2 MATPOWER.	30
3.2 Modelling of the test network with Vision and Matpower	33
3.3 Validation of the model done in Matpower based on Vision	39
3.4 Power flow results for the test network without flexibility	41
4 Implemented control methods for the study of flexibility in the test network	49
4.1 Flexible generation	49
4.2 Flexible demand	52
4.3 Flexible generation and demand	54
4.4 Flexible energy storage	56
5 Comparative assessment of different operational flexibility sources	59
5.1 Case studies proposed	59
5.1.1 Under-scaled scenario	60
5.1.2 Over-scaled scenario	61
5.1.3 Summary of the case studies and analysis methodology	63
5.2 Sensitivity analysis	64

5.3	Base line scenario	68
5.3.1	Impact of flexible generation	70
5.3.2	Impact of flexible demand	72
5.3.3	Impact of the combined flexible generation and demand.	73
5.3.4	Integration of battery systems	74
5.3.5	Loadings of the network branches	76
5.4	Comparison with the under-scaled and over-scaled scenarios	78
6	Flexibility indicators	83
6.1	Flexibility metrics	83
6.1.1	Voltage deviation	84
6.1.2	Overloadings of the network elements	86
6.1.3	Reactive power requirements	87
6.1.4	Active power requirement	90
6.2	Conclusions for the case study	93
7	Conclusions and recommendations	95
7.1	Key research findings	95
7.2	Recommendations for future work	97
	Bibliography	99
A	Data file format in Matpower	103
B	Visualisation of the Vision-Matpower converter	107
C	Validation of the coupling between Vision and Matpower	109
D	Supplementary results figures	113
D.1	Sensitivity analysis	116
D.2	Assessment of the flexibility sources	117
D.2.1	Network voltage profiles without flexibility:	117
D.2.2	Effect of the droop control characteristic on voltage regulation:	118
D.2.3	Network voltage profiles after demand response control:	119
D.2.4	Integration of battery systems in the network:	121

List of Acronyms

ADN	Active Distribution Network
DG	Distributed Generation
DGs	Distributed Generators
DSO	Distribution System Operator
DR	Demand response
DSM	Demand Side Management
DRE	Distributed Renewable Energy
EV	Electric Vehicle
ESS	Energy Storage Systems
HP	Heat Pump
HV	High Voltage
IV	Intermediate Voltage
LV	Low Voltage
MV	Medium Voltage
p.u.	per unit
P	Active Power
Q	Reactive Power
RES	Renewable Energy Sources
SAIDI	System Average Interruption Duration Index
SAIFI	System Average Frequency Index
SOC	State Of Charge
VRES	Variable Renewable Energy Sources

List of Figures

1.1	The emerging flexibility gap [7]	2
1.2	Categorization of flexibility sources [3]	6
2.1	Bus classification in a power system	12
2.2	Line model to calculate line power flows [17]	16
2.3	One-line diagram and phasor diagram of a network line [22]	17
2.4	Droop control characteristics of frequency and voltage [23]	19
3.1	Flowcharts of the the steps followed in Vision and Matpower for the calculation of the power flow	22
3.2	Colour criteria for identifying abnormal operating conditions in the network [26] . . .	23
3.3	Example of the node parameters in Vision	24
3.4	Example of the cable parameters modelled in Vision	25
3.5	Example of the parameters of a cable type considered in Vision	25
3.6	Cable model considered in Vision [26]	26
3.7	Transformer parameters considered in Vision	27
3.8	Parameters considered for the source in Vision	28
3.9	Parameters considered for the PV element in Vision	29
3.10	Branch model considered in Matpower [27]	30
3.11	Location of the selected distribution grid	34
3.12	The 2 feeders of the distribution grid chosen for the study	34
3.13	The 2-feeder distribution network developed with Vision	36
3.14	Zoom of the first feeder of the selected distribution network	37
3.15	Zoom of the second feeder of the selected distribution network	37
3.16	IEEE 33-Bus Radial Distribution System [28]	40
3.17	IEEE 33-bus radial distribution system built with Vision	40
3.18	Voltage magnitude comparison for the IEEE 33-bus distribution grid, obtained with Vision and Matpower	41
3.19	Standard residential demand profiles applied in the network loads	42
3.20	Standard industrial demand profiles applied in the network loads	42
3.21	Representative photovoltaic generation profile in a summer and winter day	43
3.22	Voltage profiles throughout the day obtained with Matlab	45
3.23	Load rates of the network branches obtained with Matlab	46
3.24	Load flow results in Vision from the combined scenario with a 50% load increase . . .	47
4.1	V-Q droop characteristic [24]	50
4.2	Flowchart of the droop control implemented in Matlab	51
4.3	Flowchart of the Demand Response for both P and Q control implemented in Matlab	54
4.4	Flowchart of the combined control of generation and demand implemented in Matlab	55
4.5	Flowchart of the logic implemented in Matlab for the detection of storage needs in the network	57
5.1	Minimum, maximum and average hourly power load values in the Netherlands in all the scenario cases proposed in the Flexnet report [33]	60

5.2	Total power load in the Netherlands for all the scenario cases proposed in the Flexnet report [33]	61
5.3	Daily demand factor profile considered for a heat pump in summer and winter	62
5.4	Daily demand factor profile considered for and electric vehicle	62
5.5	Relative voltage sensitivity factors for each load with respect to the network nodes . .	67
5.6	Relative loading sensitivity factors for each load with respect to the network branches	68
5.7	Medium-voltage profiles extremes	69
5.8	Low-voltage profiles extremes for summer and winter	70
5.9	Maximum droop control effect on the voltage profiles in summer	71
5.10	Maximum droop control effect on the voltage profiles in winter	71
5.11	Effect of the demand response control on the medium-voltage profiles	72
5.12	Effect of demand response control on the low-voltage profiles	73
5.13	Effect of droop control, demand response and the combination of both on the voltage profiles	74
5.14	Active power surplus or deficit needed per node for keeping voltage values within the allowed limits	75
5.15	Maximum load rate decrease in the network with different flexibility controls applied	77
5.16	Comparison of the medium-voltage extreme profiles for the base line, under-scaled and over-scaled demand scenarios in summer	78
5.17	Comparison of the low-voltage extreme profiles for the baseline, under-scaled and over-scaled demand scenarios in summer	79
5.18	Voltage profile comparison with summer and winter PV generation conditions in the over-scaled scenario	80
5.19	Lower LV profile extreme for all the scenarios after the action of the flexibility combined control	81
6.1	Heat map representing the magnitude of the voltage deviation for all the nodes and every hour of the day	86
6.2	Amount of reactive power needed at the individual nodes throughout the day to respect voltage constraints in the base case	88
6.3	Comparison between the amount of reactive power needed each hour to respect voltage constraints and the available one in the network	89
6.4	Amount of active power needed at the individual nodes throughout the day in the base case to respect voltage constraints	91
6.5	Comparison between the amount of active power needed each hour to respect voltage constraints and the available one in the network	92
6.6	Flexibility indicators comparison between the base case and the combined control scenario, considering the daily worst-case and average indicator values	94
A.1	Bus data (mpc.bus) structure in MatPower [27]	103
A.2	Bus data (mpc.branch) structure in MatPower [27]	104
A.3	Generator data (mpc.gen) structure in MatPower [27]	104
A.4	Power flow results in Matpower [27]	105
B.1	The developed converter Vision-Matpower	107
B.2	The results from the converter in Matpower format	108
D.1	Landscape view of the voltage profiles throughout the day obtained in Vision for the network without flexibility	114

D.2	Load rates of the network branches obtained with Vision for the network without flexibility	115
D.3	View of the relative loading sensitivity factor magnitude per load and branch	116
D.4	Medium-voltage profiles in the network for the base line case	117
D.5	Low-voltage profiles in the network for the base line case	117
D.6	Lower extreme voltage profile for the over-scaled case in summer and winter	118
D.7	Droop control voltage regulation with different k values	118
D.8	Difference of demand response control of P-Q and only P	119
D.9	Medium-voltage profiles in the network after the effect of the combined control of flexible generation and demand	119
D.10	Low-voltage profiles in the network after the effect of the combined control of flexible generation and demand	120
D.11	Upper extreme voltage profile for all the scenarios after the action of the combined control (droop and DR)	120
D.12	Power charged and discharged by each battery throughout the day	121
D.13	State of Charge of the batteries considered during the day	121
D.14	Controlled voltage profiles within the allowed limits after the integration of short-term flexible storage	122

List of Tables

1.1	List of indicators proposed for the flexibility assessment of a national grid [10]	4
2.1	Specified and unknown parameters in each bus type [15]	12
3.1	Total number of the different components present in the test network	35
5.1	Summary of the demand and generation conditions for the different case studies . . .	64
5.2	Estimated battery capacity at each node with violation of the voltage constraints . . .	75
5.3	Estimated battery capacity for voltage stability for the different case studies in summer	82
5.4	Estimated battery capacity for voltage stability for the different case studies in winter	82
6.1	Defined voltage limits and admissible voltage deviation ranges at medium and low-voltage levels	84
6.2	Worst-case voltage deviation indicator for each hour of the day in the base case and in the combined control scenario	85
6.3	Worst-case loading indicator for each hour of the day in the base case and in the combined control scenario	87
6.4	Resulting reactive power indicator each hour in the base case and in the combined control scenario	90
6.5	Resulting active power indicator each hour in the base case and in the combined control scenario	93
6.6	Indicator results for the worst-case scenario	94
6.7	Indicator results for the average scenario	94
C.1	Comparison of the IEEE-33 bus power flow results for the network nodes and loads obtained by Vision and Matpower	110
C.2	Comparison of the IEEE-33 power flow results obtained for the network branches by Vision and Matpower	111

Introduction

The purpose of this chapter is to provide the reader with an overview of the urgency and relevance of the research carried out in this thesis. With this aim, this Introduction starts with a review of the literature regarding previous studies in order to assess the academic knowledge on the field of study and identify the research gaps. Secondly, the research objectives are placed in context and the strategies followed to meet these objectives are presented. Lastly, the overall research methodology and scientific contributions to this research field are highlighted and the report outline is introduced.

1.1. Motivation

In the past years, several targets have been set in order to achieve a carbon-neutral society. The commitment of the European Union was set to reduce greenhouse gas emissions (GHG) by 85%-90% by 2050 with respect to 1990 levels [1], which illustrates the amount of coordinated effort that will be needed in order to meet this target.

Currently, renewable energy sources (RES) are leading the energy transition, especially by means of the integration of solar and wind energy into the grid. However, the increase of weather-dependent energy generation poses challenges for obtaining a real-time balance between production and demand. The European day-ahead markets provide generation forecasts, but the deviations of the actual generation from these predictions are increasing due to this intermittent renewable generation. Therefore, higher penetration rates of renewable energy sources in medium voltage (MV) and increasingly low voltage (LV) networks increase the difficulty of the operation of the distribution networks. Moreover, new types of loads such as heat pumps and electric vehicles are being integrated in the low-voltage grid level with high energy efficiency targets, imposing challenges to the distribution system operators (DSOs) for ensuring the prediction of the demand levels in the network, the reliability of electricity supply and its continuity.

In contrast to transmission networks, most of the distribution networks are radial and designed for handling unidirectional power flows [2]. However, the growth of distributed generators, the emergence of active consumers (with dual load-generator behaviour) or the presence of new equipment and services such as smart meters lead to the need of a broader range of solutions to ensure a flexible system and meet the real-time balance [3]. Power system flexibility refers in this context to the modification of the generation levels or change of the consumption patterns in reaction to an external signal, which could be a price or activation signal, with the aim of providing a service within

the energy system [3]. Power flexibility represents the ability to cope with fluctuations, responding to variations of electricity supply and demand in a set timely manner [4].

Therefore, distribution grids need to be transformed into more dynamic and complex systems. Traditional passive distribution networks need to become more active due to the opportunities that network management can bring to achieve a reliable operation of the power system [5]. In this context, the concept of active distribution networks (ADN) refers to the network capability of monitoring the whole grid in real time and improve the capacity of low-voltage networks by the control of distributed energy resources [4].

In order to satisfy the operational requirements imposed by future ADNs, controllable resources need to be integrated to ease their flexible operation. In this context, operational flexibility would be able to adapt the operational requirements of the network to the flexible adjustments needed for the capabilities of the controllable resources, responding to different operational states [6]. Operational requirements of ADNs include the economic operation, the improvement of the voltage profiles throughout the network or accommodating the integration of distributed generators [6]. In general, operational flexibility is defined as the ability to keep power balance of a system during a specific time period.

The major drivers that define the need of flexibility in a power system are the increase of variable renewable energy sources, mainly wind and solar, outages, the decommissioning of conventional energy generation, the electrification of the industrial and transport sectors or the allocation of cross-border capacity between different time horizons [3]. Particularly at the DSO level, the main concerns focus on the increasing volatility of demand, the increasing levels of behind-the-meter generation or increasing transmission congestion. Moreover, the increasing introduction of variable renewable energy (VRE) as distributed generation leads to the so-called *flexibility gap*, represented in Figure 1.1 [7], due to two main reasons. Firstly, these VREs are currently taking the market share, removing conventional power plants from the market. Secondly, VREs also lead to a bigger need of flexibility due to their inherent variable characteristics [7]. Consequently, new sources will need to fill the resulting flexibility from the three main network domains: the supply side, the demand side and the storage side. Flexibility enablers, particularly the grid and markets, will need to facilitate these new sources of flexibility in order to achieve the transition to higher VRE shares.

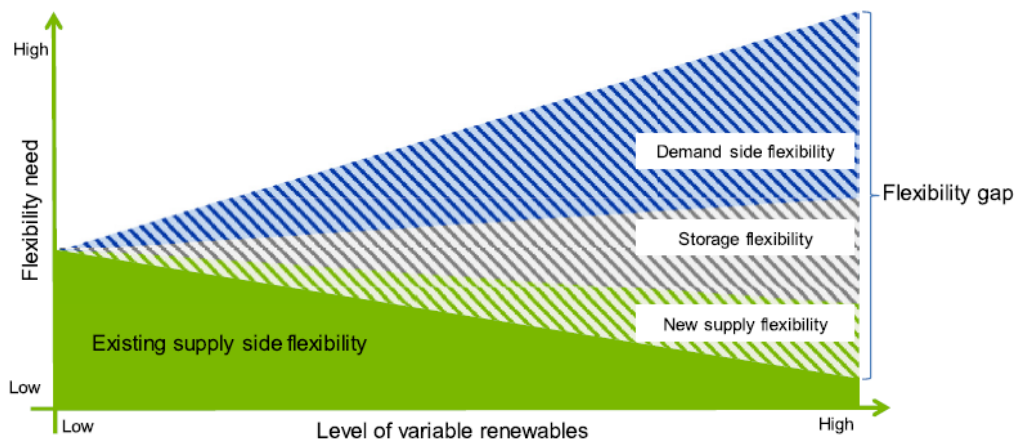


Figure 1.1: The emerging flexibility gap [7]

The time horizon considered also plays a crucial role in the evaluation of flexibility. Since changes in the system load are not normally monitored for long periods, the focus of the integration of flexibility in ADNs will be in the short term, which ranges between 15 minutes and 12 hours [3]. However, measuring the adequacy of the different flexibility sources and the flexibility potential of the overall system is a challenging task, since it will depend on the behavioural and technical boundaries for operation of each system agent/component at every moment.

Under this increasing dynamic and complex power system, flexibility would allow to respond timely to short-term variations of supply and demand. This is why its potential is being considered by the DSOs for an optimal management the current and future active distribution networks. In this context, the company Phase to Phase, together with their customers, have taken steps towards considering the integration of short-term power flexibility for the operational analysis of Dutch distribution networks. From the operational point of view, the potential of flexibility needs to be assessed in order to release operational challenges for the DSOs, especially the congestion in the transmission lines, voltage instability or the forecast uncertainty created by the distributed generators and evolving types of loads. The goal of this thesis is therefore to evaluate the performance of different flexibility sources taking as a case study a synthetic model of a typical Dutch distribution network. The creation of this test network is created based on real parameters and demand and generation levels present in a distribution network in the Netherlands, obtained from the available data included in the Phase to Phase grid models. This standard network aims to simulate voltage stability issues and congestion problems for the current network state, which could be aggravated in the near future (i.e. year 2030) and lead to unwanted disruptions and even blackouts.

1.2. Literature review

The need to better understand the impact of operational flexibility on the power system and the requirements of more flexible resources have led to the broad study of how to quantify their performance in different scenarios. In order to build upon these studies, this section explores some of the relevant flexibility indicators that have been proposed and the commonly used frameworks for carrying out a quantitative analysis of operational flexibility. The main focus for this literature review is the identification of short-term flexibility indicators, which represents the main focus of the flexibility analysis carried out for the subsequent simulations of this research. The section concludes with the knowledge gaps that this research aims to fill.

1.2.1. Flexibility quantification

Focusing on the contribution of different flexibility sources in distribution grids, several studies agree that in order to begin a transition to a higher share of variable renewable energy, methodologies to assess system flexibility and its impact to the grid will be required [8]. In this research, operational flexibility focuses on the technical capabilities of the system to modulate the fed power and energy into and out of the grid, which need to be characterized and classified into suitable flexibility metrics.

The quantification of flexibility would allow us to get a general understanding of the capability of the power system to respond to predicted and unpredicted changes in a wide variety of time horizons. The assessment of the metric obtained for the short term will facilitate that the considerations for the long-term planning process are robust for the increasing integration of VRE sources. From on the point of view of the operational flexibility of the network, the focus of the flexibility metric will

be on market-independent indicators, so that the system operator would be able to identify the technical boundaries and capabilities of the system.

Ideally, the type of flexibility metrics that is being searched would include the following characteristics [9]:

- To be able to quantify the ability of the system to respond to changes of the system load, variable renewable generation or generation outages in the short term.
- To be able to minimize the computational effort and data requirements, respecting the operational constraints of the system.
- To ensure their applicability across different power systems.

The final goal of these metrics would be the assessment of the flexibility included in a system in the short term and over an extended period of time, considering the contribution of all the elements of the system to respond to the net load changes and the flexibility sources integrated into the network. In this way, the objectives of having sufficient capacity for meeting the system load and having the ability of meeting short-term net load changes would be achieved.

Apart from the assessment of market-independent indicators, metrics that inform about the performance of operational flexibility across different networks would also be needed. In this way, a first approach about the suitability of a system to respond to unpredicted generation and load deviations, as well as the suitability for integrating more flexible resources would be analysed by the system operator. Focusing on system-wide indicators, Huang et al. [10] propose a quantitative approach to evaluate the grid flexibility of a whole country. In this case, six quantitative system indicators are proposed for the assessment of the current flexibility of a national power system: grid reliability, load profile ramp, electricity market access, forecasting systems, proportion of natural gas in electricity generation and renewable energy diversity [10]. These indicators, shown in Table 1.1, are normalised using a min-max normalization method since most of these indicators do not have a value of comparison.

Indicator	Metrics
1. Grid reliability	SAIDI, SAIFI
2. Load profile ramp	Rate of worst-case scenario demand increase (MW/h) normalized by flexible installed capacity available
3. Electricity market access	Capacity of interconnections currently operating and to be completed (MW) normalized by peak load
4. Forecasting Systems	Yes/No
5. Proportion of Natural Gas in Electricity Generation	Amount of electricity generated by natural gas in proportion to the total electricity generated
6. Renewable Energy Diversity	Number of renewable energy sources integrated in the analysed grid

Table 1.1: List of indicators proposed for the flexibility assessment of a national grid [10]

For the study of the indicators shown in the table, the overall grid flexibility score for the country will be the average of all the 6 indicators. However, the accuracy of the results does not clearly show the current flexibility performance or its preparedness of the system for the integration of flexible resources. First, most of these indicators are based on average values taken from yearly collected data for the specific country when no detailed information is available, such as the SAIDI and SAIFI

scores for the analysis of grid reliability. Moreover, other indicators considered such as the presence of forecasting systems are based on a yes-no answer. Finally, the linear normalisation proposed for each indicator adds difficulty to the comparison between specific power networks. Although this analysis for a whole country could be extrapolated to smaller-size power networks, no clear conclusions are drawn about a more specific comparison of operational flexibility performance per indicator. However, this general list of factors could be considered as a first approach for determining if these fields are already integrated into the system considered, which are related to the preparedness for the integration of flexibility in the system.

For this research, the assessment of operational flexibility within a network is performed from the point of view of the grid operator. Considering an active distribution network, it is assumed that the DSO will be able to manage and control different elements and flexibility sources in the network in order to respond to short-term variations of the parameters of interest. However, the Literature exhibits a lack of methods for the calculation of quantification regarding the amount, improvement and change of operational flexibility in ADNs. Usually, the role of the system operator for the evaluation of flexibility is related to the planning process with the aim of adapting the current practices for the measurement of flexibility. In this context, flexibility metrics could identify the time intervals at which shortages of flexible resources are expected to happen and the impact of the change or addition of flexible resources.

Lannoye et al. [9] highlight the importance of having enough ramping resources in the system that are able to respond in the time-horizon considered. In particular, the lack of ramping probability and insufficient ramping resource expectation were analysed in order to assess the regulating capacity that the system can provide. Predicting the potential deficit of fast flexible resources could help to understand the flexibility needs of the current system. This study proposes the calculation of the insufficient ramping resource expectation (IRRE), which measures the system inability of a power system to respond to the predicted and unpredicted load changes. In this case, the process of flexibility assessment is data intensive, since a distribution of the available flexible resources needs to be built for each direction and time horizon [9].

Therefore, since the flexibility should be determined by the technical features of the system components and their operation, the resources need to be temporally dependent so that flexibility is kept among the different resources. Then, the operator will decide how to respond to regulate the predicted changes in the net load. Lannoye et al. [9] state three steps for the determination of the amount of flexibility that the network resources can offer, prior to the assessment of technical features such as ramp rate constraints. These steps and their respective calculations are shown below:

1. *Resource flexibility*: availability of the resource to offer flexibility. The upward flexibility, calculated in Equation 1.1, is obtained by multiplying the upward ramp rate $RR_{u,+}$ by the by the remaining time to reach stable operation. The start-up time S_u of the unit is extracted from the time horizon considered. $Online_{t,u}$ refers to the binary online variable for each network resource. Similarly, the downward available flexibility in the network would be calculated by Equation 1.2.

$$Flex_{t,u,i,+} = RR_{u,+} * (i - (1 - Online_{t,u}) * S_u) \quad (1.1)$$

$$Flex_{t,u,i,-} = RR_{u,-} * i * Online_{t,u} \quad (1.2)$$

2. *System flexibility*: once the assessment of the flexibility provided by each resource is carried out, a system-wide resource can be proposed. The temporal dependency is kept with the aim of helping the operator in planning decisions such as unit commitment or economic dispatch,

considering the whole flexibility capability of all the resources:

$$Flex_{t,SYSTEM,i,+/-} = \sum_{\forall u} Flex_{t,u,i,+/-} \quad (1.3)$$

3. *Calculation of IRRE*: finally, the probability of insufficient flexibility can be calculated as the cumulative probability of not providing the amount of ramping every point in time. The calculation for insufficient ramping resource probability (IRRP) is performed by Equation 1.4, which depends on the available flexibility distribution $AFD_{i,+/-}$ (calculated from the system flexibility time series). The function IRRP provides the probability of insufficient ramping resources in the network.

$$IRRP_{t,i,+/-} = AFD_{i,+/-} (NLR_{t,i,+/-} - 1) \quad (1.4)$$

Where $NLR_{t,i,+/-}$ denotes the net load ramp in every direction. To conclude, the sum of the IRRP values over the whole time series provides the insufficient ramping resource expectation:

$$IRRE_{i,+/-} = \sum_{\forall t \in T_{+/-}} IRRP_{t,i,+/-} \quad (1.5)$$

The previous resource and system flexibility indicators focus on the capability of the system to respond to the expected or unexpected changes of the generation of net load. The considerations of these methods are usually applied to the planning process in the long term, leading to data-intensive and probabilistic methods. Although Equation 1.1, Equation 1.2 and Equation 1.3 could be adapted for performing a short-term assessment of the flexibility of the network resources. The time horizons for short-term flexibility range from real time (0 seconds to 5 minutes), to very short term (5 minutes to 15 minutes) to short term (15 minutes to 12 hours) [3]. The quantification of the flexibility included in the short-term time horizon can be assessed by taking into account different categories, illustrated in Figure 1.2 [3]. The larger the area in the radar chart, the more flexibility can be provided by the resource.

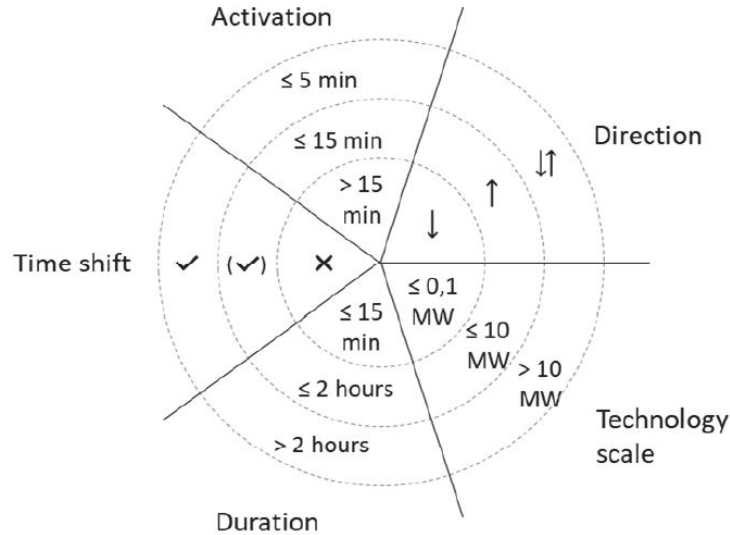


Figure 1.2: Categorization of flexibility sources [3]

Where:

- *Activation* measures how fast the resource can provide the capacity that is indicated in the specific *Technology scale* category, which indicates the scale of the technology.
- *Direction*, up or down depending on the point of power injection.
- *Duration*, referring to how long the flexibility action can be sustained.
- *Time shifting*, which indicates that the change of capacity must be compensated with an opposite action, typical for storage or demand response.

The analysis of flexibility quantification has focused on measuring the capability of the network resources to provide flexibility, as well as assessing the system-wide flexibility from the operator point of view. However, several flexibility metrics have been proposed in order to assess flexibility resources from the end user point of view. These indicators are normally based on price signals and economical benefits for the end customer. For instance, demand response has become a field of interest since it includes several aspects that can be quantified, such as energy efficiency, loss of load, thermal energy lost or the on-site generation consumed. When given a Demand Response action, it is crucial to know the cost of implementation of this request since a compensation should be given to the building or household owner by the aggregator or grid operator [8]. For instance, D'Ettorre et al. [11] investigate the performance of a cost-optimal control strategy for activating demand response actions at a building equipped with a heat pump. In this study, the consumption patterns and operational costs are assessed with the aim of evaluating the suitability of different demand response programs, focused on adapting the demand profiles to grid requirements by modifying the electric load profile of the heat pump [11]. In this case, the hourly electricity price represents an external signal which triggers the demand response request from the grid. The impact of the different demand response measures is determined with the cost-deviation from the baseline case:

$$\delta C_{flex} = C_{Daily}^{\alpha} - C_{Daily}^{ref} \quad (1.6)$$

where:

δC_{flex} is the daily flexibility cost-deviation [€]

C_{Daily}^{α} is the daily cost when added demand response [€]

C_{Daily}^{ref} is the daily reference cost without demand response [€]

For the assessment of operational assessment, the market implications of each flexibility source have been neglected. This is why the main focus is on system-wide indicators and the preparedness of the system as a whole to respond to deviations of generation and demand, considering the short-term time horizon. As already seen, flexibility indicators are often proposed for the long-term planning process, where data distribution and probability calculations are performed in order to state the expected system flexibility performance. However, short-term flexibility metrics considering several variable generation and demand scenarios [12], together with power capability for up and down regulation [13] should be further extended and considered by the DSO for the reliable operation of an active distribution network.

1.2.2. Research gaps

The different metrics that have been analysed in this literature review section focus on operational and system planning indicators for the quantification of flexibility in several time frames and fields

of application. The flexibility analysis has been found to remain limited for the short-term quantification of the impact of diverse flexibility sources integrated into the grid. Specifically, the focus on demand response predominates in the recent research from the demand side, but quantification from the grid side (system operator or aggregator) still needs to be considered.

Another challenge that has been pointed out among the different studies in the Literature is the data availability and quality, as well as the data formats. In this sense, the comparison across different networks or even countries becomes more difficult when the flexibility potential needs to be assessed. The lack of sufficient data for the assessment of the current operational flexibility in the network and for long-term planning studies represents one of the factors that hinders the creation of standardised metrics for measuring the available and potential flexibility in a power system.

In conclusion, comprehensive short-term operational flexibility indicators that include a detailed formulation of the mathematical formulation of system-wide flexibility indicators has not been proposed in the Literature. In particular, what is still missing in the ability of assessing is the available technical operational flexibility as a function of the technical control inputs such as overloadings or voltage instability signals, and the time-dependent system states [14]. In order to provide the DSOs with a methodology to evaluate the impact of flexibility resources on a distribution grid, this research aims to develop insightful flexibility indicators that evaluate the response to the variations of supply and demand in the short term. These indicators will allow us to compare the needs of flexibility of different networks, as well as the suitable action of the flexibility sources considered for each network side: demand, generation and storage.

1.3. Research objectives

As presented in this chapter, the operational challenges of active distribution networks lead to the need of new tools by the DSOs for short-term decision support. In this context, flexibility appears to be a potential source for balancing support in the short term. For the assessment of the integration of flexibility in the network, first the potential flexibility sources need to be modelled and assessed in the distribution network. Secondly, a qualitative but also quantitative analysis of the impact of these sources is required in order to prioritize the needed actions and compare the performance of these sources among different networks.

For this research, the following research objective and research questions have been proposed:

Research objective:

To propose a systematic procedure to assess the impact of different sources of flexibility by a DSO in an active distribution network.

Research questions:

- I) How could a futuristic scenario of a Dutch distribution network be confidently modelled in an open-source tool for steady-state performance assessment of flexibility?
- II) What is a mathematical insightful method to assess flexibility from different sources in future Dutch distribution networks?

1.4. Methodology

The following research steps have been identified in order to answer the aforementioned research objectives:

1. **Scope of the research**

The first milestone of the project consists in the identification of the desired outcomes of the research and to delimit the previous knowledge needed. This will be carried out considering the research questions, which constitute the final goal of the study (Chapter 1).

2. **Literature review and evaluation of the state of the art of flexibility quantification**

The second step is the review of previous studies regarding the quantification of different flexibility sources by means of different indicators. This work allows to find gaps in the Literature and to place the research topic in context. Moreover, the principles of power-flow modelling and the methods of interest need to be reviewed in order to get a proper understanding for their application in the tools used to develop the test model (Chapters 1 and 2)

3. **Model formulation and validation**

This step consists in the development of the test network, validating the results for both tools and identifying the main network components (Chapter 3).

4. **Comparative assessment of different flexibility sources**

Once the model has been built and tested, the performance of different flexibility sources is evaluated in terms of voltage stability and loadings of the test network. Voltage controls are proposed for each flexibility source analysed (Chapter 4) with the goal of determining the operational limits of the network under the conditions of different case studies and detect the critical elements of the network (Chapter 5).

5. **Development of suitable flexibility indicators and application to different scenarios**

The next step is the development of a systematic methodology to compare the flexibility impact in different scenarios that could be used by the DSO. This is done by proposing different operational flexibility indicators and drawing the required conclusions for the set case studies (Chapter 6).

6. **Conclusions**

Lastly, the results from the case studies and indicators are presented and evaluated against the aforementioned research questions, adding the recommendations for future development of this research topic and its implications (Chapter 7).

1.5. Scientific contributions of this thesis

Firstly, modelling a standard active distribution network is a topic raising much interest in the field of power system operation and planning. Most of the models are based on an optimisation nature and aim to define the benefits that different flexibility options would bring to the increasingly dynamic power system. This thesis builds upon the existing power-flow modelling techniques and contributes to the knowledge of the operational impact of flexibility sources in the future Dutch distribution networks.

The test model has been extracted from a real distribution grid managed by a Dutch DSO, aiming to represent a typical distribution network in the Netherlands with regard to its topology, load profiles, type and length of cables and size of the network elements. Therefore, the conclusions obtained for this specific case will be applicable to most of the other Dutch distribution grids. Furthermore, this test network is implemented in the software *Vision Network Analysis*, developed by Phase to Phase BV. In order to carry out the necessary simulations, a converter that exports the network data from Vision to Matpower has also been developed throughout this research. In this way, every distribution network modelled in Vision can be built and tested in an open-source tool such as Matpower,

allowing for the integration of additional scenario studies in the model. Contrary to the IEEE European Low Voltage Test Feeders, usually based on the UK and the USA distribution grid structure and values, this test network provides a typical distribution grid based on Dutch standards that can be extended and used for further academic research, as well as subsequently applied to most distribution grids across the country. In this way, more accurate conclusions can be obtained and the specifications of the power system in the Netherlands can be better simulated at a national and regional level.

Large scale validation of the principles in other networks has not been performed due to time constraints but it can certainly be a subject of future research adopting the framework implemented. The selected model for this thesis can be classified under the so-called 'engineering models', since it deals with the operational challenges of the system, considering several technical constraints. Moreover, a sensitivity analysis is performed in order to mitigate the uncertainty of the assumptions and strengthen the conclusions drawn from the analysis of the case studies.

Regarding the evaluation of operational flexibility, different operating conditions are applied to the same test network in order to draw insightful conclusions about the net load and renewable generation change in the network and the suitability of flexible resources. Taking into account the results from the different case studies, operational flexibility indicators that measure the change severity of the network variables of interest will be proposed. The main aim of these indicators is to provide a comprehensive methodology for the cross-network assessment of operational flexibility needs and the contribution of the flexibility sources integrated into the network.

1.6. Report outline

Once the motivation for this project, the state of the art of flexibility quantification and the research objectives have been introduced, Chapter 2 provides an overview of the principles of power flow modelling as well as steady-state control methods in order to provide a knowledge basis for the subsequent chapters.

The understanding of power flow calculations and the methods used in this research are necessary to comprehend their application to the tools used for the development of the test network, provided in Chapter 3. The validation of Matpower based on the software *Vision Network Analysis* is performed and the initial results are obtained and explained.

Chapter 4 details the controls that have been developed for the simulation of different flexibility sources in the test network. Then, Chapter 5 presents several case studies for carrying out a comparative assessment of diverse flexibility sources. Different levels of demand and generation are considered in the network in order to identify its operational boundaries in a futuristic context and the performance of the analysed flexibility sources, focusing on voltage regulation and congestion mitigation along the network.

Chapter 6 proposes flexibility indicators that can represent the main results obtained from the case studies analysed in Chapter 5. A methodology for short-term flexibility quantification is proposed and these flexibility indicators are compared for the different flexibility sources.

Lastly, the conclusions of this research are presented in Chapter 7, together with recommendations of future work for further development of this research.

2

Modelling of steady-state power flow

Power flow studies, also known as load flow, represent an essential tool in power system analysis. They are needed for expansion planning, economic scheduling or the control of the current system. This chapter concisely reviews the main working principles of steady-state power flow calculations, highlighting the Newton-Raphson procedure to solve the non-linear equations derived from the load flow problem and applied by the simulation tools used in this thesis. Finally, the main concepts regarding voltage control through reactive power support are also presented, which will serve as a foundation for the subsequent development of control methodologies for the integrated flexibility sources in the network.

2.1. Power flow calculations

Power flow calculations focus on the steady-state analysis of the power system network with the aim of determining the operating state of the system for a given loading. Power flow calculations are based on known input variables and consist of determining the voltage magnitudes and voltage phase angles at each bus, as well as the active and reactive power of every network line and the system losses [15].

When solving a load flow problem, balanced operating conditions are assumed in the system and a single-phase positive sequence model is used. It is also important to consider that the power flow analysis of a three-phase balanced system under steady-state conditions must meet the following requirements [16]:

- Generators need to supply all the loads and compensate the power losses of all lines. Moreover, they cannot surpass their nominal active and reactive power values.
- Voltage magnitudes of all the buses must be included within the nominal voltage limits.
- Transformers and cables should not be overloaded.

In general, each bus has four different associated variables: voltage magnitude $|V|$, phase angle δ , the active (real) power P and the reactive power Q . Moreover, the system buses are classified into three categories, detailed below. They are also represented graphically in Figure 2.1.

1. **Slack or Swing bus:** Generator bus which represents the reference bus of the power system since both voltage magnitude and angle are specified. On the other hand, the active and reactive power are not controlled: the slack bus will supply the necessary power to have a bal-

anced power system making up for the difference produced by the network losses between the scheduled loads and the generated power [17].

2. **Load bus (P-Q bus):** In general, every bus that has no generator is defined as a load bus. They are called P-Q buses since both the active and reactive power at the bus are known, while the voltage magnitudes and the phase angle of the bus voltages need to be determined [18].
3. **Generator bus (P-V bus):** At this bus, also known as ‘voltage-controlled bus’, the real power and voltage magnitude are specified. Therefore, the phase angle of the bus voltages and the reactive power are unknown, although the value of the reactive power limits are also set [17].

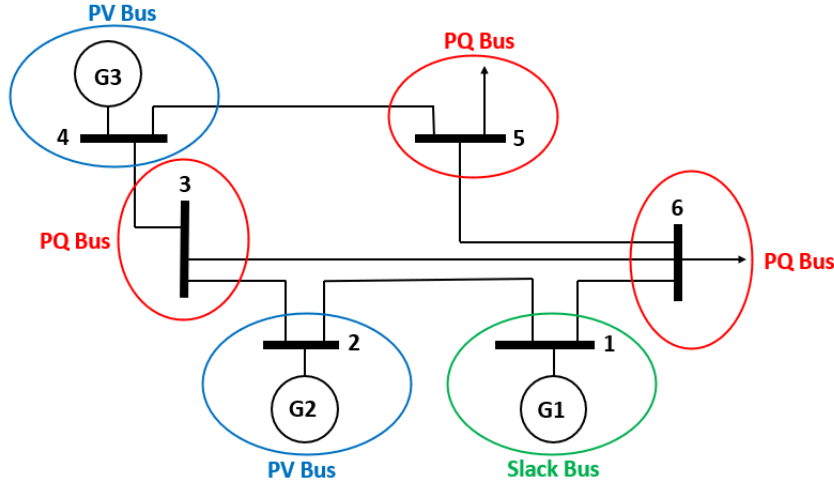


Figure 2.1: Bus classification in a power system

Therefore, for P-Q buses the voltage angles and magnitudes are unknown, whereas in a P-V bus just the voltage angle is unknown. A summary of the specified and unknown parameters at each type of bus can be found in Table 2.1.

Bus type	Specified parameters at bus i	Unknown parameters at bus i
PQ Bus	P_i & Q_i	V_i, δ_i
PV Bus	P_i & V_i	Q_i & δ_i
Slack Bus	V_i & δ_i (usually $1 < 0^\circ$)	P_i & Q_i

Table 2.1: Specified and unknown parameters in each bus type [15]

The calculation of the power flows throughout the network is based on a set of non-algebraic equations. For each line or cable, the series impedance Z and the total line admittance Y are required in order to determine the bus admittance matrix $N \times N$. The typical matrix element Y_{ij} , which represents the admittance magnitude between node i and node j is obtained following Equation 2.1 [19].

$$Y_{ij} = |Y_{ij}| \angle \theta_{ij} = |Y_{ij}| \cos \theta_{ij} + j |Y_{ij}| \sin \theta_{ij} = G_{ij} + jB_{ij} \quad (2.1)$$

Where θ_{ij} is the admittance phase angle between node i and node j , G_{ij} is the real part of the admittance between node i and node j (also called conductance) and B_{ij} is the imaginary part of the admittance between node i and node j (also called susceptance).

Other information considered includes shunt capacitor ratings, impedances, transformer ratings or transformer tap settings. Moreover, before the power-flow calculations, initial values of certain bus voltages and power injections must be known. The voltage at a bus i is represented by:

$$V_i = |V_i| \angle \delta_i = |V_i| (\cos \delta_i + j \sin \delta_i) \quad (2.2)$$

Where $|V_i|$ is the magnitude of the voltage phasor at node i and δ_i is the voltage phase angle at node i . The current that is injected at the bus i is represented in Equation 2.3 as the summation expressed in terms of Y_{ij} of Y_{bus} :

$$I_i = Y_{i1} V_1 + Y_{i2} V_2 + \dots + Y_{iN} V_N = \sum_{j=1}^N Y_{ij} V_j \quad (2.3)$$

Therefore, the net active and reactive power injected into the network at bus i , P_i and Q_i respectively, can be determined as the complex conjugate of the power injected at bus i [19]:

$$P_i - jQ_i = V_i^* \sum_{j=1}^N Y_{ij} V_j \quad (2.4)$$

Substituting Equation 2.1 and Equation 2.2 and separating the active and reactive power, the power-flow equations are obtained. Equation 2.5 and Equation 2.6 provide the calculated net active and reactive power entering the network at bus i [20].

$$P_i = \sum_{j=1}^N |Y_{ij} V_i V_j| \cos(\theta_{ij} + \delta_j - \delta_i) \quad (2.5)$$

$$Q_i = - \sum_{j=1}^N |Y_{ij} V_i V_j| \sin(\theta_{ij} + \delta_j - \delta_i) \quad (2.6)$$

The aforementioned equations can be solved mathematically by means of different iteration methods. In this respect, the most common methods used to solve non-linear algebraic equations are Gauss-Seidel, Newton-Raphson and Quasi-Newton methods. The next subsection discusses the Newton-Raphson method, performed by the tools used in this research for power system analysis and power flow simulations.

2.1.1. Newton-Raphson method

The Newton-Raphson method constitutes the most widely used method for solving non-linear algebraic equations simultaneously. It is the most efficient and practical method since the number of iterations needed to obtain a solution is not related to the system size, but functional evaluations are performed in each iteration. The basis of this method is the Taylor's series expansion for a function of two or more variables [19].

Equation 2.5 and Equation 2.6 constitute non-linear equations formed by independent variables, phase angle in radians and voltage magnitude in per unit. Each load bus (P-Q bus) is represented

by their respective P_i and Q_i equations, while each voltage-controlled bus (P-V bus) is represented just by the P_i equation. Expanding Equation 2.5 and Equation 2.6 in Taylor's series considering the initial estimate and neglecting the results of higher order terms, a set of linear equations is obtained, as shown below [17]. In this case, bus 1 does not appear since it is assumed to be a slack bus.

$$\begin{bmatrix} \Delta P_2^{(k)} \\ \vdots \\ \Delta P_n^{(k)} \\ \hline \Delta Q_2^{(k)} \\ \vdots \\ \Delta Q_n^{(k)} \end{bmatrix} = \begin{bmatrix} \frac{\partial P_2}{\partial \delta_2} & \dots & \frac{\partial P_2}{\partial \delta_n} & \left| \frac{\partial P_2}{\partial |V_2|} \right| & \dots & \left| \frac{\partial P_2}{\partial |V_n|} \right| \\ \vdots & \ddots & \vdots & \vdots & \ddots & \vdots \\ \frac{\partial P_n}{\partial \delta_2} & \dots & \frac{\partial P_n}{\partial \delta_n} & \left| \frac{\partial P_n}{\partial |V_2|} \right| & \dots & \left| \frac{\partial P_n}{\partial |V_n|} \right| \\ \hline \frac{\partial Q_2}{\partial \delta_2} & \dots & \frac{\partial Q_2}{\partial \delta_n} & \left| \frac{\partial Q_2}{\partial |V_2|} \right| & \dots & \left| \frac{\partial Q_2}{\partial |V_n|} \right| \\ \vdots & \ddots & \vdots & \vdots & \ddots & \vdots \\ \frac{\partial Q_n}{\partial \delta_2} & \dots & \frac{\partial Q_n}{\partial \delta_n} & \left| \frac{\partial Q_n}{\partial |V_2|} \right| & \dots & \left| \frac{\partial Q_n}{\partial |V_n|} \right| \end{bmatrix} \begin{bmatrix} \Delta \delta_2^{(k)} \\ \vdots \\ \Delta \delta_n^{(k)} \\ \hline \Delta |V_2^{(k)}| \\ \vdots \\ \Delta |V_n^{(k)}| \end{bmatrix}$$

The linearization is given by the Jacobian matrix for the relationship between small changes in the voltage angle and the voltage magnitude ($\Delta \delta_i^{(k)}$ and $\Delta |V_i^{(k)}|$ respectively) with small changes of active and reactive power $\Delta P_i^{(k)}$ and $\Delta Q_i^{(k)}$. The elements of the Jacobian matrix will be the partial derivatives of P_i and Q_i , evaluated at $\Delta \delta_i^{(k)}$ and $\Delta |V_i^{(k)}|$ [17]. Equation 2.7 shows this notation:

$$\begin{bmatrix} \Delta \mathbf{P} \\ \Delta \mathbf{Q} \end{bmatrix} = \begin{bmatrix} \frac{\partial \mathbf{P}}{\partial \delta} & \frac{\partial \mathbf{P}}{\partial |\mathbf{V}|} \\ \frac{\partial \mathbf{Q}}{\partial \delta} & \frac{\partial \mathbf{Q}}{\partial |\mathbf{V}|} \end{bmatrix} \times \begin{bmatrix} \Delta \delta \\ \Delta |\mathbf{V}| \end{bmatrix} \quad (2.7)$$

In the case of P-V buses, the voltage magnitudes are specified. Considering m voltage-controlled buses in the system, m equations from the Jacobian matrix that involve δV and δQ are neglected. Therefore, the Newton-Raphson calculation consists of $n - 1$ active power constraints and $n - 1 - m$ reactive power constraints [17]. The calculation of each element of the Jacobian matrix is detailed below, considering the notation from Equation 2.8.

$$\begin{bmatrix} \Delta P \\ \Delta Q \end{bmatrix} = \begin{bmatrix} J_1 & J_2 \\ J_3 & J_4 \end{bmatrix} \begin{bmatrix} \Delta \delta \\ \Delta |V| \end{bmatrix} \quad (2.8)$$

For J_1 , the diagonal and off-diagonal elements are:

$$\frac{\partial P_i}{\partial \delta_i} = \sum_{j \neq i} |V_i| |V_j| |Y_{ij}| \sin(\theta_{ij} - \delta_i + \delta_j) \quad (2.9)$$

$$\frac{\partial P_i}{\partial \delta_j} = -|V_i| |V_j| |Y_{ij}| \sin(\theta_{ij} - \delta_i + \delta_j) \quad j \neq i \quad (2.10)$$

For J_2 , the diagonal and off-diagonal elements are:

$$\frac{\partial P_i}{\partial |V_i|} = 2|V_i| |Y_{ii}| \cos \theta_{ii} + \sum_{i \neq j} |V_j| |Y_{ij}| \cos(\theta_{ij} - \delta_i + \delta_j) \quad (2.11)$$

$$\frac{\partial P_i}{\partial |V_j|} = |V_i| |Y_{ij}| \cos(\theta_{ij} - \delta_i + \delta_j) \quad j \neq i \quad (2.12)$$

For J_3 , the diagonal and off-diagonal elements are:

$$\frac{\partial Q_i}{\partial \delta_i} = \sum_{j \neq i} |V_i| |V_j| |Y_{ij}| \cos(\theta_{ij} - \delta_i + \delta_j) \quad (2.13)$$

$$\frac{\partial Q_i}{\partial \delta_j} = -|V_i| |V_j| |Y_{ij}| \cos(\theta_{ij} - \delta_i + \delta_j) \quad j \neq i \quad (2.14)$$

For J_4 , the diagonal and off-diagonal elements are:

$$\frac{\partial Q_i}{\partial |V_i|} = -2 \left| V_i \right| \left| Y_{ii} \right| \sin \theta_{ii} - \sum_{j \neq i} \left| V_j \right| \left| Y_{ij} \right| \sin(\theta_{ij} - \delta_i + \delta_j) \quad (2.15)$$

$$\frac{\partial Q_i}{\partial |V_j|} = -|V_i| |Y_{ij}| \sin(\theta_{ij} - \delta_i + \delta_j) \quad j \neq i \quad (2.16)$$

Regarding the terms $\Delta P_i^{(k)}$ and $\Delta Q_i^{(k)}$, they represent the difference between the scheduled active and reactive power entering the bus i and the calculated values, given by:

$$\Delta P_i^{(k)} = P_i^{sch} - P_i^{(k)} \quad (2.17)$$

$$\Delta Q_i^{(k)} = Q_i^{sch} - Q_i^{(k)} \quad (2.18)$$

The new estimated values for the bus voltage will be:

$$\delta_i^{(k+1)} = \delta_i^{(k)} + \Delta \delta_i^{(k)} \quad (2.19)$$

$$|V_i^{(k+1)}| = |V_i^{(k)}| + \Delta |V_i^{(k)}| \quad (2.20)$$

In summary, the Newton-Raphson procedure for the power solution starts with a first estimation of the voltage magnitude and phase angles and the corresponding injected power is calculated. The correction of the first voltage estimation will be based on the mismatch between the scheduled and the calculated injected power, obtained by evaluating the Jacobian at the present operating point and solving the resulting linear equations. The obtained correction vector will be used for a second estimation of the voltage magnitude and phase angles, and this method will continue until the injected power mismatch becomes acceptably small [20]. The detailed steps of the Newton-Raphson method are presented below [17]:

1. For the P-Q buses (load buses), the scheduled values P_i and Q_i are specified and the voltage magnitudes and phase angles are equal to the ones of the slack bus, or equal to 1 and 0 respectively ($|V_i^{(0)}| = 1.0$ and $\delta_i^{(0)} = 0.0$). In the case of the P-V buses (voltage-controlled), $|V_i|$ and the scheduled value of $|P_i|$ are specified, while phase angles are equal to the slack bus angle or 0 ($\delta_i^{(0)} = 0$).
2. $P_i^{(k)}$ and $Q_i^{(k)}$ are calculated by using Equation 2.5 and Equation 2.6, and $\Delta P_i^{(k)}$ and $\Delta Q_i^{(k)}$ by using Equation 2.17 and Equation 2.18.
3. In the case of P-V buses, $P_i^{(k)}$ and $\Delta P_i^{(k)}$ are calculated with Equation 2.5 and Equation 2.17, respectively.
4. The elements J_1, J_2, J_3 and J_4 of the Jacobian matrix are obtained from Equation 2.10 to Equation 2.16.

5. The simultaneous linear equation expressed in Equation 2.7 is solved by Gaussian elimination or ordered triangular factorization.
6. The new calculated voltage magnitudes and phase angles are obtained from Equation 2.1.1 and Equation 2.20.
7. The procedure is repeated until the differences $\Delta P_i^{(k)}$ and $\Delta Q_i^{(k)}$ are lower than a chosen precision index $\epsilon > 0$:

$$|\Delta P_i^{(k)}| \leq \epsilon \quad (2.21)$$

$$|\Delta Q_i^{(k)}| \leq \epsilon \quad (2.22)$$

2.1.2. Power flow through a line and line losses

Once the iterative solution for the bus voltages has been obtained, the next step is the computation of the line flows and line losses of the network branches. Considering the line model in Figure 2.2, the current through the line I_{ij} measured at bus i is given in Equation 2.23, specified in the positive direction $i \rightarrow j$.

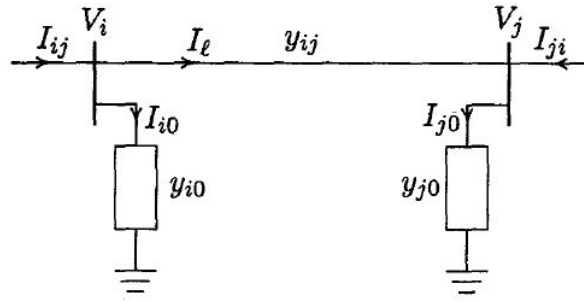


Figure 2.2: Line model to calculate line power flows [17]

$$I_{ij} = I_l + I_{i0} = y_{ij}(V_i - V_j) + y_{i0}V_i \quad (2.23)$$

Therefore, the line current measured at bus j will have the positive direction $j \rightarrow i$ and is given by Equation 2.24.

$$I_{ji} = -I_l + I_{j0} = y_{ij}(V_j - V_i) + y_{j0}V_j \quad (2.24)$$

The complex apparent power from bus i to bus j S_{ij} and from bus j to bus i S_{ji} can be obtained with the defined relationships [17]:

$$S_{ij} = V_i I_{ij}^* \quad (2.25)$$

$$S_{ji} = V_j I_{ji}^* \quad (2.26)$$

Finally, the power losses in the line i - j are represented by the algebraic sum of the power flows obtained in Equation 2.25 and Equation 2.26:

$$S_{Lij} = S_{ij} + S_{ji} \quad (2.27)$$

2.2. Voltage control and reactive power support in steady-state

The control of voltage and reactive power represents a crucial issue in the operation of the power system. Different strategies are evolving due to the characteristics and topology differences between transmission and distribution systems. In particular, control schemes to avoid a “voltage-collapse” are becoming increasingly studied in order to achieve a reliable operation of the power system. The main objectives that are being set for voltage control are [21]:

- To maintain the voltage values at the terminals of all the network equipment within the defined acceptable limits.
- To minimize the congestion at the system lines.
- To minimize active power losses.

Reactive power is essential to deliver active power to the customer through transmission and distribution systems. Elements such as synchronous generators or different types of distributed energy resource equipment are used as a support for voltage stability through reactive power variations. However, voltage-support requirements also depend on the locations and magnitudes of the generator outputs, the type of loads or the configuration of distributed generators in the distribution system. Since the characteristics of the loads vary, the power requirements in the transmission system vary as well. Reactive power can cause the voltage to fall or rise depending on the elements that are being used for reactive power compensation. It must also be considered that power flow cannot be transported over long distances due to the consequent power losses, so in this case voltage control should be applied by means of local devices located throughout the system [21]. At least, a portion of the reactive power supply should be capable of responding to changing-power demand quickly in order to maintain the voltage values within acceptable limits.

In real power grids, the effect of active and reactive power injections is evaluated in terms of voltage and frequency variations. In order to understand the relationship between voltage magnitudes, phase angles, active and reactive powers, Figure 2.3 graphically illustrates the one-line and phasor diagrams of a network line. \bar{v}_1 and \bar{v}_2 represent the phase voltages, and \bar{i}_1 and \bar{i}_2 the currents at the line extremes. Assuming that the shunt admittance is neglected, $\bar{i} = \bar{i}_1 = \bar{i}_2$ along the line. As illustrated, φ denotes the angle between \bar{i}_1 and \bar{v}_2 , thus the component of the current \bar{i} will be $I_i = I \cos \varphi$ and $I_r = I \sin \varphi$ [22]. The line impedance \bar{Z} is also represented as a function of the resistance R (real part) and the reactance X (imaginary part).

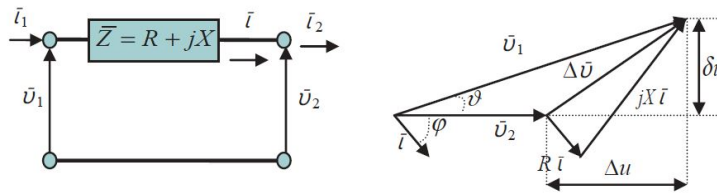


Figure 2.3: One-line diagram and phasor diagram of a network line [22]

Therefore, the voltage drop $\Delta \bar{v} = \bar{Z} * \bar{i}$ can be divided into two components, shown in Equation 2.28. Considering $\bar{i} = I_i - jI_r$, Δu and δu represent the longitudinal and transversal components of the voltage drop, respectively [22].

$$\Delta u = RI_i + XI_r, \quad \delta u = XI_i - RI_r \quad (2.28)$$

Introducing the active and reactive power into Equation 2.28 considering the relation $\bar{S} = V(I_i + jI_r) = P + jQ$, the voltage drop components become:

$$\Delta u = \frac{RP + XQ}{V}, \delta u = \frac{XP - RQ}{V} \quad (2.29)$$

The previous equation can be simplified assuming $R \ll X$ for transmission lines, resulting in the relationship:

$$\Delta u \approx \frac{XQ}{V}, \delta u \approx \frac{XP}{V} \quad (2.30)$$

Therefore, the voltage drop δu is determined by the reactive power flow along the line, while the active power affects the phase difference between \bar{v}_1 and \bar{v}_2 significantly [22]. However, the relationship between these variables is less noticeable for medium-voltage and low-voltage grids, where lines become more resistive. In these cases, both active and reactive power influence the voltage components.

The reactive power is always considered to have a direct effect on voltage stability throughout the network lines. Reactive power injection into a load bus will increase or reduce the voltage depending on the nature of the load seen by the bus (inductive or capacitive). In the case of an inductive grid, the assessment of the positive or negative effects of reactive power injection to a load bus would require a comparison between the consequent line voltage drop and the voltage increase at the bus due to this injection [22].

Reactive power sources must be coordinated to ensure voltage stability along the network during all the possible conditions of the power system. This includes plan voltage schedules, transformer tap settings, load shedding schemes or reactive device settings. Keeping voltage values within the admissible limits will prevent an increase of reactive power losses, excessive switching of reactors and shunt capacitors, reducing the reactive power margin for dealing with contingencies or the probability of voltage collapse.

However, the implementation of devices capable of regulating the reactive power injection in the network requires effort and involves several stakeholders and devices. First, metering must be present in order to capture the actual reactive consumption at different points of the power system. Moreover, grid operators and planners must set in advance the required types and locations that need reactive power correction. Finally, the reactive power devices must be maintained to provide a correct reactive power compensation. In this context, resistive distribution loads are more critical and must be compensated before the transmission reactive compensation takes place. The next subsection details the working principles of droop control, voltage control method that is mostly applied to distributed generators for local reactive power support.

2.2.1. Droop control

Frequency and voltage control in power systems can be achieved by means of diverse methods, and with or without central communication. Control methods that are based on local measurements and include a proportional frequency and voltage controller show more redundancy and reliable operation, without the need of a central communication channel [23]. Droop control is the commonly used voltage control method through reactive power Q , which consists of a decentralized control at the programmable generators, performed by their local controllers. This control is currently applied to programmable and dispatchable generators, despite being a category in which renewable energy generators are not normally included.

As introduced in this section, power angle depends mainly on the active power P , while voltage difference is directly related to the reactive power Q . In other words, the angle δ is controlled through P , and the voltage U_1 can be controlled by regulating Q [23]. These principles form the frequency and voltage droop regulations, which can be included in the local controllers of the generation units in order to adjust active and reactive power outputs following specific droop characteristics. Thus, this type of regulation will change the set point along the respective characteristic according to load conditions, and modifying the steady-state frequency and voltage errors. This droop control adjustment is represented in Equation 2.31 and Equation 2.32 [24]:

$$f - f_0 = -k_p (P - P_0) \quad (2.31)$$

$$U_1 - U_0 = -k_q (Q - Q_0) \quad (2.32)$$

where:

f_0 and U_0 refer to the nominal values of frequency and grid voltage, respectively

P_0 and Q_0 are the inverter set points for active and reactive power

k_p and k_q are the frequency and voltage droop control characteristics, representing the negative slopes

The previously mentioned droop control characteristics and their relation to the frequency and voltage variables included in the equations are shown graphically in Figure 2.4.

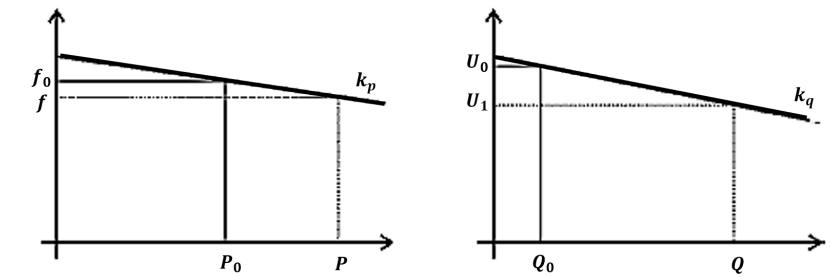


Figure 2.4: Droop control characteristics of frequency and voltage [23]

The main objective of this control, when applied to distributed generators, is to keep frequency and voltage at appropriate levels for given values of P and Q based on predefined droop characteristics [25]. The slope of the droop characteristics defines until which threshold the programmable generators can share power among them and the ability to bring frequency and voltage back to their nominal values.

3

Development of an open test model of an active distribution network

Chapter 2 outlined the key concepts regarding power flow calculations and concisely reviewed the Newton-Raphson procedure, used for solving the power flow problem in the selected power systems simulation tools for this research: Vision Network Analysis v9.1 and Matpower v7.0. Matpower was selected in addition to Vision since it represents an open-source tool that performs steady-state power flow calculations in the same way as Vision. Additionally, this chapter first presents how each of these tools adapts the mathematical models of power flow calculations for the subsequent development of the test network used in this thesis. Secondly, the validation of the model developed in Matpower based on the power flow results obtained with the model implemented in Vision is performed. Finally, the first results with the test network are obtained without the integration of flexibility with the aim of illustrating that power flow calculation results match for both tools. The impact of the different flexibility sources on the network operation will be presented in Chapter 5.

3.1. Power flow calculations in the tools Vision and Matpower

After having stated the theory behind power flow calculations, the main aim of this section is to further explain how Vision Network Analysis and Matpower treat and implement these concepts for obtaining the power flow results. For this purpose, a first introduction of each tool is presented, as well as the modelling considerations of each network element. A particular emphasis is placed on the input parameters needed and calculations performed by Vision Network Analysis, since it is an industrial tool that has not been previously tested with another open-source tool for power system analysis.

Before describing the main characteristics of each software separately, a flowchart that illustrates the input data needed, the steps followed for performing the power flow calculations and the type of results obtained is represented in Figure 3.1 for both Vision and Matpower. With this comparison, it can be observed that Vision needs less steps for obtaining the results, but both apply the Newton-Raphson method and use the same type of input data for the analysis of power networks. The particular features of each tool are detailed in this section.

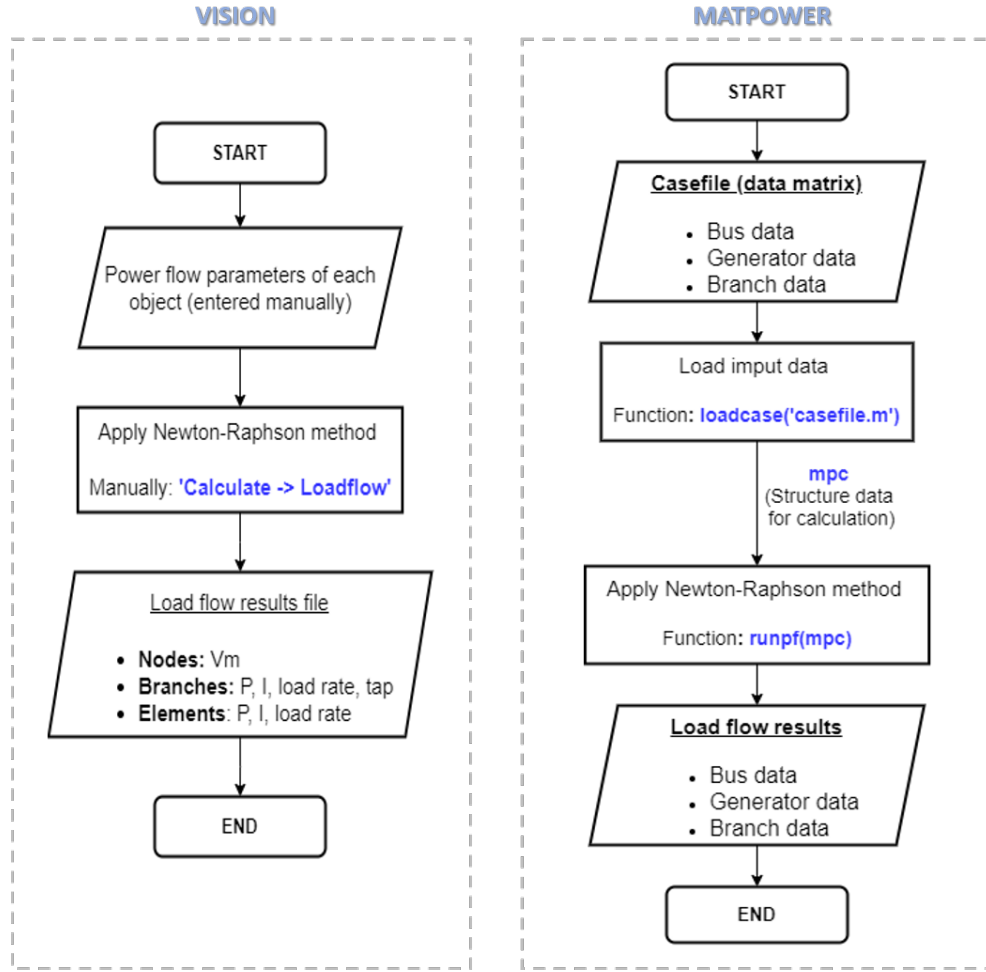


Figure 3.1: Flowcharts of the the steps followed in Vision and Matpower for the calculation of the power flow

3.1.1. Vision Network Analysis

Vision Network Analysis is a tool designed by Phase to Phase BV focused on the analysis of transmission, distribution and industrial networks, and used for power flow calculations, fault analysis and short-circuit calculations. When modelling the network, a database that includes commonly used cables, transformers, reactance coils, generators, motors, protection relays and busbar systems is accessible. The network model is object-oriented and the objects are graphically interconnected in order to build the desired power system model. The layout of the test network modelled for this research will be illustrated in the next section of this chapter.

In general, this tool carries out power flow calculations following a regular load flow with the aim of calculating voltages and currents in all operating conditions. The load flow is solved by using the typical Newton-Raphson method, following the iterative process that was already detailed in Chapter 2. This process will stop when it reaches a sufficient accuracy or the solution does not converge. Vision sets the maximum number of Newton-Raphson iterations to 15 by default, and its accuracy is defined as the maximum power mismatch allowed in p.u., which is set at 10^{-5} by default [26].

Each power system is modelled in Vision using as many equations as nodes in the system. The solution of the iterative process for this set of equations requires the reference of the complex voltage

at one node, the swing bus. As introduced in the previous chapter, this bus has a specified voltage value in magnitude and angle. In the standard power flow calculations, the swing bus is integrated in the external grid, also called the network source. At this bus, the nominal voltage is multiplied by a reference voltage U_{ref} , set by the user. The voltage angle is usually zero, but it can also be modified by the user [26]. Since the voltage is fixed for the swing bus, the complex power variable is chosen ($P+jQ$). Therefore, the difference between the generated power in the network and the demand plus the network losses will be provided or absorbed by this external grid. The results of the power flow analysis are directly perceived by the colour indication set in Vision so that possible problematic areas can be easily identified. The criteria for this colour indication are illustrated in Figure 3.2. Then, detailed information about each network element can also be accessed and visualised.

Object	Limit	Condition	Colour
Nodes	$U > U_{max}$	Fault situation	Higher
Nodes	$U > U_{max}$	Nomal situation	High
Nodes	$U < U_{min}$	Nomal situation	Low
Nodes	$U < U_{min}$	Fault situation	Lower
Branch/Elements	Load percentage $> B_{max}$	Fault situation	Higher
Branch/Elements	Load percentage $> B_{max}$	Nomal situation	High
Brach/Elements	Load percentage $< B_{min}$	Nomal situation	Low
Protection devices	$I > I_{nom}$ or $I > I_{protection}$		High

Colour indication

- Higher
- High
- Low
- Lower
- Attention

Figure 3.2: Colour criteria for identifying abnormal operating conditions in the network [26]

The results from the power flow calculations also present the following sign conventions [26]:

- Branch: positive for a power or current when they flow from the node into the branch.
- Load, motor, coil or battery: positive for a power or current when they are consumed by the element.
- External grid, wind turbine, PV, generator or capacitor: positive for a power or current when they are supplied by the element.

Each network component is now detailed in terms of their modelling and parameters that are taken as inputs for the power flow analysis. In particular, the objects present in the analysed test network include:

- Nodes
- Branches: cables, links and transformers.
- Elements: external grid, synchronous generator, PV element, load and transformer load.
- Switches, breakers, protections: load switches, fuses, circuit-breakers, short-circuit indicators and measurement units can be added to the branches and elements.

For each analysed element, a screenshot of an example of the parameters considered in Vision is added. It is important to highlight that the parameters coloured in blue are the ones that are being considered for the load flow, while the rest represent additional information for other type of calculations, such as short-circuit or fault analysis.

Nodes

Nodes represent busbar systems or stations, connected through branches. Figure 3.3 shows the node parameters that are considered for the power flow calculations, coloured in blue. First, U_{nom} represents the nominal operating voltage, which is set for the test network at 10,5 kV for the medium-voltage level, and 400-420 V for the low-voltage level.

Moreover, all the loads that are connected to a node are corrected by a simultaneity factor, which represents the fraction of the expected active load connected at the time when the demand peak occurs, shown in Figure 3.3 as 'Simultaneity of loads'. It is also known as the 'coincidence factor', which can be given for each node. Then, all the loads and transformers loads connected to the node will be multiplied by the corresponding factor, as illustrated in Equation 3.1 and Equation 3.2.

$$P_{load,calculation} = Simultaneity * P_{load} \quad (3.1)$$

$$Q_{load,calculation} = Simultaneity * Q_{load} \quad (3.2)$$

The image shows a software interface for defining node parameters. The 'Node' window has several tabs: General, Rail, Diverse, Geography, Reliability, Specifics, Notes, Presentation, Selection, and Variations. The 'General' tab is selected. The following parameters are visible:

- Name:** 25495014
- Unom:** 0,42 kV
- ID:** (empty field)
- Short name:** (empty field)
- Function:** (empty field)
- Simultaneity of loads:** 0,765

Figure 3.3: Example of the node parameters in Vision

Branches

In this category, the parameters and modelling logic applied in Vision for links, cables and transformers are further detailed.

1. Link:

Connection between two nodes with the same nominal voltage, and with almost zero impedance. The link includes a rated current I_{nom} and a maximum short-circuit current I_k [26]. If they are not specified, the link will be assumed as infinitely strong.

2. Cable:

A cable represents a three-phase connection between two nodes, which also specifies data of the conductor type. The cable is formed by one or several cable parts in series, as shown in Figure 3.4. For each cable part, the number of parallel three-conductor cables is defined, as well as the cable type. This number of parallel cables, the cable length, the defined nominal current I_{nom} for each cable part and the ampacity factor need to be stated for calculating the power flow through the cable.

The screenshot shows the 'Cable' window in Vision software. The 'General' tab is active, displaying a cable diagram between two busbars: 'WILLEMSSEN INT. BOUW (29307491)' and 'BML 10-1RF1 (29270545)'. The voltage is 10,5 kV, and the length is 1481 m. The cable name is '11WT64'. Below the diagram, a table lists 'Cable parts in series'.

#Parallel	Type	Length (m)	Inom	Ampacity factor	Year		
1	3x240Al GPLK 10kV	44	310 A at 0,75 Km/W	1			
1	3x240Al GPLK 10kV	201	310 A at 0,75 Km/W	1			
1	3x240Al GPLK 10kV	244	310 A at 0,75 Km/W	1			
1	3x240Al GPLK 10kV	246	310 A at 0,75 Km/W	1			
1	3x240Al GPLK 10kV	198	310 A at 0,75 Km/W	1			
1	3x240Al XLPE 10kV	108	360 A at 0,75 Km/W	1	2009		
1	3x240Al GPLK 10kV	195	310 A at 0,75 Km/W	1			

Figure 3.4: Example of the cable parameters modelled in Vision

Furthermore, the specified cable type includes a more complete set of parameters, found at Figure 3.5. As mentioned previously, the ones coloured in blue are considered for the load flow calculation: operational resistance, reactance and capacitance (R_{ac} , X and C), dielectric loss angle $\tan(\delta)$ and specified nominal currents set for the cable type.

The screenshot shows the 'Cable type' window in Vision software. The 'Type' is '3x240Al GPLK 10kV'. The 'Short' is '240 Al'. The 'Unom' is 10 kV. The 'Price' is 0 €/m. The parameters are as follows:

Parameter	Value	Unit
Rac	0,139	Ohm/km at 50 °C
X	0,075	Ohm/km at 50 Hz
C	0,47	µF/km
Tan delta	0,003	
R0	1,18	Ohm/km
X0	0,631	Ohm/km
C0	0,235	µF/km
Inom0	225	A in the air
Inom1	340	A at 0,5 Km/W
Inom2	310	A at 0,75 Km/W
Inom3	290	A at 1 Km/W
Ik (1s)	20,4	kA at 160 °C
Pulse velocity	168	m/µs

Figure 3.5: Example of the parameters of a cable type considered in Vision

In general, the nominal current of the cable depends on the permissible conductor and jacket temperature. As observed in the cable type parameters, I_{nom} depends on three different values of the thermal resistivity of the soil G . These values of G will be used in the calculations to select the maximum current loading. In the case of several cable parts, the weakest will

determine the cable loading.

Regarding the cable modelling, the so-called pi model is used, illustrated in Figure 3.6 and already introduced in Chapter 2. This model is valid for cables with a length until 50 km [26]. R represents the resistance, L the inductive reactance, C the capacitive reactance and R_{shunt} the shunt resistance.

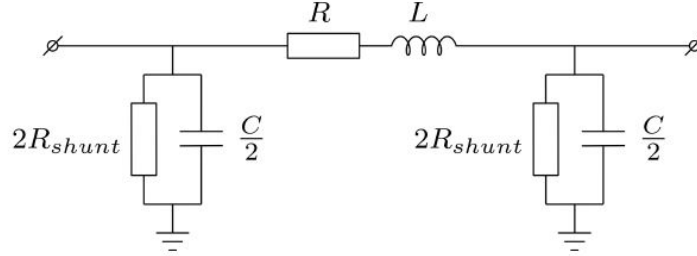
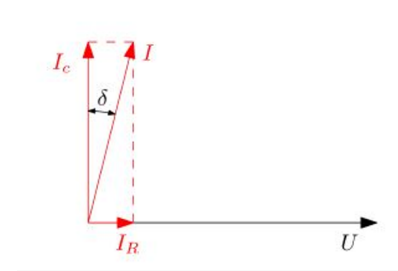


Figure 3.6: Cable model considered in Vision [26]

In this case, R_{shunt} is calculated by using $\tan(\delta)$, specified in the cable type parameters. δ represents the dielectric loss angle, which measures the ageing of the cable connection. Thus, $\tan(\delta)$ depends on the type of insulation, the temperature of the cable and the ageing, among other factors. The derivation used for calculating R_{shunt} from the dielectric loss factor $\tan(\delta)$ is detailed below, I_R being the resistive current component, I_C the capacitive current component and ω refers to the angular frequency.



$$\tan(\delta) = \frac{I_R}{I_C} = \frac{\sqrt{I^2 - I_C^2}}{I_C}$$

$$\tan(\delta) = \frac{U / R_{shunt}}{U / \left(\frac{1}{\omega C}\right)} = \frac{1}{R_{shunt} \omega C}$$

$$R_{shunt} = \frac{1}{\tan(\delta) \omega C}$$

3. Transformer:

The transformer connects subsystems that are at different voltage levels. In the test network used, 52.5/10.5 kV, 10.5/0.42 kV and 10.5/0.4 kV transformers are present. Focusing on the defined transformer parameters in Figure 3.7, $U_{nom,w1}$ and $U_{nom,w2}$ are based on the nominal voltage of the nodes to which each winding is connected, between the $0.8 \cdot U_{nom}$ and $1.2 \cdot U_{nom}$ for both nodes. Moreover, the minimum, nominal and maximum tap position of the transformer are specified. In this case, the minimum tap position refers to the lowest number of windings, which yields the largest voltage ratio [26]. The nominal apparent power S_{nom} has also been included in the given parameters in order to indicate a possible overload after carrying out the power flow calculations. On the other hand, the relative short-circuit voltage u_k , short-circuit loss P_k , no-load loss P_o and no-load current I_o are used for analysing short-circuit and no-loss conditions, respectively.

Figure 3.7: Transformer parameters considered in Vision

Additionally, the voltage ratio of the transformer depends on the tap side, which is determined by using the equations [26]:

$$\text{Tapside } w_1 : (U_{\text{nom},w1} + \text{tap standardised} * \text{tapsize}) / U_{\text{nom},w2}$$

$$\text{Tapside } w_2 : U_{\text{nom},w1} / (U_{\text{nom},w2} + \text{tap standardised} * \text{tapsize})$$

Finally, the transformer impedance, resistance and reactance are calculated as follows [26]:

$$\text{Impedance: } Z_{eq} = \frac{U_k}{100} \cdot \frac{U_{nom}^2}{S_{nom}} \quad (3.3)$$

$$\text{Resistance: } R_T = \frac{P_k/1000}{S_{nom}} \cdot \frac{U_{nom}^2}{S_{nom}} \quad (3.4)$$

$$\text{Reactance: } X_T = \sqrt{Z_{eq}^2 - R_T^2} \quad (3.5)$$

Elements

In this category, the parameters and modelling logic applied in Vision for the source, synchronous generator, load and PV generator are further detailed.

1. Source:

The source is needed for carrying out the power flow calculations since it represents the swing bus. It is a fictitious network element that supplies the mismatch between generation and load plus the network losses, also seen as an infinitely powerful network.

In Vision, every network usually has only one source, with a set voltage magnitude and angle. A reference voltage U_{ref} can be used for defining the voltage of the source per unit and it is calculated as a factor of the nominal voltage of the node U_{nom} to which the source is added (keeping the same angle as the node) [26]:

$$|U| = U_{ref} * U_{nom \text{ node}}$$

The source parameters that are used for the load flow are coloured in blue in Figure 3.8. As stated, only the reference voltage and the angle play a role in the calculations. Moreover, a profile can be added, defining an hourly, weekly or monthly behaviour of the external grid.

Figure 3.8: Parameters considered for the source in Vision

2. Synchronous generator:

In power flow calculations, the synchronous generator can be controlled by the power factor $\cos(\phi)$ or it can be voltage-controlled. For this research, all the synchronous generators present a $\cos(\phi)$ control, which sets a defined relation between the real power P and apparent power S . This is a typical control mode used for generators in Dutch medium-voltage distribution networks. Therefore, the synchronous generator is represented as a negative constant power load, being the active power P_{load} and reactive power of the load Q_{load} (assuming a non-zero $\cos(\phi)$) [26]:

$$P_{load} = -P_{ref}$$

$$Q_{load} = -P_{ref}^* \sqrt{(1 - \cos(\phi)^2) / \cos(\phi)} \text{ (capacitive)}$$

$$Q_{load} = +P_{ref}^* \sqrt{(1 - \cos(\phi)^2) / \cos(\phi)} \text{ (inductive)}$$

3. Load:

The load behaviour sets the voltage dependency of the load. In this case, all loads are set with a 'constant power' behaviour, thus 100% constant P and Q . Therefore, the rated power is always constant, independently of the calculated voltage $|U|$ at the node. In summary:

- If $|U|$ increases, I_{load} decreases.
- If $|U|$ decreases, I_{load} increases.

Instead of a single load, a **transformer load** can also be connected to a node. This element combines a transformer and a load, which is connected at the secondary side of the transformer. The needed parameters for the load flow calculations are the combined ones of the transformer and the load.

Regarding the modelling of the load for the power flow calculations, a subdivision between constant power (P, Q) and constant impedance (R, X) is made for the real and imaginary part of the load. A particular ratio between P and R (or Q and X) is selected, and the voltage dependence will vary between 0 and the quadratic form:

$$P_{load} = P * [(\text{const.}P / 100) + (\text{const.} R / 100) (|U| / U_{nom})^2] \quad (3.6)$$

$$Q_{load} = Q^* [(const. Q/100) + (const. X/100) (|U|/U_{nom})^2] \quad (3.7)$$

where:

P, Q represent the load power at nominal node voltage

|U| is the calculated node voltage

U_{nom} is the nominal node voltage

const. P is the constant real power proportion in %

const. Q is the constant imaginary power proportion in %

const. R is the constant real impedance proportion in %

const. X is the constant imaginary impedance proportion in %

Being:

const. P + const. Q = 100%

const. Q + const. X = 100%

4. PV element:

The photovoltaic element represents the generation of electric energy by means of a solar panel. The needed property is the nominal power of the set of panels, and the irradiation of the PV element is calculated depending on its location, day of the year and time of the day, as shown in Figure 3.9. For the power flow calculations, the voltage-dependent behaviour of the PV element is constant power, as for the loads.

Panels	P _{nom} (MWp)	Orientation (°)	Tilt (°)
#1	0,2362	180	30
#2	0	180	30
#3	0	180	30

Figure 3.9: Parameters considered for the PV element in Vision

3.1.2. MATPOWER

Matpower is a Matlab package that aims to solve power flow calculations and optimal power flow problems. It focuses on standard steady-state models for power flow analysis. The Matpower input data are introduced by means of a set of matrices, packaged as a Matlab struct, called the *Matpower case file* and denoted by *mpc*. The main fields of the struct is the scalar *baseMVA*, and the matrices: *bus*, *branch*, *gen*, and optionally *gencost* [27]. In general, *baseMVA* is a scalar value that represents the system MVA base used for transforming the power input data into per unit quantities. Each row from the matrices corresponds to a bus, branch or generator, the number of rows from the matrix *bus*, *branch* and *gen* being: n_b , n_l and n_g , respectively. The details of the Matpower case format and the fields for each matrix can be found in Appendix A.

As in the case of Vision Network Analysis, the main elements that are modelled in Matpower are nodes, branches (lines and transformers) and generators. The mathematical formulation and main aspects considered for the power flow calculations in Matpower for these fields are detailed below. Afterwards, the power flow method used, the network equations and the results obtained are stated.

1. Branches:

The branch model includes all the lines, transformers and phase shifter elements of the network. As in Vision, it consists of the pi transmission line model, with series impedance $z_s = r_s + jx_s$ and a total charging susceptance b_c , in series with a phase shifting transformer, as illustrated in Figure 3.10 [27]. In this case, the transformer has a tap ratio τ and phase shift angle θ_{shift} , located at the initial extreme of the branch ('from').

The represented current injections i_f and i_t at the initial and end extremes of the branch ('from' and 'to') can be expressed by means of the branch admittance matrix Y_{br} , with their respective terminal voltages v_f and v_t :

$$\begin{bmatrix} i_f \\ i_t \end{bmatrix} = Y_{br} \begin{bmatrix} v_f \\ v_t \end{bmatrix} \quad (3.8)$$

Considering the series admittance element, present in the pi model of Figure 3.10, as $y_s = 1/z_s$, the previous branch admittance matrix can be expressed as:

$$Y_{br} = \begin{bmatrix} \left(y_s + j\frac{b_c}{2}\right)\frac{1}{\tau^2} & -y_s\frac{1}{\tau e^{-j\theta_{\text{shift}}}} \\ -y_s\frac{1}{\tau e^{j\theta_{\text{shift}}}} & y_s + j\frac{b_c}{2} \end{bmatrix} \quad (3.9)$$

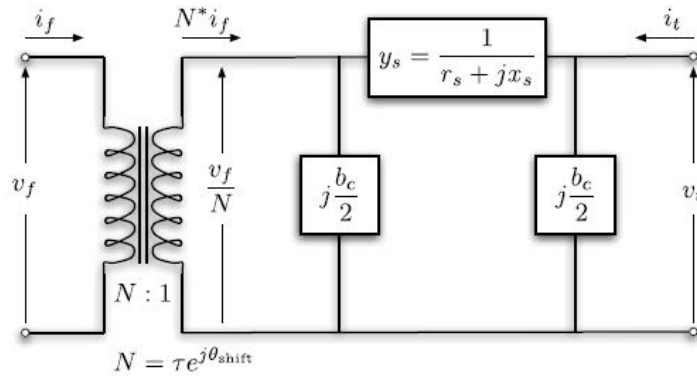


Figure 3.10: Branch model considered in Matpower [27]

If for branch i the elements of the matrix are labelled as shown in Equation 3.10, four vectors Y_{ff} , Y_{ft} , Y_{tf} and Y_{tt} with a dimension $n_l \times 1$ (number of branches as rows and 1 column) can be constructed, in which each i -th element is extracted from the corresponding element of Y_{br}^i .

$$Y_{br}^i = \begin{bmatrix} y_{ff}^i & y_{ft}^i \\ y_{tf}^i & y_{tt}^i \end{bmatrix} \quad (3.10)$$

Moreover, the $n_l \times n_b$ connection matrices C_f and C_t are used to build the system admittance matrices, for which the $(i, j)_{th}$ element of C_f and $(i, k)_{th}$ element of C_t are 1 for the branch i if it is connected from bus j to bus k . Otherwise, the elements of C_f and C_t will be zero.

2. Generators:

Matpower models the generator as a complex power injection at a specific bus. The injection for generator i is expressed in Equation 3.11. n_g being the number of rows in the generator matrix, there will be $n_g \times 1$ vectors of power injections.

$$s_g^i = p_g^i + jq_g^i \quad (3.11)$$

Being $S_g = P_g + jQ_g$ the $n_g \times 1$ vector representing these power injections. The generator matrix in Matpower expresses p_g^i and q_g^i in MW and MVar, specified in the columns PG (2) and QG (3) for each row i of the *gen* matrix (Figure A.3 from Appendix A). Being $n_b \times n_g$ the generator connection matrix C_g , its $(i, j)_{th}$ element is 1 if a generator j is located at bus i , and 0 otherwise. Therefore, the generators bus injections can be defined as $S_{g, bus} = C_g \cdot S_g$.

3. Loads:

In Vision Network Analysis, the loads could be modelled with different behaviours, but the constant power loads were selected for this research. Matpower also models the loads with a constant power behaviour, thus with a specific value of active and reactive power consumed at the bus. For bus i , the load can be expressed as:

$$s_d^i = p_d^i + jq_d^i \quad (3.12)$$

Being $S_d = P_d + jQ_d$ the $n_b \times 1$ vector representing the complex loads at all buses [27]. The generator matrix in Matpower expresses p_d^i and q_d^i in MW and MVar, specified in the columns PD (2) and QD (3) for each row i of the bus matrix (Figure A.1). Negative values can also be included in order to represent fixed distributed generation at some buses. On the other hand, dispatchable loads are represented as negative generators, thus including negative values in S_g .

Once the network buses (including their loads), branches and generators have been modelled, the corresponding network equations that define the power flow problem are obtained. For a network with n_b buses, the constant impedances of the model can be included in a $n_b \times n_b$ bus admittance matrix Y_{bus} , expressed in Equation 3.13 [27]. It relates the current injections at the nodes I_{bus} to the node voltages V :

$$I_{bus} = Y_{bus} V \quad (3.13)$$

In the same way, a network of n_l branches will present a $n_l \times n_b$ branch admittance matrix Y_f and Y_t ('from' and 'to'). These relate the bus voltages and the $n_l \times 1$ vectors I_f and I_t of the branch currents:

$$I_f = Y_f V \quad (3.14)$$

$$I_t = Y_t V \quad (3.15)$$

Considering Y_{ff} , Y_{ft} , Y_{tf} and Y_{tt} the diagonal of the admittance matrix, each system admittance matrix 'from' and 'to' (Equation 3.16 and Equation 3.17) defines the admittance matrix of the bus, expressed in Equation 3.18.

$$Y_f = [Y_{ff}] C_f + [Y_{ft}] C_t \quad (3.16)$$

$$Y_t = [Y_{tf}] C_f + [Y_{tt}] C_t \quad (3.17)$$

$$Y_{\text{bus}} = C_f^\top Y_f + C_t^\top Y_t + [Y_{sh}] \quad (3.18)$$

By using the corresponding current injections presented in Equation 3.14 and Equation 3.15, the complex power injections can be described as functions of the complex bus voltages:

$$S_{\text{bus}}(V) = [V] I_{\text{bus}}^* = [V] Y_{\text{bus}}^* V^* \quad (3.19)$$

$$S_f(V) = [C_f V] I_f^* = [C_f V] Y_f^* V^* \quad (3.20)$$

$$S_t(V) = [C_t V] I_t^* = [C_t V] Y_t^* V^* \quad (3.21)$$

Finally, the AC nodal power balance equations are formed by matching the nodal bus injections and the injections from loads and generators. These are expressed in a complex matrix form, expressed as a function of the complex bus voltages and the generator injections:

$$g_S(V, S_g) = S_{\text{bus}}(V) + S_d - C_g S_g = 0 \quad (3.22)$$

The power flow calculations performed in Matpower aim to solve the power balance equations presented in Equation 3.22. Matpower follows the same methodology as Vision for solving the power flow problem by applying the Newton-Raphson method, with an updated Jacobian at each iteration. As previously explained in this chapter, the load flow problem consists of solving a set of voltages and flows in the network for specific conditions of load and generation. Moreover, Matpower includes power flow calculations for both AC and DC problems. One of the main differences with Vision is that Matpower lacks an automatic adjustment of the transformer taps.

The focus for this research is on AC power flow. As in the conventional methods, a generator bus is selected as a reference for both voltage magnitude and angle (slack bus). The active power generation at the slack bus is considered unknown so as not to overspecify the problem. The rest of the generator buses are classified as PV buses, which set the active power injection and voltage magnitude given in the generator matrix: columns PG (3) and VG (6) of Figure A.3, respectively. Since Matpower specifies P_d and Q_d of the loads, all the non-generator buses are classified as PQ buses, the active and reactive power injections being the PD (3) and QD (4) columns of the bus matrix (Figure A.1), respectively. In the traditional AC power flow problem, Equation 3.22 is split into the active and reactive power components as functions of the voltage magnitudes V_m and angles Θ , and P_d and Q_d generator injections [27]. In this case, the load injections are constant and given. These two power components are shown in Equation 3.23 and Equation 3.24.

$$g_P(\Theta, V_m, P_g) = P_{\text{bus}}(\Theta, V_m) + P_d - C_g P_g = 0 \quad (3.23)$$

$$g_Q(\Theta, V_m, Q_g) = Q_{\text{bus}}(\Theta, V_m) + Q_d - C_g Q_g = 0 \quad (3.24)$$

Considering that $g(x) = 0$ represents the set of equations to solve, its formulation can be stated taking the real power balance equations from Equation 3.23 for the non-slack buses and the reactive

power balance equations from Equation 3.24 for the PQ buses, including the reference angle, loads and known voltage magnitudes and generator injections:

$$g(x) = \begin{bmatrix} g_P^{\{i\}}(\Theta, V_m, P_g) \\ g_Q^{\{j\}}(\Theta, V_m, Q_g) \end{bmatrix} \quad \forall i \in \mathcal{I}_{PV} \cup \mathcal{I}_{PQ} \quad (3.25)$$

Finally, the remaining unknown voltage quantities at the non-reference buses, and the voltage magnitudes at the PQ buses can be expressed as [27]:

$$x = \begin{bmatrix} \theta_{\{i\}} \\ v_m^{\{j\}} \end{bmatrix} \quad \begin{array}{l} \forall i \notin \mathcal{I}_{ref} \\ \forall j \in \mathcal{I}_{PQ} \end{array} \quad (3.26)$$

The vector x represents the resulting set of non-linear algebraic equations that needs to be solved. Once the solution of x is obtained, the remaining active power balance equation yields the generator active power injection in the slack bus and, in the same way, the reactive power balance equations lead to the generator reactive power injections.

Each Newton-Raphson iteration will calculate the mismatch $g(x)$ (Equation 3.25) forming the Jacobian, which is based on the sensitivities of these differences on the x values, and solving the updated value of x by updating the Jacobian. In general, these AC power flow tools solve the power flow problem without generator limits, voltage magnitude limits or branch flow limits constraints. In Matpower, the power flow is executed by calling the command *runpf*, applied to the case struct file. By default, *runpf* solves the AC power flow problem following the Newton-Raphson method. The *results* struct will include the *mpc* struct input data with some additional columns. Details about the fields obtained in the power flow results can be found in Figure A.4 (Appendix A).

3.2. Modelling of the test network with Vision and Matpower

In this chapter, the two software tools used for the development of this project have been detailed, including the models of the different network components and the mathematical models considered for carrying out the required power flow calculations. On the one hand, Vision Network Analysis has been used for the user interface, network modelling and collection of the first power flow results. On the other hand, Matpower will be used for modifying the system for the integration of the different flexibility sources and analysis the power flow results under different network conditions.

For this purpose, first the test distribution grid needs to be chosen and modelled in Vision, represented in Figure 3.11. This network is operated by a Dutch DSO and it is located in the province of Guelders (*Gelderland* in Dutch), between Nijmegen and Arnhem. Each colour defines a different network feeder and the visible points represent the different nodes of the power grid, which are not related to the colour indication that Vision uses for the analysis of the power flow results. Due to the magnitude and complexity of this grid for the study, with almost 400 nodes, only two feeders were selected, shown in Figure 3.12. The selection of this portion of the system is suitable for the aim of this research, with a resulting radial network of 100 nodes. These feeders were selected due to the variety of locations of the nodes and the different nature of loads. Moreover, the size of the grid is suitable for the analysis of different levels of demand and generation along the network, as well as for the introduction and simulation of flexibility sources.

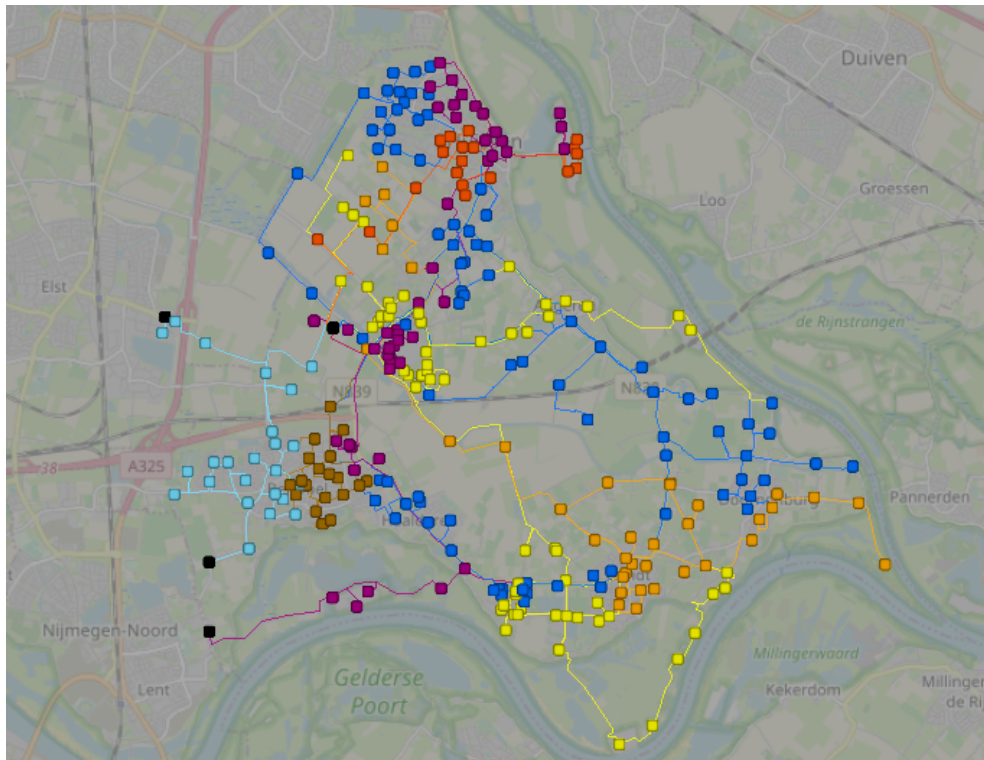


Figure 3.11: Location of the selected distribution grid

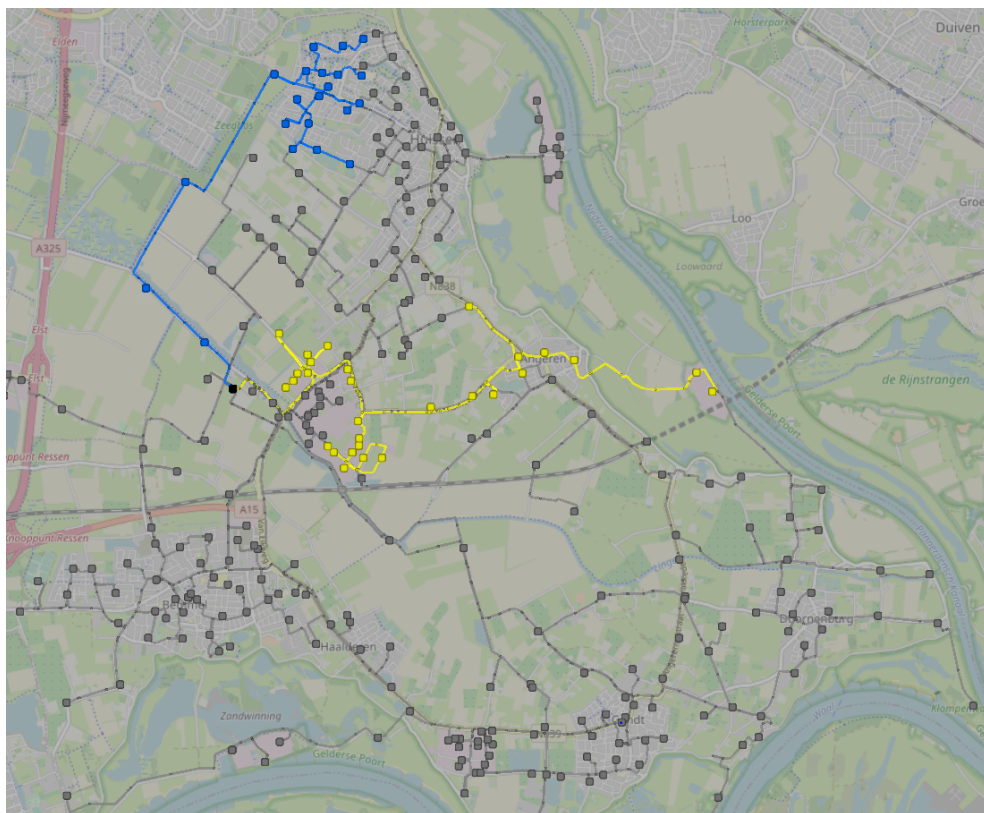


Figure 3.12: The 2 feeders of the distribution grid chosen for the study

The single-line diagram of the network is presented in Figure 3.13, as shown in the Vision interface. Information regarding the number of the different components present in the network can be found in Table 3.1.

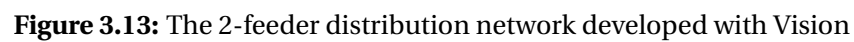
Element	Number
Nodes	100
Sources	1
Synchronous generators	2
Loads	47
PV	28
Cables	50
Links	11
Transformers	38
Measure fields	48

Table 3.1: Total number of the different components present in the test network

In power systems engineering, the single-line diagram constitutes a simplified notation for the representation of a balanced power system. This network represents the medium-voltage level of the distribution grid. It is important to consider how Vision categorises the different voltage levels:

- High Voltage: greater than 100 kV
- Intermediate Voltage: between 20 and 100 kV
- Medium Voltage: between 1 and 30 kV
- Low Voltage: less than 1 kV

Both medium-voltage and low-voltage loads are present in the network and important considerations about their modelling need to be pointed out. Firstly, they are aggregate loads and they do not represent individual households. Each load represents an equivalent that can include consumers with different profiles and different possibilities for power curtailment. Going deeper to the level of a specific low-voltage customer is out of the scope of this research but can be a subject of future investigation.



Zooming into both feeders, a detailed organisation of the different components is illustrated, as well as the actual names of the nodes as shown in the low-voltage grid operated by a Dutch distribution system operator. Figure 3.14 shows the configuration of the blue feeder of the network and Figure 3.15 depicts the configuration of the yellow feeder previously presented in Figure 3.13. This feeder also details to which component corresponds every symbol represented in the network.

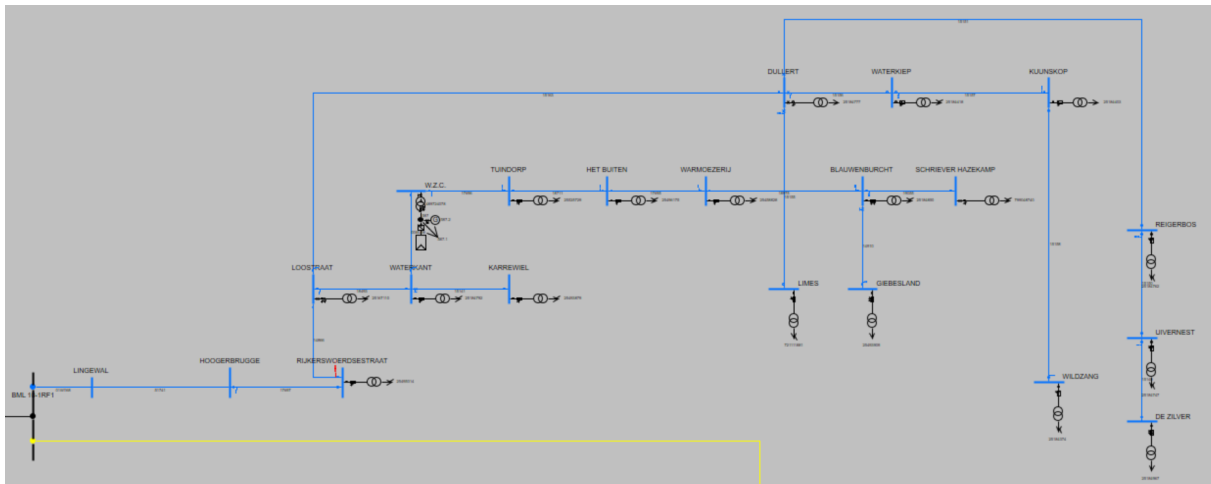


Figure 3.14: Zoom of the first feeder of the selected distribution network

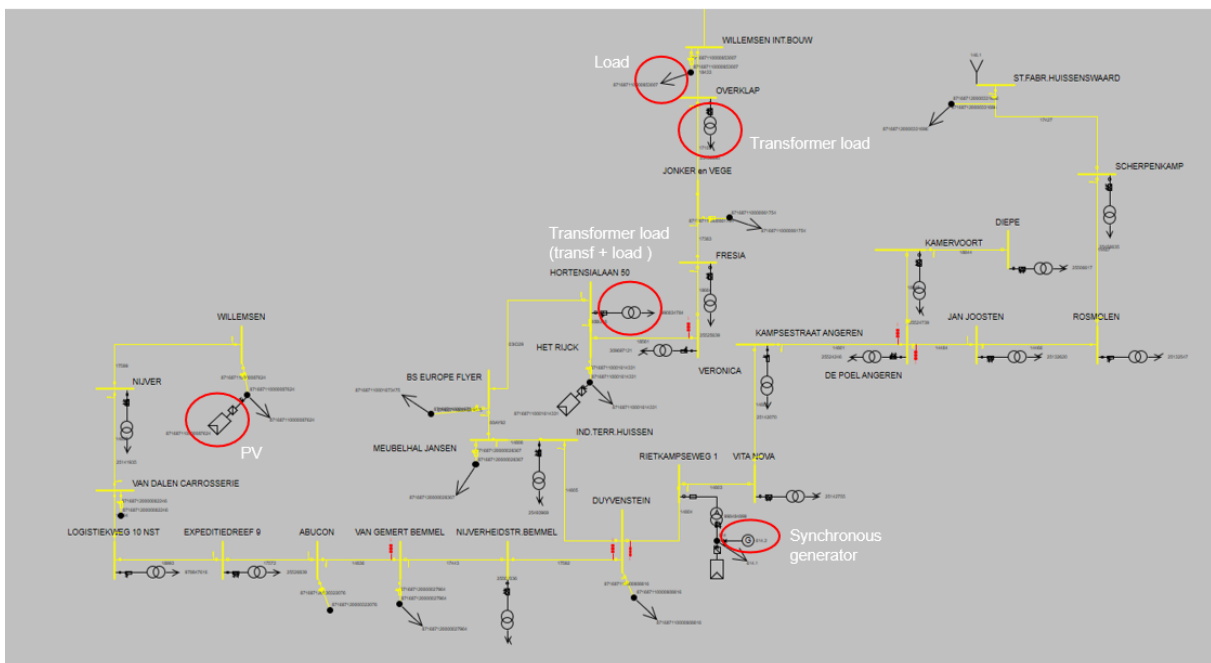


Figure 3.15: Zoom of the second feeder of the selected distribution network

Once the test network has been developed in Vision and the power flow results are obtained and checked, the network file must be built into Matpower for its subsequent simulations. For this purpose, a converter was developed that exports and transforms the network data from Vision to the needed Matpower file format. The considerations and steps followed in order to obtain the Matpower network file are detailed in this section. Afterwards, the validation of the power flow results in Matpower is carried out by their comparison with the Vision load flow results for the same network.

First, the active and reactive powers of the different Vision network components were determined. Both active and reactive power were then split into two parts: the constant power and constant impedances, which represent the PD, QD and GS, BS columns in Matpower, respectively. PD and QD correspond to the real and reactive power demand, while GS and BS correspond to the shunt

conductance and susceptance, all included in the bus data matrix (Figure A.1). The active powers are directly exported in MW and reactive powers in Mvar.

During the conversion process, the simultaneity factor of the nodes is also considered. In other words, the powers of the loads connected to each node are scaled to the set factor. This is applied to all the elements except the external grid and the synchronous generators, which are included in the generator matrix structure of Matpower instead on the bus one. On the other hand, the external grid will be seen as a synchronous generator in voltage control mode with very broad reactive power limits.

The load at each bus is taken in an equivalent form, so all loads and constant power generators connected to the bus are summed up with their respective signs: positive for loads and negative for PV generators. Moreover, bus types are determined considering the rules below:

- If an external grid is connected to a bus, this becomes the reference (slack) bus.
- If the bus has no external grid connected but a synchronous generator in a voltage control mode, it is a PV bus type.
- If the bus is not classified into a slack or PV bus, then it is a PQ bus.

Branches are represented in Vision as the components that connect two nodes with each other, and they are exported to the branch matrix structure from Matpower. Focusing on the cables, first an equivalent resistance R_{Ohm} , reactance X_{Ohm} and shunt branch capacitance $C_{\mu F}$ of all the cable parts between two network nodes are determined and then transformed to per unit. These parameters were calculated by using Equation 3.27, Equation 3.28 and Equation 3.29.

$$R_{pu} = \frac{R_{Ohm}}{Z_{base}} \quad (3.27)$$

$$X_{pu} = \frac{X_{Ohm}}{Z_{base}} \quad (3.28)$$

$$B_{pu} = 2\pi f_{nom} \cdot C_{\mu f} \cdot 10^{-6} \cdot Z_{base} \quad (3.29)$$

Where the base impedance in p.u. Z_{base} is determined from the nominal voltage of the connected buses and the base apparent power in p.u. S_{base} , calculated by using Equation 3.30. The base frequency and base apparent power can be selected by the user in the conversion process; by default, they are 50 Hz and 10 MVA, respectively.

$$Z_{base} = \frac{U_{base}^2}{S_{base}} = \frac{U_{nom_bus}^2}{S_{base}} \quad (3.30)$$

The most critical component to convert from Vision to Matpower is the transformer due to its tap changer, which can be placed in the primary or secondary sides. It is important to pay attention to the transformer modelling since the tap changer can deviate the transformer nominal voltages from the bus nominal ones. Matpower requires that the taps refer the primary voltages to the secondary side, while the transformer impedances are always referred to the secondary side. Therefore, if the tap changer is at the primary side in Vision, the Matpower 'Tap' parameter is defined as the calculation performed in Equation 3.31. On the other hand, if the tap changer is at the secondary side, the 'Tap' parameter can be expressed as described in Equation 3.32.

$$Tap_{primary} = \frac{U_{nom \text{ prim}} + \Delta U \cdot \text{Tap position}}{U_{nom \text{ bus1}}} \cdot \frac{U_{nom \text{ bus2}}}{U_{nom \text{ sec}}} \quad (3.31)$$

$$\text{Tap}_{\text{secondary}} = \frac{U_{\text{nom prim}}}{U_{\text{nom bus1}}} \cdot \frac{U_{\text{nom bus2}}}{U_{\text{nom sec}} + \Delta U \cdot \text{Tap position}} \quad (3.32)$$

where:

$U_{\text{nom prim}}$ and $U_{\text{nom sec}}$ are the nominal voltages of the primary and secondary transformer windings, respectively.

$U_{\text{nom bus1}}$ and $U_{\text{nom bus2}}$ are the nominal voltages of the primary and secondary buses.

ΔU is the voltage step size of the tap changer.

Tap position is the actual position of the tap changer.

Finally, the transformer impedance Z_{tr} is first converted from the transformer per unit form to the global one (Equation 3.33) and then referred to the secondary side (Equation 3.34).

$$Z_{tr_global} = Z_{tr} \cdot \frac{S_{base}}{S_{nom}} \quad (3.33)$$

$$Z'_{tr_global} = Z_{tr_global} \cdot \left(\frac{U_{\text{nom bus2}}}{U_{\text{nom sec}}} \right)^2 \quad (3.34)$$

Shunt branches of the transformer related to no-load losses and magnetizing currents are neglected for the purpose of this project. To conclude, the Vision components that cannot be converted from Vision to Matpower are listed below:

1. PV and wind turbines with advanced inverter controls. In particular, the steady-state controls Q(U), Q(P) and P(U), which adjust active and/or reactive power depending on the bus voltage.
2. Battery storage systems.
3. Three-winding transformers.

The graphical visualisation of this converter tool can also be found in Appendix B.

3.3. Validation of the model done in Matpower based on Vision

The previous subsection exposed the different steps, parameters and calculations considered in order to export the required input data in Matpower from the Vision distribution network. In order to check and validate the developed Vision-Matpower converter, the IEEE 33-Bus Radial Distribution System was selected, since it has a smaller size for the comparison between both tools. This 33-bus Matpower case file can be found within the Matpower installation folder and its structure is shown in Figure 3.16. Considering the input data presented in the Matpower network and the interconnection between the different elements, the same network was manually built in Vision. Its layout is presented in Figure 3.17.

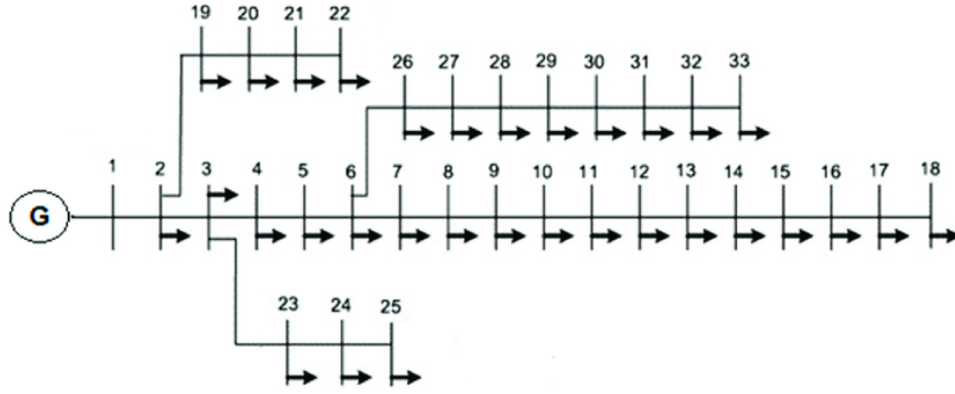


Figure 3.16: IEEE 33-Bus Radial Distribution System [28]

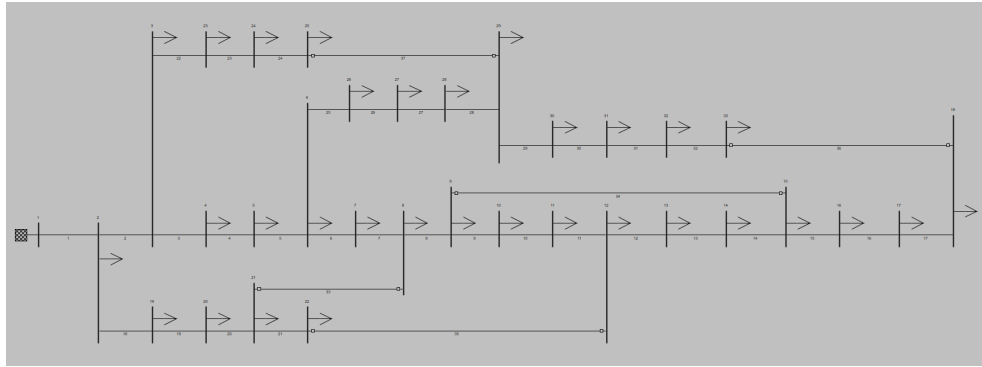


Figure 3.17: IEEE 33-bus radial distribution system built with Vision

The next step was to transform the Vision network to the Matpower network format by means of the developed converter. In this way, the power flow results obtained with the original IEEE 33-bus network and the ones obtained with the converted Matpower network can be compared in order to check the reliability of the converter.

A detailed comparison of the power flow results is presented in Appendix C: Table C.1 shows the voltage magnitude comparison for the different nodes and the active and reactive power set for the network loads. Secondly, Table C.2 presents the load flow results at the branches provided by Vision and Matpower. Finally, the comparison of the voltage magnitudes in both software tools is presented graphically in Figure 3.18.

It can be noticed that, for every variable, the load flow results obtained by both softwares are practically the same. The only difference is the active and reactive power for the first node. This is because Vision provides the value of total power provided by the external grid, while Matpower refers the value to the power consumed at that node. For the aim of this research, it can be concluded that Vision Network Analysis is a robust tool for the analysis and simulation of the network proposed due to the matching of the results with Matpower. The couple of both tools is expected to bring accurate results and it will be further used for simulations and network analysis studies.

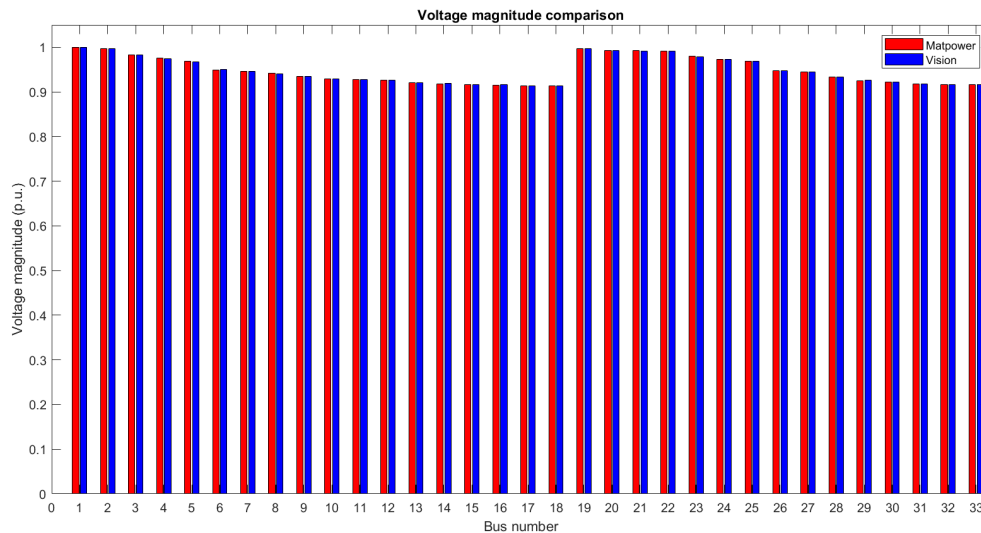


Figure 3.18: Voltage magnitude comparison for the IEEE 33-bus distribution grid, obtained with Vision and Matpower

3.4. Power flow results for the test network without flexibility

Once the coupling of both tools has been performed and validated, the next step is to adapt the test network in order to simulate a complete day. The daily demand and generation conditions will be modified in the next chapters to consider different operating situations. For this purpose, the daily demand and generation profiles need to be constructed and integrated into the network. Then, the voltage and loading results are compared between Vision and Matpower to ensure that they are the same and that both tools can be interchanged for subsequent simulations with the integration of flexibility.

Focusing on the daily load profiles in the distribution network, DSOs in the Netherlands can only access aggregated households meter data due to privacy restrictions, such as the aggregated loads represented in Vision. In order to assess the different assets of a typical distribution grid and where and when overloads are expected to occur throughout the day, power load time series with an hour resolution have been constructed. Several average load profiles representing different load behaviours can be selected and applied to the different loads in Vision, where each profile determines the relation of power of an aggregated load as a function of time. All the profiles are normalized between 0 and 1, so they are included in the model as a factor that is multiplied by the active and reactive power set for the load in order to consider the hourly demand variations throughout the day. These hourly load profiles for the regional DSO grid level were built by Phase to Phase using internal data sources.

Four representative profiles have been selected with the aim of considering different types of customers and consumption patterns. Figure 3.19 displays typical residential demand profiles and Figure 3.20 typical industrial demand profiles. In particular, Figure 3.19a illustrates a residential demand profile for a household whose consumption is electrical except for the heating system (powered by natural gas) and Figure 3.19b includes a residential demand profile whose consumption is all electric. On the other hand, Figure 3.20a represents the electricity demand consumption of a typical industrial load (i.e. factory) and Figure 3.20b shows the demand profile of a commercial load, such as a shop or other type of commercial business.

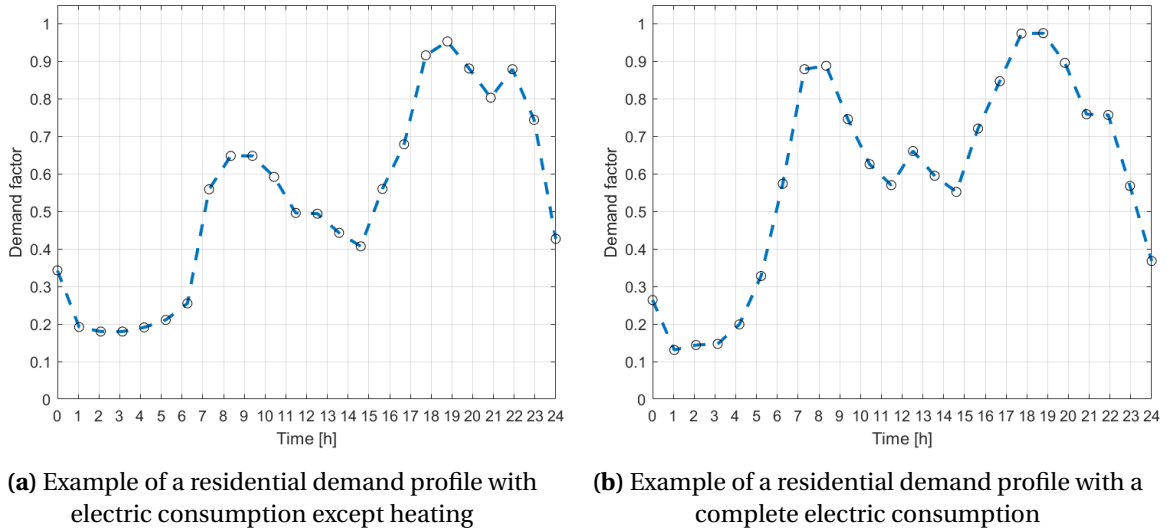


Figure 3.19: Standard residential demand profiles applied in the network loads

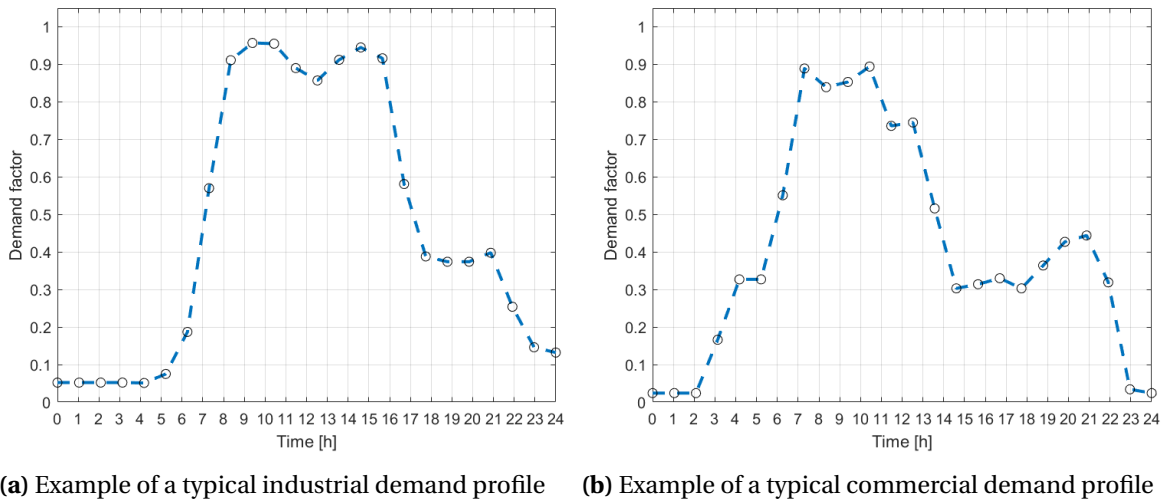


Figure 3.20: Standard industrial demand profiles applied in the network loads

A combination of these four profiles was included in the test network to distribute the demand peaks during the day and consider the different types of customers that are typically connected to a distribution network. The load profiles were integrated among all the network loads in a random manner but also considering that the low-voltage grid mainly supplies households and small-scale enterprises, while medium-voltage loads normally include large-scale customers. Following these voltage criteria and the different areas in the Netherlands represented for the test network (Figure 3.12), residential profiles were prioritized for urban areas or villages, while industrial profiles were included in more isolated locations.

In general, all the previous residential loads present a base load that varies significantly during the day from the night (hours 3-4) to the peak loads, around hours 9-10 in the morning and particularly hours 18-19 in the evening. Moreover, although the weekly change is not analysed in this research,

the demand is usually higher during the working days than in the weekend. On the other hand, industrial load profiles also show a peak in the morning that remains during the midday hours, when the commercial activity is higher. In this case, the demand peak in the evening is less notorious than in the representative residential profiles.

Moreover, it is assumed that only solar PV generation will make a significant contribution in the residential areas. In order to get the hourly PV generation during summer and winter, two real representative days were selected and the PV profiles were normalised, as shown in Figure 3.21. Moreover, the normalised winter factors were under scaled considering that solar panels generate less energy during this period. For these specific profiles, the solar PV generation is around 40% less than in summer. In general, the obtained PV generation varies significantly depending on the day and the week due to the changing weather conditions. Still, the daily pattern is more regular than then one for wind generation. The PV output normally peaks in the middle of the day, around hour 13, whereas there is no generation in the late evening hours and during the night.

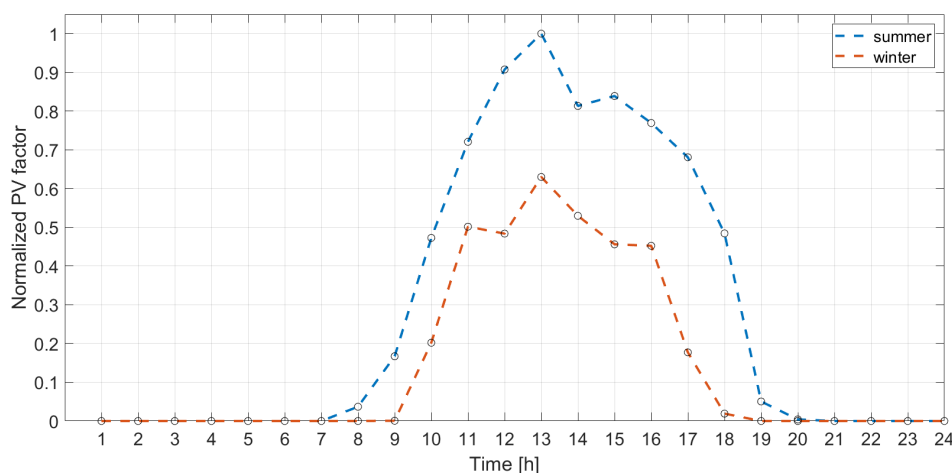


Figure 3.21: Representative photovoltaic generation profile in a summer and winter day

Power flow calculations with the test network are firstly carried out without any source of flexibility in order to compare the power flow results with Vision and Matpower. For this purpose, the previous four normalised demand profiles were distributed among the network loads and the summer normalised PV profile was also integrated in all the PV generators. The aim of these simulations is to identify the current operating conditions of the network in this scenario, as well as the main voltage and overloading problems that could arise. The results will allow to identify the needs of flexibility, the most critical points of the network as well as the time periods in which the operating limits have the risk to be exceeded. In this case, grid reinforcement is neglected, with the assumption that only the current practices performed by the DSO can be performed. In this context, under operating conditions of voltage instability or congestion issues, the main actions to take would be:

1. **Transformer tap change:** this mechanism is used to vary the voltage relations between the transformer windings, allowing to regulate the output voltage in the second winding. When calculating the power flow in Vision, the tap is adjusted automatically thanks to the transformer controls already included.
2. **Load curtailment:** decreasing the active power generated or consumed is the next action that the DSO would apply if significant congestion issues are still present. Special attention needs

to be given to the specific energy regulations and agreements between generators and consumers. For this research, it is assumed that the aggregated loads are highly controllable, which might be a valid assumption in the long term, when dynamic local electricity pricing and/or smart appliances with demand response capabilities might be widely applied.

After calculating the power flow for this test network, Vision is able to represent the voltage profiles for all the nodes at every hour of the day. These voltage profiles are shown in Figure D.1 of the Appendix for a better visualisation. Then, the same load and PV generation profiles were also integrated in Matlab in order to simulate the same scenario (Figure 3.22). It can be noticed that the voltage profiles follow the same trend in both tools, although the values are not exactly the same. However, the error is kept below 2% for all the voltage values. These differences are mainly caused by:

1. The change of the transformer tap. When running the load flow in Vision, the tap changer is automatically modified to get the best voltage relation; by contrast, Matpower does not take the tap into account and directly considers the resulting hourly voltages due to the limitations of the developed converter.
2. The solar energy generated by the PV elements in Vision is defined by an internal algorithm. Hence, Vision still scales the different generation values depending on the hour of the day by means of an internal algorithm. This is why the voltages are more similar at noon, when the PV generation reaches the maximum (1 p.u.) and Vision presents the same solar generation as Matpower.

It is important to consider that both medium voltage nodes (10,5 kV) and low voltage nodes (400-420 V) are represented in the same graph but each level presents different allowed operating limits (detailed in Figure 3.22). For the medium-voltage nodes, voltage values must range between 0,95 and 1,05 p.u. and low voltage-nodes between 0,9 and 1,06 p.u. These values are already defined in Vision for identifying overvoltage or undervoltage operating conditions.

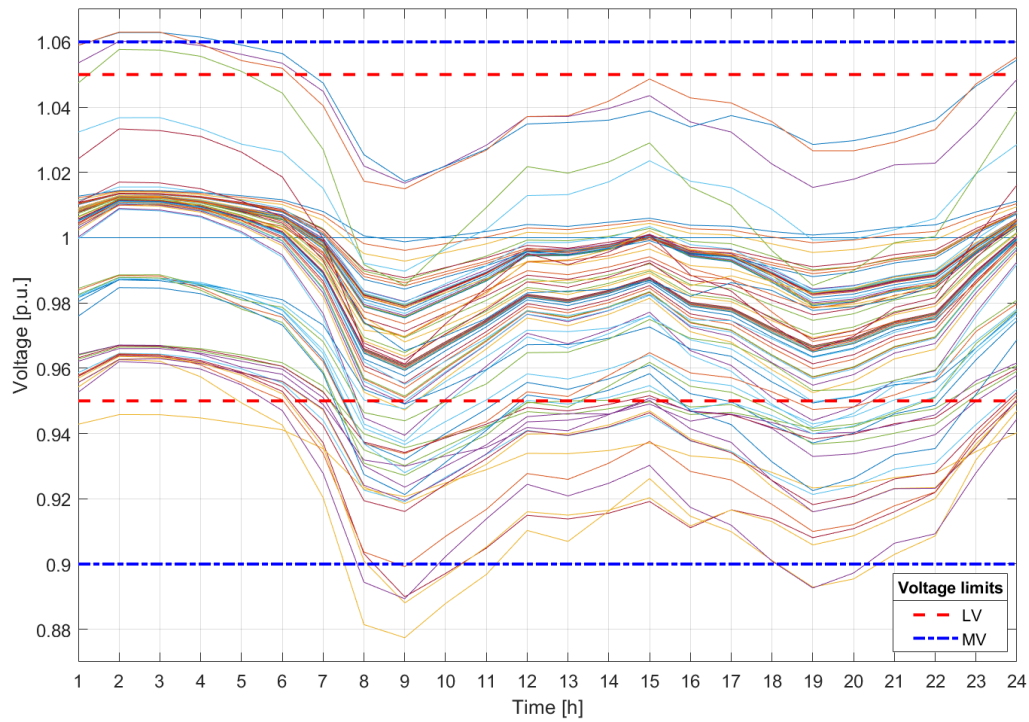


Figure 3.22: Voltage profiles throughout the day obtained with Matlab

Apart from voltage regulation, the main aim of flexibility sources is to mitigate the potential overloads in the network. Figure D.2 of the Appendix illustrates the load rates for all network branches throughout the day for this base case, directly obtained from Vision. These loading levels can also be obtained in Matlab, as shown in Figure 3.23. It can be observed that there are periods that could experience possible overloading situations, with elements that present 96% loading values. These periods correspond to the demand peaks, especially in the morning peak between 9:00-10:00 am. Chapter 5 will compare the state of the load rates of the network branches between the base case and after the action of different flexibility sources in order to check the suitability of these sources for congestion management.

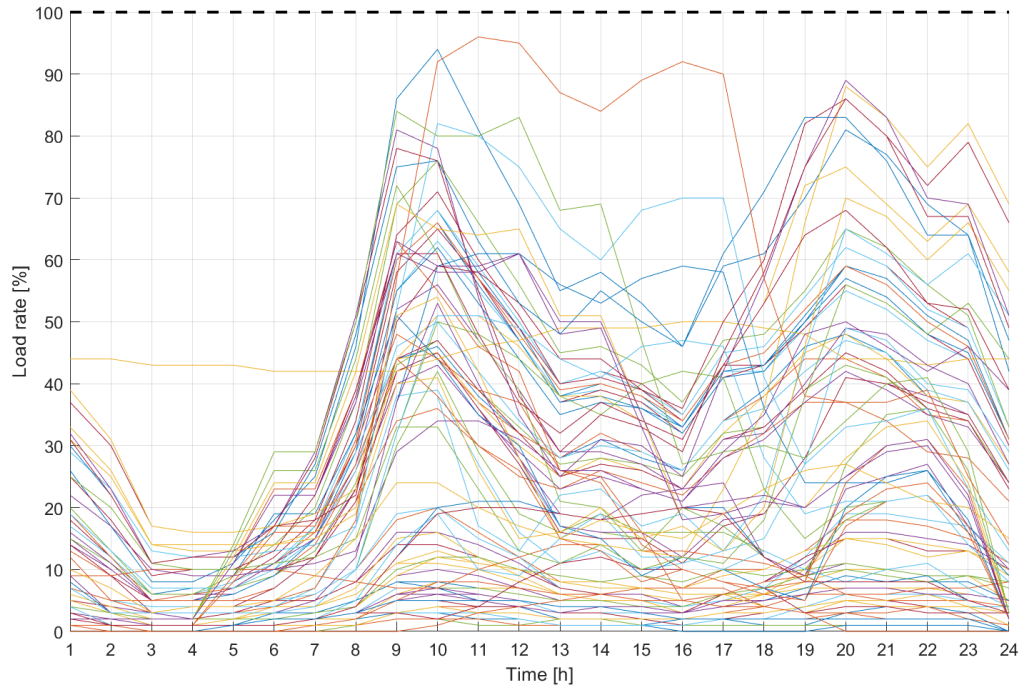


Figure 3.23: Load rates of the network branches obtained with Matlab

On the other hand, considering that demand is expected to increase in the coming years and that consumption patterns keep changing, congestion issues throughout the network are also expected to increase. In order to identify the most critical points of the network in this scenario, the load flow was calculated with a demand increase of 50%, represented in Figure 3.24. Following the colour indication set in Vision (detailed previously in Figure 3.2), it can be noticed that there are several overloaded elements in the network, coloured in orange and red. Higher load levels and under voltage problems arise even though the transformer tap was automatically updated by Vision. The DSO would proceed to apply load curtailment if the problems persist, but this is not a common practice in the low-voltage level.

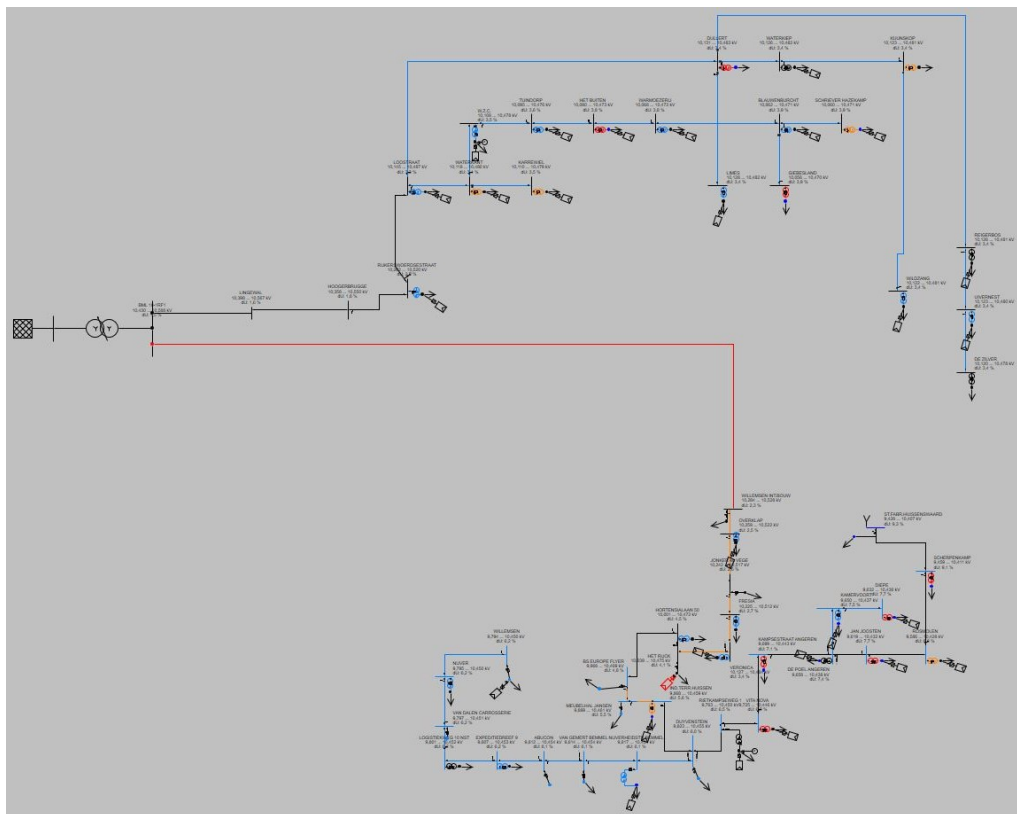


Figure 3.24: Load flow results in Vision from the combined scenario with a 50% load increase

Load curtailment programs involve an agreement between the customer and the utility or power provider, in which the customer agrees to decrease their power consumption at the utility's request in order to meet the required power needs [29]. This power drop is normally notified in advance and are usually quite expensive for the utility or system operator. In response, some industrial customers are able to power up their own generators and transfer the required loads to the generators, reducing the total demand of the utility and grid congestion. Once the peak of demand is over, the customer would be able to transfer the loads back to the utility [29].

The case of curtailment of residential loads would be more critical, since the security of electricity supply is fundamental in order to avoid potential economic losses and socioeconomic disruptions. Supply systems that are integrating renewable energy sources have a higher probability of experiencing outages at the transmission and distribution level due to their intermittency and challenging regulation when periods of high demand appear. While the grid configuration keeps unchanged, the presence of new sources of distributed generation and the higher grid electrification impose operational challenges for the system operator in terms of congestion of the lines or voltage stability issues along the network. This transformation of the power system has a critical effect on the distribution networks, in which the current practices of the DSOs might be limited for balancing purposes. In this sense, power system flexibility would allow to respond timely to the variations of supply and demand in the short-term [30].

4

Implemented control methods for the study of flexibility in the test network

The previous chapter highlighted the current operational risks in a futuristic ADN in terms of voltage regulation and congestion, mainly due to the increasing demand levels and the changing trends of power consumption. Under these conditions, operational flexibility could be a cost-efficient option for the current infrastructure challenges without resorting to grid reinforcement. With the aim of assessing the impact of different flexibility sources in the operation of the test network, specific controls have been developed in Matlab. Each flexibility source presents a specific control that simulates its potential impact on the daily network operation. The controls will modify the variables of the Matpower case file, improving the power flow results considering the constraints defined. It is important to highlight that these controls focus on voltage regulation, while the impact on the branches loadings will be analysed afterwards for each case in the next chapter to check that potential congestion problems do not arise.

The logic for the development of the Matlab controls is presented as follows. First, the individual impact of the presence of flexible generation is analysed, focusing on the integration of droop control in the PV distributed generators. Secondly, only the presence of flexible loads is considered by means of the integration of demand response in selected loads. Then, the combination of both flexible demand and generation is applied, which are based on a droop control; the obtained results will be compared with the performance of each control separately in the next chapter. Finally, storage has also been added as a potential flexibility source in distributed networks and the logic for its integration in the different case studies is detailed.

4.1. Flexible generation

The main working principles of droop control were introduced in subsection 2.2.1. Focusing on its integration into distributed energy generators, usually primary and secondary droop controls are implemented in the distribution grid by means of local measurements, reducing the communication between generators. A central controller could be added to speed up the response to perturbations.

In this study aims to explore, the effect of a decentralized droop control on the network voltage profiles due to the injection or absorption of the reactive power determined by the applied droop

characteristic, as shown in Figure 4.1. The droop control acquires the network data, the voltage magnitude in this case, at the interconnection point between the PV inverter and the grid. If the measured voltage does not meet the set constraints, the individual parameters of the distributed generation will be adapted in order to compensate for the voltage error and adjust its set point within the acceptable range [31]. This control follows Equation 4.1, which changes the voltage set point (U_1) along the respective characteristic (k_q), modifying the steady-state voltage error $U_1 - U_0$.

$$U_1 - U_0 = -k_q (Q - Q_0) \quad (4.1)$$

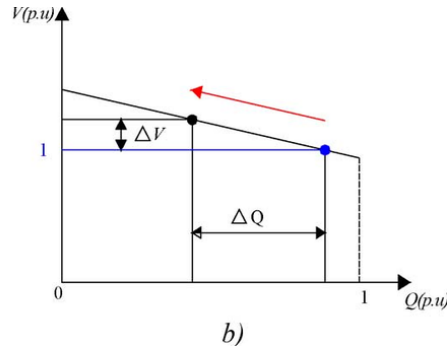


Figure 4.1: V-Q droop characteristic [24]

Since the size and number of distributed generators are not high for this network, the droop control has been integrated into all the PV generators with the aim of noticing its maximum impact: there are 28 out of 100 buses that include a PV element.

This control has been simulated in Matlab and the flowchart reproduced in Figure 4.2 shows the logic followed in terms of power flow calculations. To begin with, the hourly voltage results from the base case without flexibility are taken as the starting point of the control. Then, the voltage values are checked for every node that includes a (controllable) PV generator. Starting with the first hour, if a violation of the voltage limits occurs at those nodes, the droop control acts and calculates the required reactive power Q_i that needs to be injected or absorbed by the PV inverter. It is important to underline that this network includes photovoltaic DGs in both medium-voltage and low-voltage levels, which present different voltage constraints: the medium-voltage limits are set between 0.95 and 1.05 p.u. and low-voltage limits are between 0.9-1.06 p.u. For this case, the most restrictive condition has been applied to all nodes.

As shown in Figure 4.2, the calculated Q_i for each node depends on the voltage set point V_i at that hour, the nominal voltage value V_{nom} (always 1 p.u. in this case) and the droop characteristic k . This equation is derived from Equation 4.1. Moreover, the resulting equation is multiplied by the power of the inverter for that hour S_{hour} to express Q_i in MVar instead of p.u., as considered in the Matpower case file. It has also been assumed that the hourly apparent power of the inverter is equal to the maximum peak active power it can deliver during that hour (MWp), which corresponds to the hourly PV generation already set in the generation profiles of Vision and Matpower.

Moreover, a limitation of the amount of reactive power to inject or absorb by the PV inverter has been added. For these simulations, the reactive power head room has been set at $\pm 20\%$ and the droop slope presents a fixed value of $k=1$. Usually, the droop characteristic ranges between 1 and 5 for distributed generators but a low value has been chosen due to the small size of the PV generators currently considered [32]. Summarizing, for each PV inverter:

$$S_{hour} = P_{hour} \text{ (MWp)}$$

$$Q_{max} = 0.2 * P_{hour}$$

$$Q_{min} = -0.2 * P_{hour}$$

$$Q_i = ((V_o - V_i)/k) * S_{hour}$$

The next step will be to substitute the new calculated values of reactive power for every hour in the Matpower network file and run the power flow again in order to check the voltage results. It is important to note that droop control will only act once when there is a violation of the voltage limits at the selected nodes since the amount of reactive power that can be adjusted is limited. This process will be performed for every hour of the day. The final outcome will be the corrected voltage profiles throughout the day due to the action of droop control when required. The impact of droop control in the test network will be presented in the next chapter for summer and winter solar generation conditions.

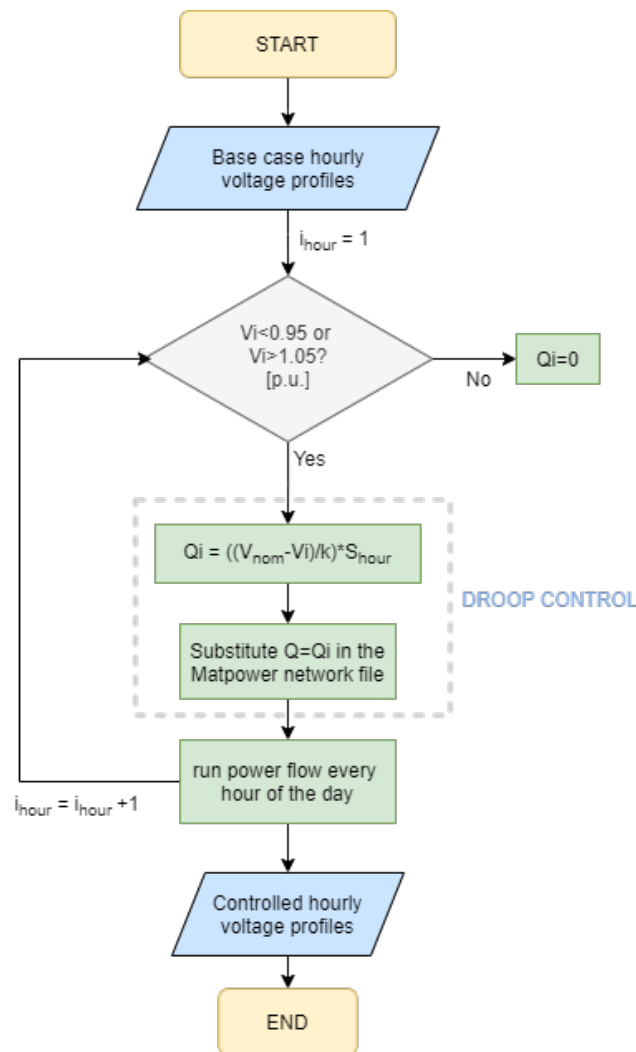


Figure 4.2: Flowchart of the droop control implemented in Matlab

4.2. Flexible demand

Demand response presents a large potential to meet flexibility needs in the Dutch power system, particularly in industrial demand applications which are expected to grow in the coming years, such as power-to-gas (P2G), power-to-heat (P2H) or power-to-ammonia (P2A) [33]. Additionally, households have been pointed out as candidates for providing demand response services, but its potential highly depends on price incentives, human behaviour or the emergent role of the aggregator in the low-voltage networks. Demand side management mechanisms would provide opportunities for the consumers to play a crucial role in the grid operation by reducing their power consumption or shifting the electricity usage during some periods, depending on financial incentives or time-based rates [34]. In fact, demand response programs are already being tested by system operators for balancing purposes.

In this context, residential loads have a huge potential for adopting demand side management (DSM) programs due to several reasons. First, the energy consumption from both buildings and the construction sector combined represent nearly 40% of the total CO₂ emissions. Energy demand from households increases every year, encouraged by the bigger ownership of energy-consuming devices [35]. Particularly, space heating represents 68% of the end-use energy in the residential sector [36]. The different devices that consume energy in the households, together with the expected demand increase in the coming years, lead to a potential integration of demand response programs in distribution grids, focusing on the mitigation of overloads.

Demand Response is usually defined as a shift of part of the peak power demand from an hour to another, forward or backwards. It can be divided into different categories, mainly non-dispatchable (price-based) and dispatchable load (incentive-based) [37]. Nevertheless, direct control programs can also be set, which give power companies the ability to turn some devices on and off, such as power heaters or air conditioners, during high-demand periods. As a reward, the customers receive some financial incentives or lower electricity bills.

Although peak shifting is the demand response method that is mostly implemented in several pilot projects, the direct control by the system operator is chosen for these simulations. For this research, only one day is being analysed while in real operation, the shift of demand can be set from one hour to another hour of the week or month. Therefore, the analysis of demand response for this study will focus on the effect of power variations, performed by the DSO, during the hours of the day which present the highest demand rates. An overview of the steps followed is illustrated in Figure 4.3. This control has been applied to a quarter of the network loads (13 out of 47) in order to notice its local effect on voltages and loadings. The type of load behaviour selected for the integration of demand response is the residential load with a 100% electricity consumption. In this way, there are higher chances of regulating the energy used in the household by means of these programs.

Using a similar procedure to the one used for droop control in distributed generators, demand response control takes as a starting point the voltage results from the power flow calculations without flexibility. However, this time the control does not act at each node depending on the voltage set point at that hour, but as a whole set. If at least one of the nodes with Demand Response violates the voltage limits, the control is activated and the voltage condition is checked for all the nodes with a controllable load. As expected, the network aggregate loads are highly controllable and fully manageable by the DSO. For this research, just the overall impact on the network operation in terms of power flow calculations is investigated.

In general, decreasing the power of a load entails that the current required decreases accordingly. As a consequence, the voltage increases based on the Ohm law ($V(V) = R(\Omega) * I(A)$), and it decreases while the power demand increases. The method shown in the flowchart follows this rationale: if

the node presents undervoltage, the value of active and reactive power of the load at that hour is decreased by 10%; if the node presents overvoltage, the active and reactive power are increased by 10% in order to bring back the voltage values within the allowed range. In a similar way to the droop control applied to the distributed generators, the demand response control proposed also varies active and reactive power depending on the variation of the voltage values beyond the admissible limits. However, there is not a defined slope for the variation of P and Q depending on the variation of the voltage. In this case, the voltage values are continuously checked each hour ('while' loop) and, if the voltage limits are still violated for that hour, P and Q are varied a fixed 10% of the P and Q values set in the previous load flow loop. Since the active and reactive powers can be decreased until zero if the iterations continue and the voltages are not regulated, a limit of 50% of active power (real consumption of the customer) that can be increased or decreased has been defined.

Therefore, the variation of active power P performed by demand response in this study considers the limits below. P_{max} refers to the maximum amount of active power that the load can increase under overvoltage conditions with respect to the initial active power set for that hour (without flexibility). On the other hand, P_{min} corresponds to the maximum amount of active power that the load can decrease if undervoltages occur, with respect to the initial hourly active power values before the introduction of flexibility. The increase and decrease of P is performed proportionally depending on the voltage deviation, applying the theory of droop control.

$$\begin{aligned} P_{max} &= 1.5 * P_{hour} \\ P_{min} &= 0.5 * P_{hour} \end{aligned}$$

Once the updated values of P and Q reach the previous limits or the voltages are corrected with less iterations, the new calculated values of active and reactive power are substituted in the Matpower case file and power flow calculations are carried out. This process will be repeated for each hour of the day until the voltage profiles are regulated for the whole day, considering the set assumptions and constraints.

The variation of both active and reactive power is usually applied to industrial loads, which include motors than can regulate better the reactive power, either injected or absorbed. However, while most of the electric companies do not directly charge for reactive power, they benefit from power factor correction since the lines carrying additional reactive current cost them more money. The economic benefits that power factor correction can offer to a typical household are normally ignored in comparison to the savings and other benefits that businesses with large industrial loads can offer. In general, reactive power is paid in the form of energy losses originated by the reactive currents flowing into the households. These losses are expected in the form of heat and cannot be returned to the grid. In this research, the effect of reactive power regulation by demand response programs has also been considered for the selected residential loads since the most energy-intensive domestic devices such as the washing machine and the dishwasher include motors that could perform this task. The final goal of this control is to prove to what extent this type of regulation could be a source of voltage control in the residential level.

In general, the reactive power that is added by the lines represents a hurdle for the grid operator. With low demand conditions, for example during the night, parallel reactors might be necessary in order to consume the additional capacitive reactive power introduced. During the peak hours, voltages are expected to drop, which are aggravated by the inductive reactive power present in the lines. Hence, the reactive power control should be considered, especially if large inductive industrial loads are the subject of study.

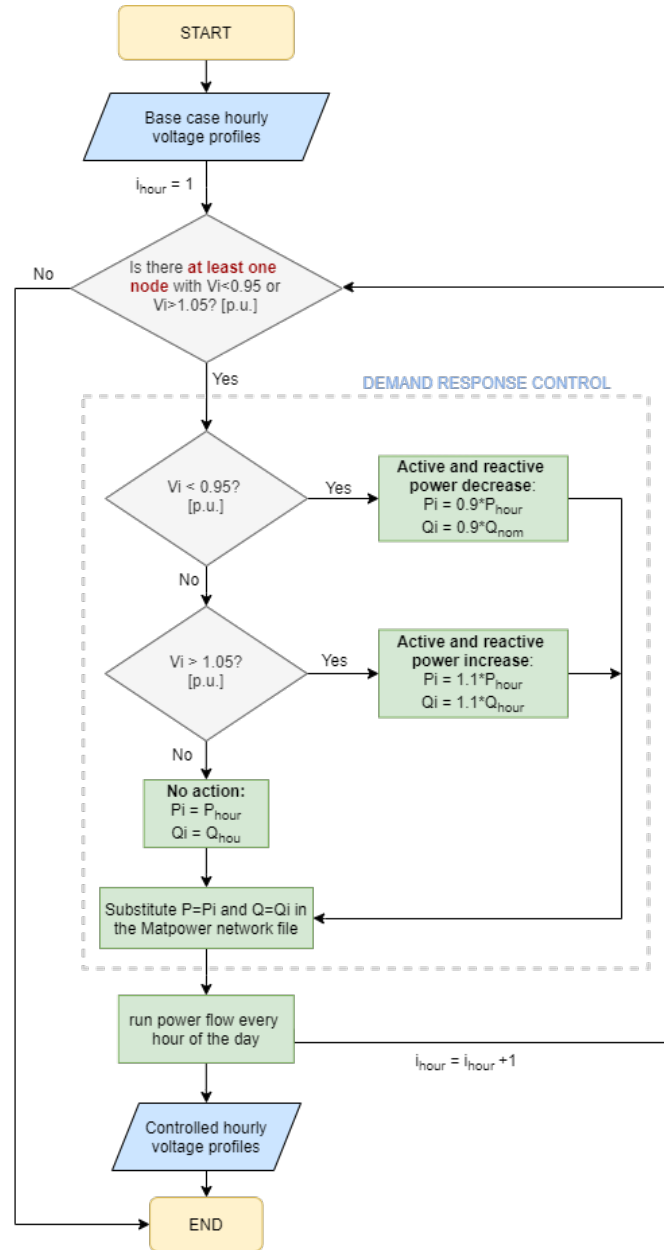


Figure 4.3: Flowchart of the Demand Response for both P and Q control implemented in Matlab

4.3. Flexible generation and demand

Along this chapter, the logic for the separate integration of flexible generation and demand in the test distribution network has been presented. However, the effect of the combined control of distributed generation and demand in the network could lead to interesting results in terms of voltage regulation. Its impact will be explored in the next chapter.

As presented in the previous sections, the proposed controls for the simulation of flexible generation and demand consist of a droop control with $k=1$ and $Q_i = \pm 20\%$, as well as demand response regulating both P and Q with a variation range of $\pm 50\%$. Similar to previous subsections, the control logic that has been followed in this case is represented in Figure 4.4 in a two-stage approach. It has been considered that droop control is first applied and then, the resulting voltages are corrected by

demand response. In this way, the customer side is the last one to be modified in order not to compromise the security of supply and to avoid the higher costs that the demand response programs involve as much as possible.

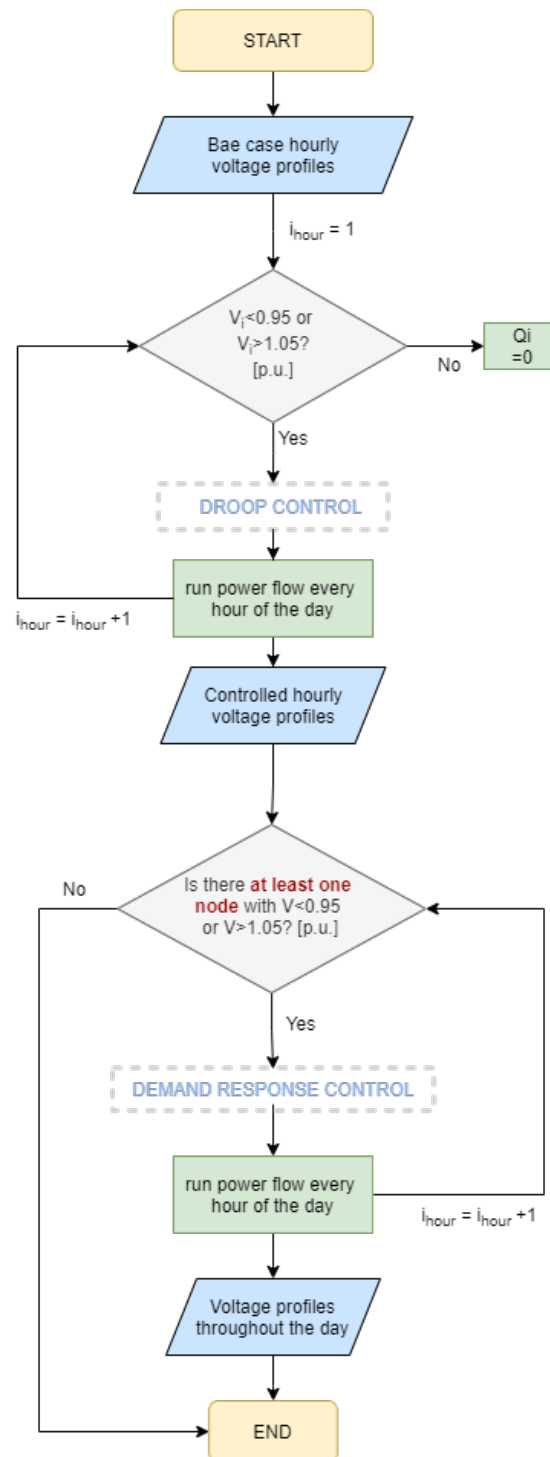


Figure 4.4: Flowchart of the combined control of generation and demand implemented in Matlab

Therefore, first the voltage values at all the nodes with distributed generation are regulated by the droop control with the injection or absorption of the corresponding reactive power Q at each node. Once the droop control has been applied, the corrected voltage values are checked again and, if violation of the voltage limits still persists at the nodes with controllable demand, demand response acts for all the network flexible loads. The value of P and Q will be therefore decreased or increased by the control in order to bring back the voltages close to their nominal values at every node. First, droop control checks the voltage profiles every hour of the day, and then demand response also acts throughout the complete day. In this case, the dashed-line boxes include the droop and demand response control steps that were also within the dashed boxes in Figure 4.2 and Figure 4.3 to simplify the flowchart.

4.4. Flexible energy storage

In general, the role of energy storage for flexibility services is limited due to its relatively high costs. This specially applies to long-term storage functions that could meet the expected flexibility needs or, at a regional level, for congestion management purposes [33]. Storage options are usually more expensive than the alternatives, such as demand response, curtailment or even grid reinforcement. However, the role of storage would be more significant for meeting balancing needs considering the uncertainty generated by the distributed renewable energy sources, and particularly for providing primary and secondary power reserves.

Focusing on energy storage at a regional level, the use of battery systems purely for congestion management in the short-term was found to not outweigh the costs. Relatively large batteries would be required for this function and taking into account the costs of a battery system, additional energy losses and complexity (and, therefore, higher operational risks), it can be concluded that the integration of battery systems instead of opting for grid reinforcement is economically feasible for a few number of cases [33]. However, the use of batteries when the system includes other sources of voltage support or back-up power, could be profitable. The application of energy storage for this research aims to explore the impact of battery systems on a network which already presents other voltage regulation sources in the form of the presented flexibility controls. Energy storage is proposed as a flexibility source for regulating the pending voltage profiles after the action of droop control and demand response in order to achieve a suitable voltage regulation and congestion management along the network.

For each case study analysed in Chapter 5, the following steps have been taken in order to evaluate the need of battery systems, as well as the dimension of their required capacities and location in the network:

1. **Active power difference needed per node for voltage regulation:**

As already stated, it is assumed that droop control and demand response have already taken place, while energy storage acts as an extra measure for voltage regulation. In this context, the nodes that still violate the admissible voltage limits after the action of flexibility need to be detected. Each of these nodes will present a connected battery system, which must charge and discharge the required energy to achieve voltage regulation during the specified hours. The first step is to define the amount of active power that still needs to be increased or decreased at each node every hour in order to bring back the voltage profiles within the allowed limits. This power would be covered by individual battery systems connected to each node of interest. For this purpose, the steps represented in Figure 4.5 are followed.

The starting parameters are the voltages values throughout the day, previously corrected by droop control and demand response actions. Then, the voltage value of each node is checked

every hour. If the node presents overvoltage ($V_i > 1.06$), the active power of the selected nodes is increased by 0.01 MW for the corresponding hours and the power flow is run again. The process continues until the overvoltage values disappear. On the other hand, if undervoltages are detected along the network, the power is decreased by 0.001 MW for the necessary nodes in order to bring back the voltage values within the allowed limits. Similarly, the power flow is calculated again and the active power will be corrected until the voltages are completely regulated. In the end, the active power for all the nodes will be unchanged if there are no voltage violations, or P_{hour} will be updated by the control. The difference between the final and initial active power at each node every hour defines the amount of active power that needs to be charged or discharged by the battery systems during the day.

For this case, the voltage limits have been set between 0.9 and 1.06 p.u., which corresponds to the low-voltage constraints set in Vision and used by their clients for the identification of voltage stability issues in the network. This is why it was found that medium-voltage profiles were corrected more easily by the other flexibility sources, while low-voltage profiles still presented some voltage instability that required storage applications.

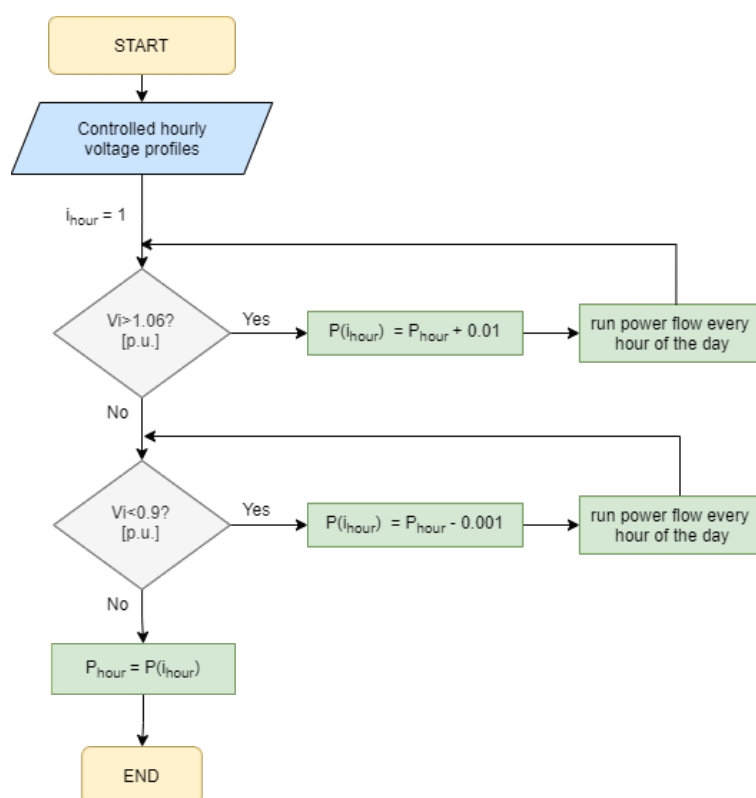


Figure 4.5: Flowchart of the logic implemented in Matlab for the detection of storage needs in the network

2. Capacity estimation for the required battery systems:

With the set theoretical amount of active power to decrease or increase per node, a first calculation of the needed battery capacity at each node can be worked out. For this, it has been assumed that the State of Charge (SoC) of all batteries can vary between 10% and 90% in order to avoid undercharging and overcharging conditions [38]. The SoC refers to the current available capacity of the battery with respect to its nominal capacity, a discharged battery being

SoC = 0% and a completely charged battery being SoC = 100% . Therefore, in this case study the total variation range of the SoC has been set at 80%, meaning that only that percentage of the full battery capacity can be used considering the charging and discharging constraints.

The estimated capacity for each battery is directly influenced by this SoC rate. The capacity will be calculated as the total amount of power that needs to be decreased or increased at that node during the complete day, divided by the SoC range (0,8) to take into account the actual capacity that can be varied. Equation 4.2 shows this calculation. The capacity of the battery connected to a node 'n' will be obtained by considering all the active power that needs to be injected (discharged) or absorbed (charged) by the battery with the aim of regulating its voltage values during the complete day, adding the SoC constraints defined. The number of nodes n whose active power is corrected by the control defines the number of required battery systems in the network.

$$\text{Capacity } (n) = \sum_{i_{\text{hour}}=1}^{i_{\text{hour}}=24} \frac{P_n(i_{\text{hour}})}{0.8} \quad (4.2)$$

3. Logic for the charged and discharged energy by the batteries throughout the day:

Once a first estimation of the number of battery systems that would be required in the network and their theoretical capacity is made, their charging and discharging logic during the day needs to be defined. In this sense, it is important that the charging and discharging periods of the batteries do not influence other voltage profiles in an undesirable way.

During the overvoltage periods, all the batteries will charge in order to increase the demand at the selected nodes and lower the voltage values. By contrast, during undervoltages periods, the batteries will discharge in order to cover part of the demand and increase the voltage values. During the rest of the hours, the batteries will do the opposite in order to present the optimal conditions when the critical time periods are reached. Thus, being completely charged at the time when they need to start discharging due to the presence of undervoltages, and in the same way being completely discharged when the overvoltage values are detected. Therefore, the rest of the hours the batteries will charge or discharge the same amount of energy every hour, always considering their influence in the global network voltage profiles.

4. Check the State of Charge (SoC) of the batteries throughout the day:

After implementing the charging-discharging logic of the battery systems throughout the day, their State of Charge is checked. This is a way of ensuring that the batteries are charged and discharged respecting the SoC constraints (between 10 and 90%) assuming their estimated capacity. The hourly SoC is calculated dividing the capacity of the battery system during that hour by the total estimated storage capacity connected to that node, as shown in Equation 4.3.

$$\text{SOC} = \frac{\text{Capacity } (n_{\text{hour}})}{\text{Capacity } (n_{\text{total}})} \quad (4.3)$$

Finally, the network voltages can be illustrated after the introduction of the battery system control, which must be within the admissible voltage limits. The different steps followed for the integration of flexible storage systems will be applied in different case studies in the next chapter. The differences found regarding the size of the battery systems and their location will draw conclusions about the suitability of this flexibility source under changing operating conditions, and how feasible its integration would be in a future ADN in the Netherlands.

5

Comparative assessment of different operational flexibility sources

The demand for flexibility of a distribution network can be covered from the supply side, demand side or by means of flexible storage systems. Droop control, demand response and flexible battery systems have been proposed respectively as potential flexibility sources that could be integrated in an action distribution grid in the Netherlands. The controls presented in Chapter 4 for the simulation of these sources in an hourly basis are now applied to the developed test network under different operating conditions.

First, the characteristics of the case studies analysed for the assessment of the different sources of flexibility are presented. Then, a sensitivity analysis is carried out prior to the analysis of each case study in order to identify the interrelation between the network variables of interest and how they influence each other. Finally, the sources of flexibility are integrated in the case studies proposed and conclusions are drawn regarding their performance when the test network is exposed to changing levels of demand and generation.

5.1. Case studies proposed

The test network built in Vision and Matpower represents the 'base line case' for this analysis. The results for the defined generation and demand levels in the network have already been shown in Chapter 3, in terms of voltage regulation and loading of the branches. In order to get more insightful conclusions about the performance of the sources of flexibility considered after their integration into the network, other two case studies have been considered. The same network is simulated with lower demand values than the base line case, and higher demand levels with some peaks of demand during the day are also introduced.

In this way, it is easier to spot the differences regarding the resulting voltage profiles and their subsequent regulation by the flexibility controls proposed in Chapter 4. Therefore, the suitability of these sources for each case will be assessed in order to obtain a comparative assessment about the performance of flexibility under different operating conditions in the same network.

For this analysis, a complete day is analysed for all the study cases, considering 1-hour resolution. Moreover, two representative days, one in summer and one in winter, are assessed for each case in order to identify the differences of the network in terms of power flow results, considering seasonal differences of solar generation. Both PV generation profiles were already presented in Figure 3.21

above. Before the integration and assessment of the different flexibility sources for different levels of demand and generation, the assumptions made for the under-scaled and over-scaled case study are presented.

5.1.1. Under-scaled scenario

Both under-scaled and over-scaled scenarios are derived from the base line case already set up in the test network. The conditions for both case studies were extracted from the FLEXNET project report, developed by Alliander and ECN [39]. This project aims to assess the demand and supply of flexibility of the Dutch power system up to 2050 at both regional and national levels. In order to analyse the demand of flexibility in the Netherlands, it proposes two types of scenarios: the Reference scenario (accepted policy scenario) and the Alternative scenario, which assumes a strong growth of the electrification of the energy system, specially by means of electric vehicles (EV), heat pumps (HP) and other additional types of electrification. The Alternative scenario will be the one considered for the analysis of the under-scaled and over-scaled case studies in this network.

From now on, the interest will rely on the scenario 'A2030' proposed by FLEXNET, which considers the expected values of the Dutch power system for 2030. These values are based on data and different models developed by research centers and DSOs in the Netherlands in order to assess the grid performance in the near future. Moreover, additional electrification of the national network will be considered.

Focusing on the under-scaled scenario, the demand levels have been extrapolated from Figure 5.1, proposed by FLEXNET. The average load is considered as our base line case study in order to define the under-scaled case as the 'minimum load' represented in the graph. In this way, for the Alternative scenario in 2030, the average and minimum load differ in a factor of 0,61. Hence, in order to build a representative day with low levels of demand, the demand from the base line case has been decreased in a factor of 61%. The solar PV generation will not be changed, but both summer and winter differences will be assessed for this case.



Figure 5.1: Minimum, maximum and average hourly power load values in the Netherlands in all the scenario cases proposed in the Flexnet report [33]

5.1.2. Over-scaled scenario

The main aim of the over-scaled scenario is to assess the way in which higher rates of electrification of the power system of the Netherlands have an impact on the demand for flexibility, and how the proposed sources of flexibility are able to respond to this increase of demand. For higher levels of electrification, the grid could be loaded beyond its limits.

Taking as a reference A2030 scenario already considered for the under-scaled scenario and following Figure 5.2, a significant increase of electrification demand is expected by 2030. Moreover, the contribution of additional load created by electric vehicles (EVs) and heat pumps (HPs) is already noticeable. For the over-scaled case study proposed for this research, apart from the additional electrification rates, the added daily demand from EVs and HPS is also considered.

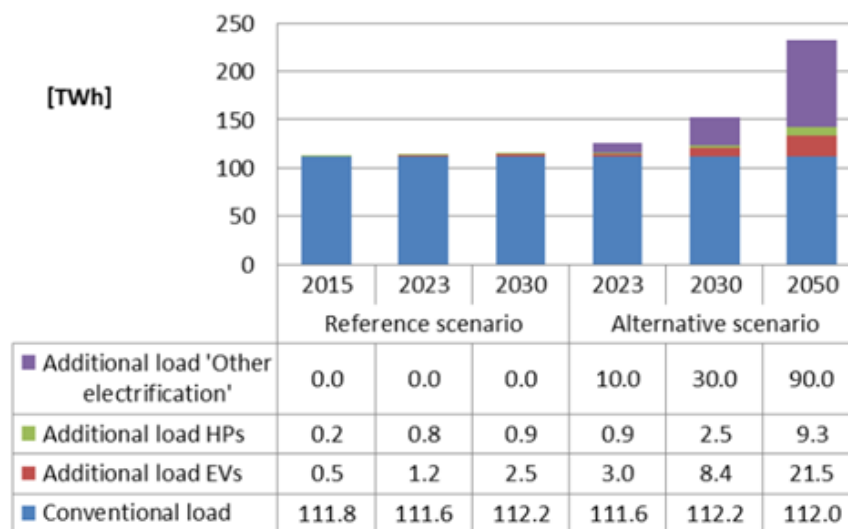


Figure 5.2: Total power load in the Netherlands for all the scenario cases proposed in the Flexnet report [33]

Particularly, three representative hourly profiles have been developed for three variables in the demand side (base load, additional load for EVs and additional load for HPs), apart from the PV generation profiles (summer and winter) in the supply side. All these profiles have been normalised to represent a factor between 0 and 1, such as the different load profiles already presented in Chapter 3. Each profile will be multiplied by the respective input values for each case study in order to simulate the daily variations of demand and generation in the network.

The HP demand profiles at the regional level were extrapolated from national data regarding the expected electricity consumption of heat pumps, and the seasonal differences were taken into account in order to create a HP demand profile of a representative summer and winter day, as represented in Figure 5.3. It can be observed that, in winter, the contribution of heat pumps to the total demand profile is quite significant and highly depends on the variation of the hourly temperatures and the household activities. For instance, it can be noticed that in the midday hours, when the temperature rises again, the heat pump's load decreases. In general, the base load period is found in the afternoon (13-15h), while the demand peaks occur in the morning (7-9h), when people start heating their houses, and in the evening (18-20h), when people arrive home from work and start heating the homes again. In the case of summer, the power demand is much lower since HPs are usually used

for heating tap water and not for space heating. However, the demand profiles also vary during the day, with two peaks in the morning and in the evening.

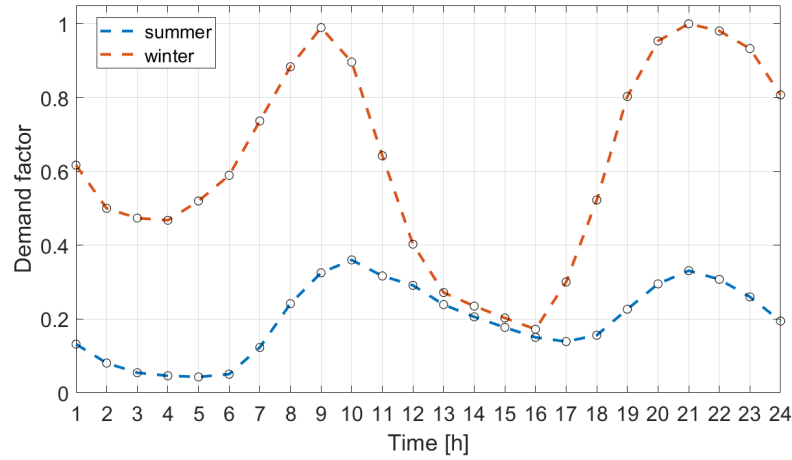


Figure 5.3: Daily demand factor profile considered for a heat pump in summer and winter

The daily EV power demand has also been extrapolated from DSOs data regarding the expected arrival time to the EV chargers and the charging periods during the day. At the aggregated level, the EV load profile presents two outstanding peaks, around 9:00 and 18:00. This is due to the fact that, during working days, it is assumed that passenger EVs charge their vehicle when they arrive to the charging station and when they come back home. This is also combined with relatively large charging times. Moreover, the morning and evening peaks of the EV daily demand profile unfavourably coincide with the demand profile peaks of a typical household.

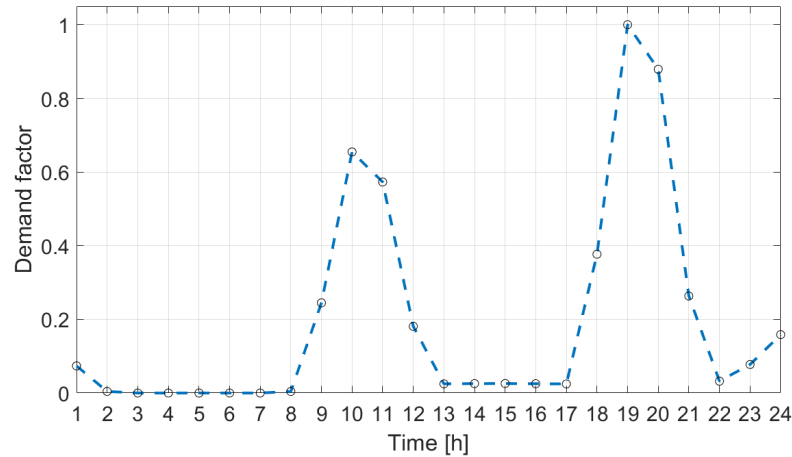


Figure 5.4: Daily demand factor profile considered for an electric vehicle

The main issue of the increasing integration of EV and HP in the distribution grid is that they are usually active during the same time periods of the day on a local level, as shown in Figure 5.3 and Figure 5.4, leading to peak loads on the grid. Local penetrations of the previous technologies could create loading peaks, leading to potential loading issues. Moreover, these technologies will not be uniformly distributed along the network, creating additional challenges for the network operation.

by the DSO [33]. In the A2030 scenario considered in Figure 5.2, it is assumed that there will be a 20% share of heat pumps among the total number of residential households, and 32% share of electric vehicles in all the passenger cars in the Netherlands [33]. These penetration rates were also considered for integrating these technologies into the test network.

The previous expected penetration rates were considered for the integration of HPs and EVs in the over-scaled scenario of the analysis. In the case of the addition of HPs, only the loads with demand response were considered, since heat pumps present high potential for providing flexibility in the residential level. Having 47 loads in the network and 20% increase of the presence of heat pumps, the additional HP demand profile was added to 10 loads (out of 13 loads with demand response). On the other hand, 32% of the residential loads were added the daily EV demand profile also focusing on their expected penetration rate in 2030. In this case, the EVs were equally distributed between the two types of residential loads present in the network.

In this way, the load profile for each particular load was modified based on the expected adoption of these technologies along the network. In particular, the impact of EVs and HPs on the demand profile will be noticed after carrying out the power flow calculations. To achieve this, the forecasted share of these technologies at the national level have been transferred to the regional level following the same penetration rates.

For the development of the over-scaled scenario, a weighted sum of the different demand levels presented in Figure 5.2 was performed. First, a general demand increase for the whole network was considered due to the expected additional electrification of the system by 2030. For this purpose, the total demand in the A2030 scenario (obtained from the sum of all the values in the column, equal to 153.1 TWh) was divided by the total demand in the A2023 scenario, considered as the base line case. This results in a general demand increase factor of 1.22, which was multiplied by all the load demand profiles every hour of the day. Then, the additional demand provided by HPs and EVs was also added to the selected loads by a weighted sum considering the values in the A2030 scenario shown in Figure 5.2.

Therefore, if a residential load is considered to present a HP and EV at the same time, its daily demand profile would additionally present the general demand increase factor (1.22), the weighted HP demand factor ($2.5/153.1$) multiplied by the winter or summer demand profile respectively and the weighted EV demand factor ($8.4/153.1$) multiplied by the EV normalised demand previously presented. The resulting demand values for each load were multiplied by the daily demand profiles considered in Matpower in order to simulate an increase of demand in a futuristic scenario for the same test network.

For the households with a HP and that also own an EV, the highest demand peak will occur in the evening: the household evening demand peak coincides with the evening charging peak, and the heat pump also contributes to this peak, especially in winter. The impact of the integration of these technologies into the daily network demand profile will be noticed after carrying out the power flow calculations.

5.1.3. Summary of the case studies and analysis methodology

As presented in this section, three different demand levels will be included in the network in order to analyse its operational limits, as well as the suitability of the proposed flexibility sources under different scenarios. The base demand considered in the power flow calculations without flexibility is now under-scaled and over-scaled in order to simulate a typical day with low and high demand rates. Moreover, for the over-scaled scenario, expected demand values for 2030 in the Netherlands

are considered, including higher rates of electrification and penetration of heat pumps and electric vehicles.

Apart from the variation of the network demand levels during the day, a representative summer and winter day were analysed for each case, taking the daily PV generation profiles already presented in Figure 3.21. In this way, the role of the generation levels in the network on voltage stability and congestion of the lines will be also analysed. The different scenarios are summarized in Table 5.1.

		24-hour Demand Profile		
		Under scaled	Base line	Over scaled
PV generation	Summer	Case 1a	Case 2a	Case 3a
	Winter	Case 1b	Case 2b	Case 3b

Table 5.1: Summary of the demand and generation conditions for the different case studies

For each case study, first the power flow results without the integration of flexibility will be assessed in order to identify the influence of different demand and generation levels in the network operation. Then, the controls proposed in Chapter 4 will be integrated into each case study in order to simulate the action of the different flexibility sources considered. The representative differences in the results between the case studies will be presented, mainly focusing on:

1. Sensitivity analysis of the voltages and loadings to active power curtailment and reactive power control. Prior to the assessment of the results from the different scenarios, a sensitivity analysis will be performed for each case in order to identify the critical points of the network in terms of voltage stability and congestion.
2. Voltage stability. The controls proposed for the supply, demand and storage flexibility sources focus on the regulation of the voltage profiles within the admissible range. Their performance for the different network conditions will be assessed, identifying the critical time periods of the day in terms of voltage deviations.
3. Loadings of the network branches. Despite the focus on the control of voltage regulation, the load rates of the network cables and transformers need to be considered after the action of the different flexibility sources, to check their suitability for short-term congestion management.

The next section details the sensitivity analysis performed for the assessment of the variations of the node voltages and branch loadings throughout the network under active and reactive power changes.

5.2. Sensitivity analysis

Before presenting the flexibility assessment for the different case studies, a sensitivity analysis was carried out in order to identify how the network operation is affected by changes in the different parameters. This sensitivity analysis will determine how different values of the variables of interest, active and reactive power in this case, affect other dependent variables under given assumptions (voltages and loadings). The main aim of this analysis is to identify the most critical points of the network under different operating conditions. For this research, the main interest lies in:

1. The voltage variations at every network node due to the active and reactive power variations at any other node.

2. The loading variation of every network branch due to the active and reactive power variations at any other branch.

To begin with, Chapter 2 presented the theory of power flow calculations and derived the net active and reactive power equations P_i and Q_i , which represent the power injections at a bus i (Equation 2.5 and Equation 2.6). In real electricity distribution networks, where the inductive nature of the loads predominates, the effects of active and reactive power injections into the system buses are commonly analysed in terms of voltage variations [40]. Considering the dependence of the voltages at a bus i on the net powers of all the buses in the network:

$$V_i = f(P_1, P_2, \dots, P_n, Q_1, Q_2, \dots, Q_n)$$

The differential function V_i can be expressed as [41]:

$$dV_i = \sum_{j=1}^n \frac{\partial V_i}{\partial P_j} dP_j + \sum_{j=1}^n \frac{\partial V_i}{\partial Q_j} dQ_j \quad (5.1)$$

Where the partial derivatives $\frac{\partial V_i}{\partial P_j}$ and $\frac{\partial V_i}{\partial Q_j}$ represent the voltage sensitivity coefficients with respect to the power variations at the network nodes. Considering that there are n equations given by the previous expression (Equation 5.1), these coefficients build the sensitivity matrices $\partial V/\partial P$ and $\partial V/\partial Q$, denoted S_p and S_q respectively [40]:

$$[S_p] = \begin{bmatrix} \frac{\partial V_1}{\partial P_1} & \dots & \frac{\partial V_1}{\partial P_n} \\ \dots & \dots & \dots \\ \frac{\partial V_n}{\partial P_1} & \dots & \frac{\partial V_n}{\partial P_n} \end{bmatrix}, [S_q] = \begin{bmatrix} \frac{\partial V_1}{\partial Q_1} & \dots & \frac{\partial V_1}{\partial Q_n} \\ \dots & \dots & \dots \\ \frac{\partial V_n}{\partial Q_1} & \dots & \frac{\partial V_n}{\partial Q_n} \end{bmatrix} \quad (5.2)$$

Focusing on the analytical definition of the derivative of a function f , being $f : U(x_0) \subset \mathbb{R} \rightarrow \mathbb{R}$ be a real valued function defined in an open neighborhood of a real number $x_0 \in \mathbb{R}$. The derivative of the function f at the point x_0 is equal to the limit (if it exists):

$$f'(x_0) = \lim_{x \rightarrow x_0} \frac{f(x) - f(x_0)}{x - x_0} = \lim_{\Delta x \rightarrow 0} \frac{f(x_0 + \Delta x) - f(x_0)}{\Delta x} = \lim_{\Delta x \rightarrow 0} \frac{\Delta f(x)}{\Delta x} \quad (5.3)$$

Since the power flow equations P_i and Q_i present an implicit relation in terms of voltage magnitudes and angles, $P = f_1(|V|, \theta)$ and $Q = f_2(|V|, \theta)$, the derivation process becomes complex. For the aim of this study, the partial derivatives are approximated by finite differences to build the sensitivity matrices $\partial V/\partial P$ and $\partial V/\partial Q$:

$$\frac{\partial V_i}{\partial P_j} \approx \frac{\Delta V_i}{\Delta P_j}, \quad \frac{\partial V_i}{\partial Q_j} \approx \frac{\Delta V_i}{\Delta Q_j} \quad (5.4)$$

In the same way and considering the loadings L of the network branches, it has been assumed:

$$\frac{\partial L_i}{\partial P_j} \approx \frac{\Delta L_i}{\Delta P_j}, \quad \frac{\partial L_i}{\partial Q_j} \approx \frac{\Delta L_i}{\Delta Q_j} \quad (5.5)$$

The sensitivity coefficients will depend on the characteristics of the loads and lines and they will represent the changes in either voltages, reactive power flows or line losses, both locally and remotely. For each of the six case studies proposed, the sensitivity matrices $\frac{\Delta V}{\Delta P}$, $\frac{\Delta V}{\Delta Q}$, $\frac{\Delta L}{\Delta P}$ and $\frac{\Delta L}{\Delta Q}$ were obtained. The value of ΔP and ΔQ for building the sensitivity matrices was selected in order to be

sufficiently small but large enough to notice the variation of node voltages and branch loadings due to the injections of active and reactive power. After carrying out different practical experiments, it was decided that:

- For the voltage sensitivity coefficients: $\Delta P = 10^{-5}$ and $\Delta Q = 10^{-5}$.
- For the loading sensitivity coefficients: $\Delta P = 10^{-3}$ and $\Delta Q = 10^{-3}$.

From the voltage control point of view, the most relevant sensitivity matrix is $\partial V/\partial Q$, whose coefficients for a given column represent the voltage variation contribution at each bus with respect to the injection into the bus linked to the specific column. The sensitivity coefficients $\partial V_i/\partial Q_j$ were compared with the $\partial V_i/\partial P_j$ ones and it was found that the variations of reactive power influences up to 10 times more the voltages of the corresponding network nodes. Therefore, the analysis of the voltage variations along the network will focus on the results of the sensitivity matrix $\partial V/\partial Q$. In the same way, the loadings of the network branches are more influenced by the active power flows through the lines. Therefore, the focus on the load rate variation at every network branch will focus on the sensitivity matrix $\partial L/\partial P$.

In order to obtain insightful conclusions about the influence of the different parameters in the network operation conditions, the active and reactive power variations ΔP and ΔQ were applied only at the loads with demand response (13 out of 47). The aim of this analysis is to identify the loads that mostly compromise the voltage stability in the network and have more potential for creating congestion problems in specific lines. In this way, the loads that present higher sensitivity coefficients would require a demand response program with more urgency in order to prevent their power variations and to decrease their influence in the network nodes and loadings.

The analysis of the weight of every load in the voltages and loadings variations was carried out with the calculation of a relative sensitivity factor. Considering that, for the $\partial V/\partial Q$ sensitivity matrix, each row represents a network node and each column shows a load with demand response, each sensitivity coefficient $\partial V_i/\partial Q_j$ has been divided by the total sum of the coefficients of each row in order to find the contribution of each load to the voltage variation of the node. The value is multiplied by 100 to express these relative sensitivity factors as percentages (%). In the same way, each row of the sensitivity matrix $\partial L/\partial P$ represents a network branch and each column pictures a controllable load. Therefore, the relative sensitivity factor for the network loadings was obtained by dividing every sensitivity coefficient $\partial L_i/\partial P_j$ of each row by the total sum of all the coefficients of the row.

The results of these relative sensitivity factors are graphically shown in Figure 5.5 and Figure 5.6. Figure 5.5 represents the influence of each load in the variation of the voltage nodes, while Figure 5.6 represents the influence of each load in the variation of the loadings of the different branches. The analysis focuses on the results obtained for the base line case in summer, since similar conclusions were obtained from each case study in terms of voltages and loadings sensitivities.

First, the relative voltage sensitivity factors obtained for each load is analysed in Figure 5.5, which shows the weight of the sensitivities obtained in the matrix $\Delta V/\Delta Q$. It can be noticed that, among the demand response loads considered, reactive power changes from the loads 9 to 13 highly influence the voltage values along the network. In particular, load 9 presents sensitivity factors that reach 85%, while the rest of the loads make up the pending 15% for the same node. As expected, the node that experiences the highest sensitivity to reactive power changes is node 101, to which load 9 is connected. Not only is the magnitude of the factor crucial, but also the number of times voltage sensitivity peaks that can be found for the same load. Only one noticeable peak can be found for loads 1, 7 and 8, while two peaks are observed for loads 9 to 13, hence highly influencing two nodes under minimum variations of reactive power. Looking at the magnitude and location of these fac-

tors, especially loads 9, 10 and 11 turn out to be the most critical ones among the demand response loads. This analysis would serve as a first indication of the network loads that would require a demand response agreement with more urgency. On the other hand, loads 2 to 5 show low voltage sensitivities under reactive power changes from all the selected loads and do not present the need to be controllable from the point of view of voltage regulation.

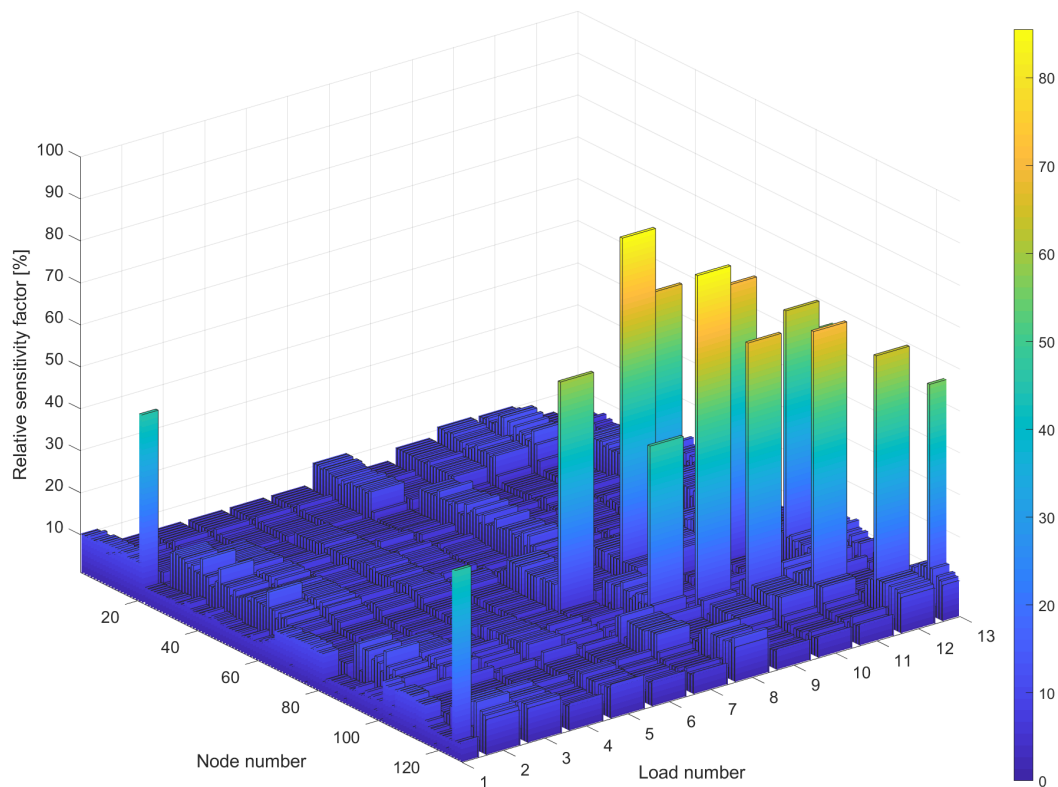


Figure 5.5: Relative voltage sensitivity factors for each load with respect to the network nodes

Opposite to the localized influence in the voltage variations along the network, the relative loading sensitivity factors shown in Figure 5.6 do not follow a visible trend. These factors represent the results obtained for the sensitivity matrix $\Delta L/\Delta P$, which measure the influence of the active power changes of the demand response loads in the load rates of the network branches.

Although it is not clearly seen in the graph, the maximum value occurs for load 1 for branch. This cable is located at the end of the feeder, where congestion issues are more likely to turn up. On the other hand, all loads present high loading sensitivity factors for several branches except loads 3, 4 and 5. The amount of branches that are being affected per node can be easily identified in Figure D.3, in section D.1 of the Appendix. In general, loads 2 and 7 present a higher number of branches with relatively high sensitivity factors, while 8 to 13 present isolated high peaks for specific branches. Moreover, most of the loading sensitivity peaks displayed in Figure 5.6 present a value close to 100%, meaning that changes of the active power of most of the loads have a direct effect on the loadings of specific branches.

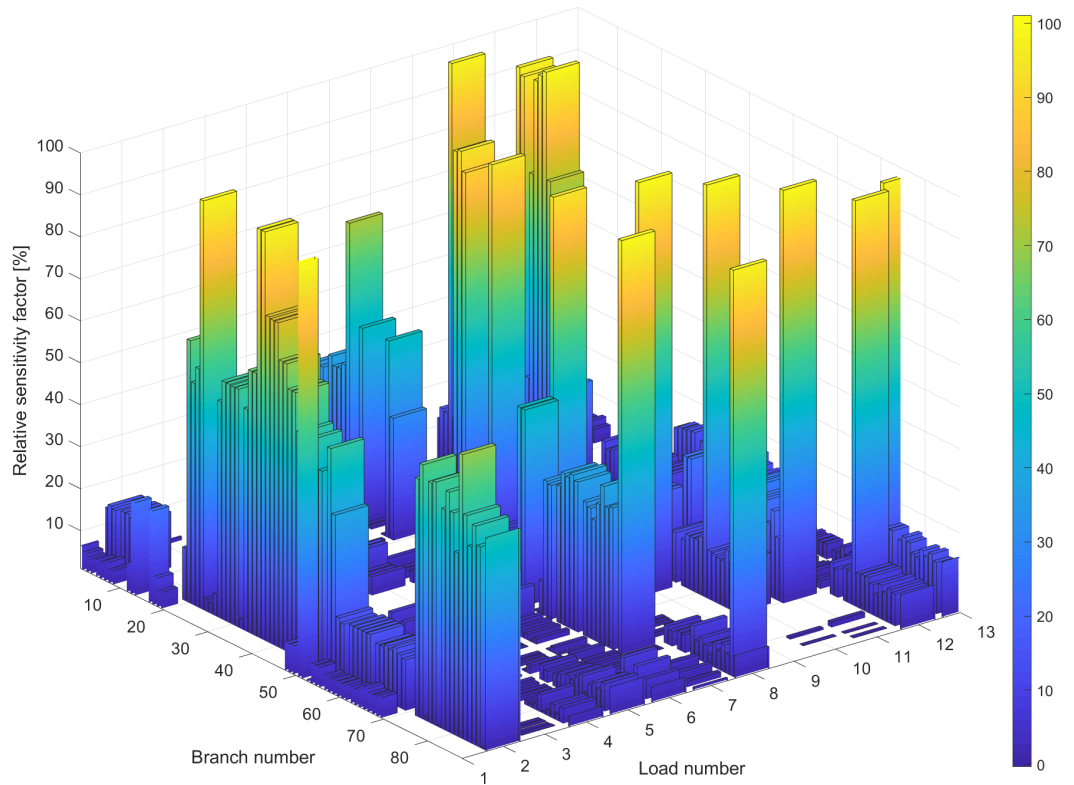


Figure 5.6: Relative loading sensitivity factors for each load with respect to the network branches

In this case, the combination of the sensitivity matrices $\partial V/\partial Q$ and $\partial L/\partial P$ can bring insightful conclusions about the needs of flexible demand in a network. The changes of both active and reactive power of the load will influence the node voltage profiles and branches, respectively. Under demand peak situations, demand response would allow to control the active and reactive of the loads that include this type of local flexibility, reducing the risk of excessive voltage deviations and possible congestion issues along the network. By this type of sensitivity analysis, a ranking of the most critical loads for the reliable network operation could be performed by the DSO in order to detect the locations that require the control of certain network variables.

After having carried out the sensitivity analysis for the variables of interest, the next section presents the impact of the considered flexibility sources on the base line case. Afterwards, the performance of these sources will be compared for the under-scaled and over-scaled case studies, which include lower and higher demand requirement in the test network, respectively.

5.3. Base line scenario

A more detailed analysis of the integration of flexibility sources is presented for the base line case, focusing on the summer PV generation conditions. Then, the main representative differences found under different levels of demand and generation will be highlighted in order to detect the operating limits of a standard distribution network.

The voltage profiles resulting from this case study without flexibility integration was already presented in Chapter 3 (Figure 3.22). For a more insightful understanding of the voltage behavior along the network, the MV and LV levels have been represented separately in Figure 5.7 and Figure 5.8, respectively. The corresponding voltage limits for each level are also defined: between 0.95 and 1.05 p.u. for MV and between 0.9 and 1.06 p.u. for LV. These limits are defined in Vision and are the ones considered by their clients, DSOs among them, for detecting voltage deviations along the network.

Moreover, only the upper and lower voltage profiles are illustrated in order to easily identify the extreme voltage values every hour of the day. The rest of the corresponding MV and LV profiles are included within these extreme profiles. The complete voltage profiles for the network nodes can be found in Figure D.4 and Figure D.5 of the Appendix.

For the base line conditions of demand and generation defined for the test network, undervoltages appear for both MV and LV levels. These undervoltage peaks correspond to the electricity consumption peaks in the morning and evening, at 8-10 am and 18-20 pm. It can be observed that the morning demand peak is the most critical one, since the voltage deviations are the highest at 9 am. Particularly, the LV profiles present more variability during the day, with overvoltages present in the first hours, from 1 to 4 am. In general, the changes in demand along the network will be better observed in the changes that LV profiles experience since the test distribution network is mostly residential.

Finally, the voltage differences considering summer and winter PV generation conditions are also presented. The difference can only be noticed in the LV profiles, where most of the distributed PV generators are located. Due to the decrease of solar power generation in winter, the net demand of the network increases, leading to lower voltages than in the case of the selected summer day. These differences are only noticeable during daytime, from 9 to 19h in the case of a representative winter day.

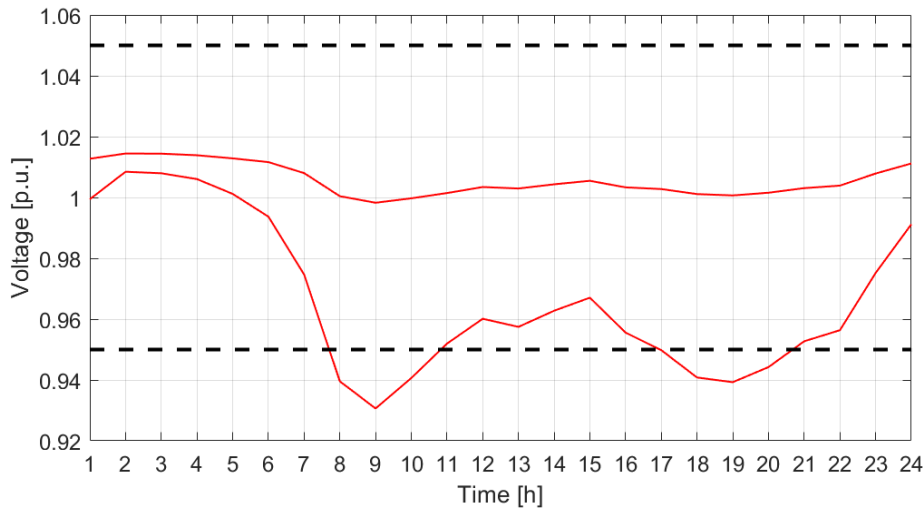


Figure 5.7: Medium-voltage profiles extremes

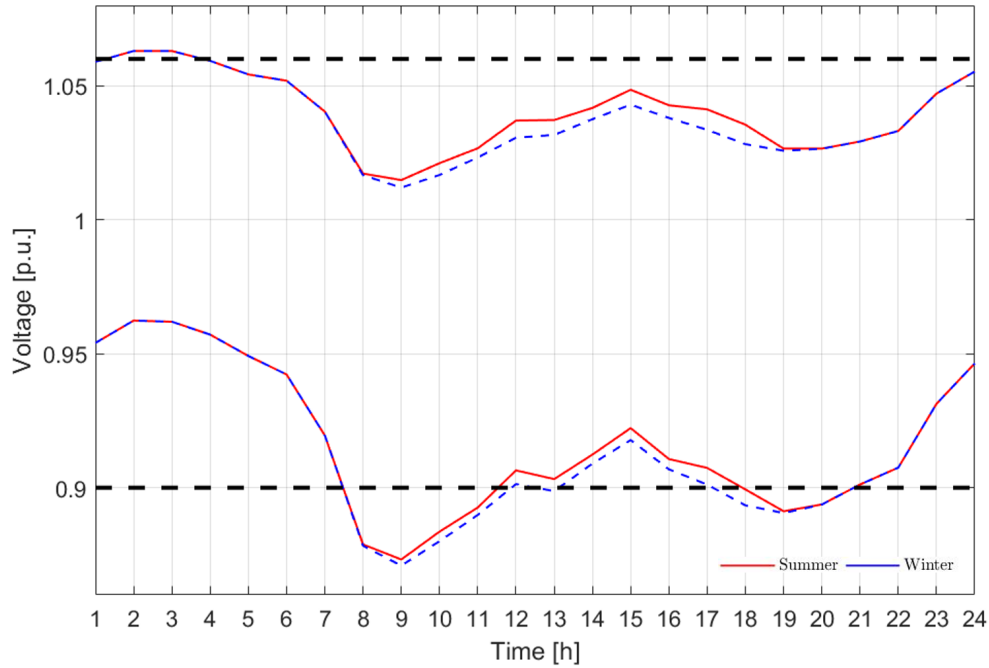


Figure 5.8: Low-voltage profiles extremes for summer and winter

5.3.1. Impact of flexible generation

In the previous subsection, the voltage profiles in the base line case were presented without any source of flexibility. Under these conditions, the impact of the integration of flexible generation is analysed by means of the addition of a droop control (presented in Chapter 4) in the distributed PV generators. This control acts only if the voltage set point at that node and that hour is outside the allowed range. Moreover, since the maximum and minimum amount of reactive power that the PV inverter can inject or absorb is defined as a percentage of the maximum active power that the generator can provide at that time, the impact of the control will be higher during the periods of the day with higher PV generation, that is, around midday.

Since the global effect of droop control performed by the distributed generators is not noticeable, the local effect on a single node is analysed. Figure 5.9 shows the maximum voltage regulation performed by the control in a summer day, while Figure 5.10 shows its maximum effect in a winter day. Since the control only acts when the PV panels are generating solar energy, a closer view of the corresponding daily hours for summer and winter is presented for each case. In general, the voltage change carried out by droop control is in the order of 10^{-3} p.u. Particularly, the maximum net regulation during summer is 0.016 p.u., and 0.012 p.u. during winter. In both cases, the maximum regulation occurs when the solar generation is at its peak, around 13h.

This local effect is inappreciable network-wide and, although undervoltage values in the base line case present a slight improvement after the control, these voltages are still not within the desired range. This is especially due to the influence of the generation profile and the limitations that PV inverters present for providing reactive power.

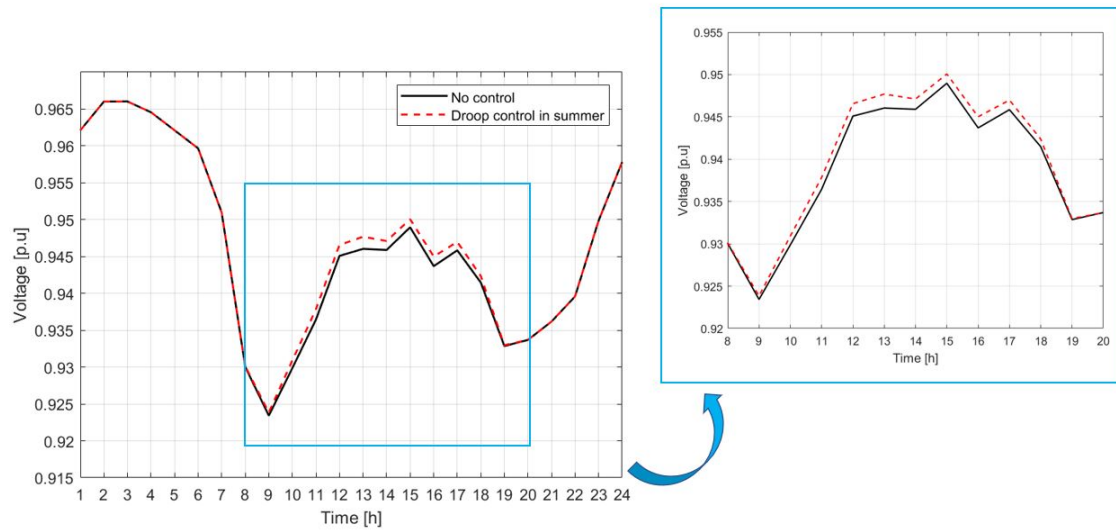


Figure 5.9: Maximum droop control effect on the voltage profiles in summer

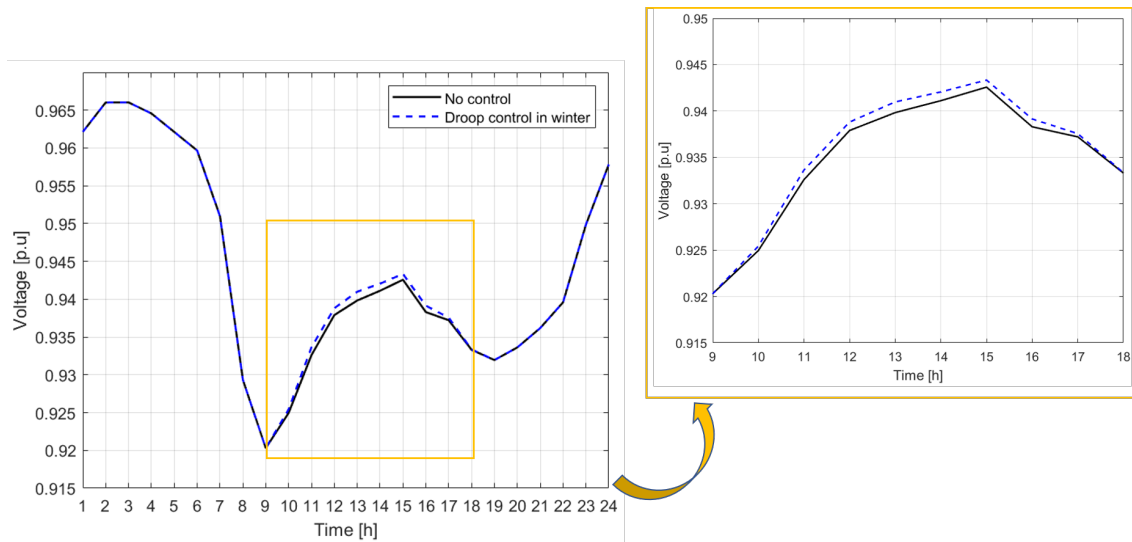


Figure 5.10: Maximum droop control effect on the voltage profiles in winter

In order to implement a suitable decentralized control in networks with different features, a sensitivity analysis should be carried out in order to define the different variables of the control. Figure D.7 (Appendix) shows how the voltage profiles change with different values of the droop characteristic k , present in the droop control formulation (Equation 4.1). In general, this slope has a low value for distributed generators and can vary between 0 and 5 for small-scale installations [42]. As shown in Equation 4.1, it is when the value of k is the lowest that the biggest voltage change occurs. For values bigger than 1, the control is practically not noticeable.

It is important to highlight that these control methods cannot consider changes in the network due to rapid modifications in the output power of renewable energy sources. Moreover, the control function adapts the voltage of the individual distributed generators, instead of through the interaction with other DGs or other points of the system [31].

5.3.2. Impact of flexible demand

This subsection analyses the effect of demand response in the selected loads of the network (13 out of 47), without having flexible generators. The impact of the integration of flexible loads will be directly related to their capability when variations in the voltage profiles throughout the day are involved, as well as to the limit of the variable range of active power set in the control. For the non-flexible network, it could be noticed that undervoltage values during periods of peaks in demand were the main issue that needed to be tackled. The presented demand response control directly influences the demand levels at the most critical hours of the day, which is also visible in the voltage results after the control action. Figure 5.11 and Figure 5.12 represent the network voltage profiles at the medium- and low-voltage levels (in summer) adding the comparison of the extreme voltage profiles after the action of the demand response control.

The most noticeable effect occurs for the medium-voltage nodes, which present all the voltage profiles within the admissible limits in comparison with the non-flexible MV network. For this purpose, the control has decreased P and Q at the nodes that presented undervoltage in order to bring back the voltage profiles within the allowed range. For the lower voltage profile shown in Figure 5.11, demand response has increased the voltage value from 0.875 to 0.9 at 9 am. This node does not present a flexible load but it is influenced by the control actions in the surrounding nodes. Focusing on the morning demand peak at 9 am, demand response has decreased the value of active power by a maximum of 50%, as set in the control. However, only 5 loads out of 13 decrease the power of the load until that threshold. The rest of the loads only curtail part of the power, until the voltage value of the node at that hour is within the allowed range.

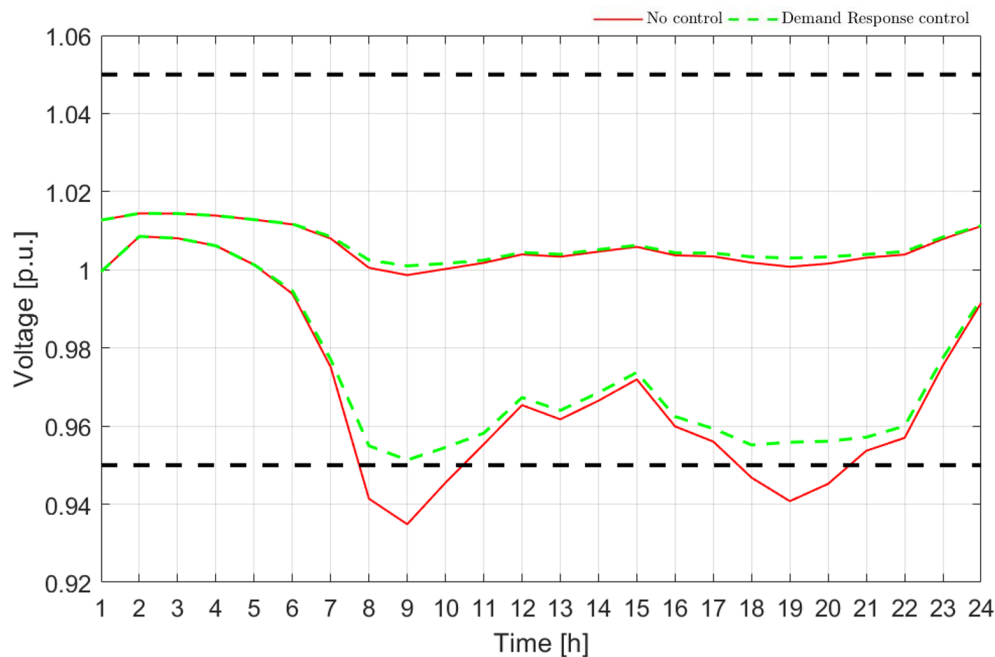


Figure 5.11: Effect of the demand response control on the medium-voltage profiles

On the other hand, the voltage values at the nodes located at the low-voltage level also show an improvement with respect to the base case, but the ideal network state is still not reached. Figure 5.12 illustrates how the time period between 8 a.m and 11 a.m presents voltage values below the defined limit despite the action of the control. In this case, the voltage values cannot be improved further

since the values of P and Q during this period have already decreased until the 50% of their nominal values in the non-flexible base case.

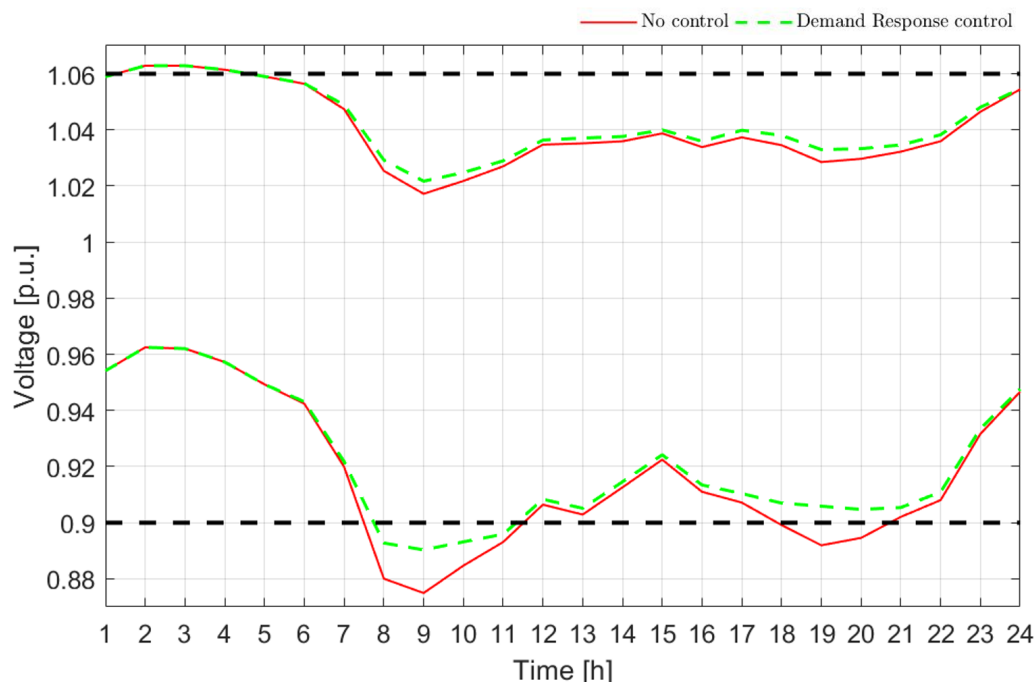


Figure 5.12: Effect of demand response control on the low-voltage profiles

The presented demand response control considers the regulation of both active and reactive power for voltage regulation. When the topic of flexibility is addressed, especially in the residential sector, it is often assumed that only the active power is shifted from demand peaks to other periods with better operational and economical conditions. This flexible demand represents the real power variation for which the customers would need to change their consumption behaviour under these agreements. Moreover, the value of lost load (VLL) is usually expensive and needs to be covered by the DSO or the different stakeholders involved in the contract. In this way, this shifted power represents both the investment needed by the system operator and the financial incentives for the consumers. The voltage profile comparison between the P-Q control and only P control can be observed in the Appendix (Figure D.8). It can be noticed how the addition of reactive power in the control leads to better voltage results. In the case of flexible residential loads, the value of active power approximately doubles the defined reactive power. This is why the control of P alone also leads to sufficient voltage control.

5.3.3. Impact of the combined flexible generation and demand

As analysed during this section, the controls applied to flexible generation and flexible demand yield positive results in terms of voltage regulation when they are integrated separately. In order to notice the impact of the combination of both in the network, its local effect at two different buses is shown in Figure 5.13. Specifically, Figure 5.13a represents a node that includes flexible generation while Figure 5.13b represents a node with a flexible load.

The main conclusion that can be drawn is that this combined control leads to a better voltage regulation in every case, no matter if a flexible load or PV element is connected to the analysed node.

However, one control will be more dominant depending on the time of the day and the network conditions. For example, it can be observed how droop control integrated in PV generators predominates over demand Response when solar generation is at its peak (Figure 5.13a) since the node is directly influenced by this type of voltage regulation. On the other hand, Figure 5.13a presents better results for the demand response control throughout the day since a flexible load is connected. In all cases, droop control will provide a slight improvement in the voltage set point with enough solar generation, since the value of Q will be accordingly modified each hour. Demand response will always offer a noticeable voltage regulation during demand peaks. In conclusion, the impact of each control on the network voltages will depend on the proximity of the controls to the selected nodes, as well as the specific conditions such as renewable energy generation and amount of demand that must be met.

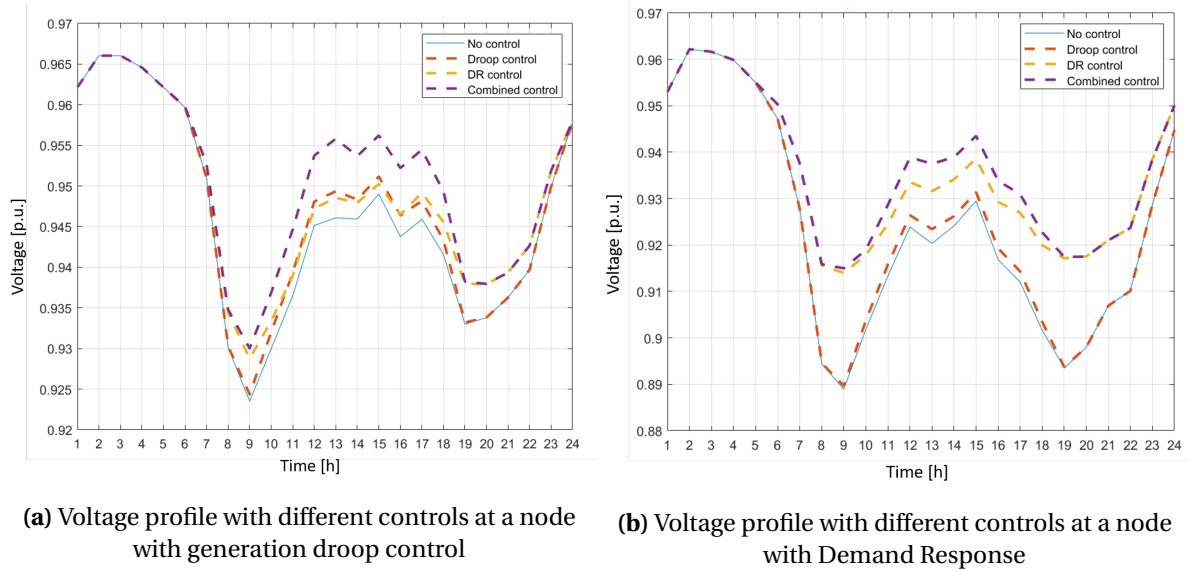


Figure 5.13: Effect of droop control, demand response and the combination of both on the voltage profiles

5.3.4. Integration of battery systems

In the previous subsections, droop control and demand response have been investigated as potential flexibility controls in the generation and demand sides, respectively. The biggest regulation of the voltage profile occurs with the combined control of flexible generators and loads, but still some voltage peaks violate the set limits. In this context and with the aim of having a full control for voltage stability, energy storage is proposed as a potential flexibility source in distribution grids.

Figure 5.12 above showed that demand response cannot correct the overvoltages present in the first hours of the day and the undervoltages in the morning demand peak, from 8 a.m. to 11 a.m. These will be the critical periods in which batteries will need to be able to charge and discharge the required energy for regulating the pointed voltage profiles. For this analysis, the voltage profiles regulated by the combined control of flexible generation and demand are taken as an input for the storage assessment. Since the effect of droop control by the PV generators is not noticeable, the profiles are practically the same as the ones obtained after the action of demand response. All the network voltage profiles after the combined control action are represented in Figure D.9 and Figure D.10 of the Appendix, for the MV and LV levels, respectively.

Following the control logic proposed in Chapter 4 for the integration of battery systems, Figure 5.14 shows the active power difference that needs to be covered by the batteries at the network nodes 'n' in order to respect the allowed voltage range. As expected, during the night (1 a.m. to 5 a.m.) the active power needs to be decreased in order mitigate the overvoltage values, while during the morning demand peak (8 a.m to 11 a.m) the power needs to be increased to remove undervoltages. This would be translated into battery systems connected to each presented node, which would absorb power during overvoltage periods and inject power to the grid when undervoltages are present.

Table 5.2 details the storage capacity that needs to be connected to each identified node. One aspect that stands out is the high capacity required at the nodes with overvoltage, when these voltage profiles showed that the limits are just slightly exceeded during the night. This is because of the mutual influence of the voltage profiles, since that period presents several nodes with voltages that exceed upper limit, while the batteries only act at one node. Hence, the active power that needs to be decreased at these two individual nodes with overvoltage will be higher in order present an impact on their separate voltage values. On the other hand, the undervoltage values present a higher peak below the limit, but they are quite isolated with respect to the other voltage profiles. This is why the battery capacity for these nodes represent more accurately the amount of active power to increase depending on the proximity to the set limit. As expected, node 94 needs a bigger capacity since it presents the highest voltage deviation of the network.

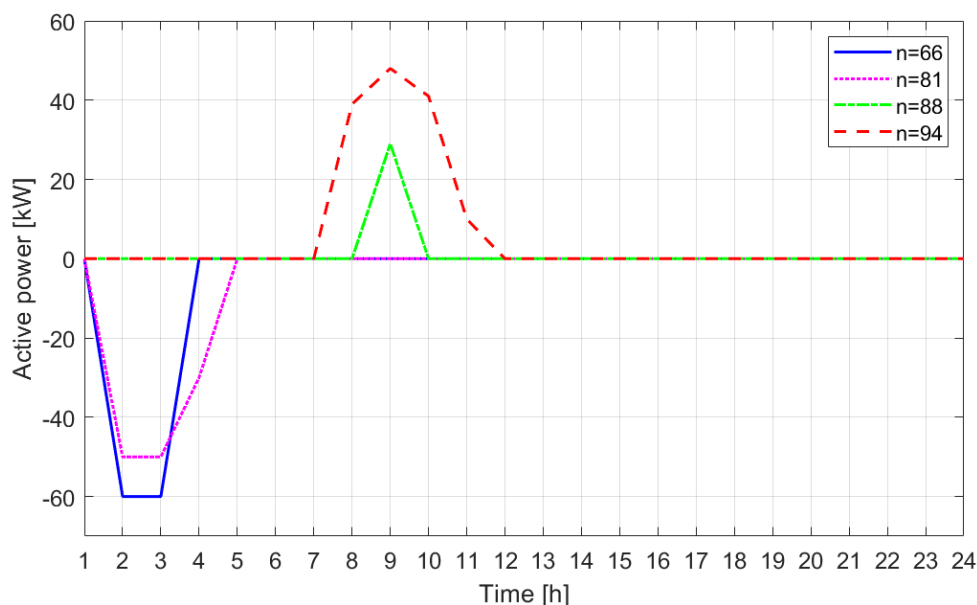


Figure 5.14: Active power surplus or deficit needed per node for keeping voltage values within the allowed limits

	Node	Battery capacity [kWh]
Overvoltage	66	150
	81	162
Undervoltage	88	36
	94	172

Table 5.2: Estimated battery capacity at each node with violation of the voltage constraints

The estimated capacity values are relatively high, considering its integration into the distribution grid. For instance, node 94 would require a battery with a capacity of 172 kWh, while the Tesla Powerwall, also used for residential or light-commercial services, presents a capacity of 13,5 kWh. However, it must be considered that the low-voltage loads that are being studied in this network are aggregated to the medium-voltage distribution grid and can represent several households and even a neighborhood or village. In this sense, the previous total capacities estimated for each node could be the parallel connection of several small batteries between different households.

Following the control logic presented in Chapter 4, the charging and discharging periods of the battery system are defined, as well as the conditions for their state of charge (SOC), which are added in the Appendix for this base line case. They are represented in Figure D.12 and Figure D.13 respectively. The final impact of the integration of short-term flexible battery storage systems on the network voltage profiles can be observed in Figure D.14 of the Appendix.

To conclude, it has been proved that the combination of flexibility sources applied to generation, demand and storage is able to keep the voltage profiles within the admissible voltage range in the distribution grid throughout the day. It must be pointed out that batteries are only correcting the low-voltage profiles since demand response was already able to regulate all the profiles properly at the medium-voltage level. The battery needs obtained for this base line case will be contrasted in the next subsection under the presence of different levels of demand and generation in the network.

5.3.5. Loadings of the network branches

Due to the changes of active and reactive power imposed on by flexibility controls, the load rates of the network branches could be affected in a negative way. This is why a final step in order to get a more fine-grained assessment of the performance of the different flexibility sources proposed is the analysis of the change of the load rates along the network branches.

Figure 5.15 shows the biggest load rate difference at one network branch throughout the day for the base line case, comparing the load rates results of the combined control with the separated controls of flexible demand and generation. The individual effect of droop control on the network loadings has been neglected since the difference ranges from 1% to 3%. The main conclusions from each control can be drawn from this graph: during the period of high demand in the base case, the effect of demand response is quite noticeable, while from 11 a.m. to 5 p.m. the combined control predominates since the effect of droop control is at its maximum. During this period, the injection of extra reactive power Q at a selected node decreases the voltage difference ΔU with the adjacent node, improving the active power transmission and releasing congestion. The total current through the line decreases, hence the power losses also decrease accordingly. In this way, integrating droop control in certain points of the network could be an advantage if these midday hours are expected to have peaks of demand, which would put the branches at risk of experiencing overloadings.

The highest congestion release is achieved after the action of demand response occurs, since the decrease in the loadings through the branches ranges from a small percentage to 30-40% for some nodes. This reduction is quite significant considering that the highest difference occurs during peaks of demand, which present higher risks of leading to congestion issues. These periods also correspond to undervoltage values, meaning that the necessary decrease of P and Q will be performed by the control in order to bring back the voltages closer to the nominal values. It must be taken into account that the demand response control applied is only related to the voltage results, but the regulation through P and Q will directly impact the load rates of the system. For instance, the branch illustrated Figure 5.15 presents load rates over 80% in the base line case: under unexpected

demand peaks, for example due to electric vehicles charging or lack of renewable energy generation, these load rates could be over 100% and become a threat for the well-functioning and maintenance of the different network elements.

In general, the loadings of all the network branches decreased after the action of the flexibility controls proposed, especially due to the power curtailment performed by demand response during the critical periods of high demand during the day. In this sense, the effects of power variations by means of flexibility sources could be beneficial when congested locations are expected or are closer to a 100%. In conclusion, a mix of flexibility sources in the network would be the best option in order to keep voltage stability and mitigate grid overloads, considering the specific characteristics and operational limits of the network under analysis.

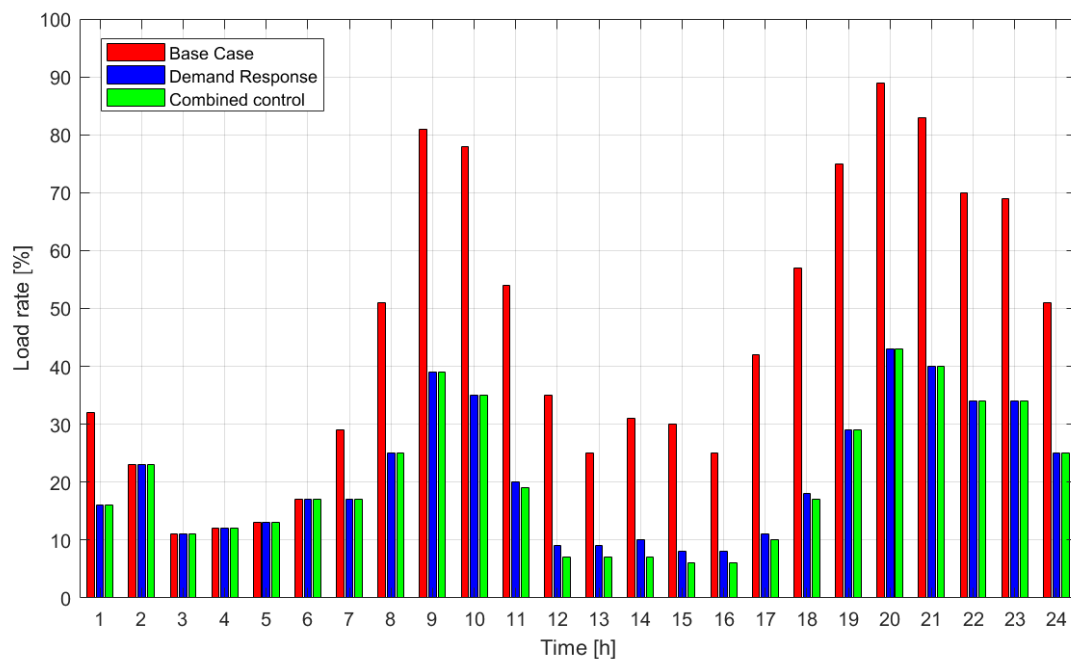


Figure 5.15: Maximum load rate decrease in the network with different flexibility controls applied

5.4. Comparison with the under-scaled and over-scaled scenarios

After the extended analysis of the base line case, the same flexibility assessment was performed in the presented under-scaled and over-scaled scenarios with the aim of identifying the main differences in terms of the regulation performed by the flexibility controls.

First, both extreme case studies were simulated without the integration of flexibility. As in the base line case, MV and LV profiles are represented separately in order to notice the critical time periods of the day and the magnitude of the voltage deviation for both voltage levels, considering the summer PV generation profile. To begin with, Figure 5.16 displays the upper and lower MV profile extremes for all the case studies proposed. On the other hand, Figure 5.17 illustrates the upper and lower LV profiles extremes for each case study.

In general, the lower demand levels present in the under-scaled case make all the medium- and low-voltage profiles (coloured in blue) remain within the allowed limits. It is that the demand is increased by a certain factor when the overvoltages and undervoltages start to appear during the lowest and highest consumption periods of the day. In the case of the already analysed base line case, the demand is 40% higher than in the under-scaled case study. Considering this increase, the peaks of demand in the morning and evening already impose undervoltages on the network. If the demand increases even more while keeping the same generation rates, the voltage profiles in the network experience a general severe decrease. The lower voltage profile extreme for both medium-voltage and low-voltage levels presents high voltage deviations beyond the allowed limit. The over-scaled scenario proposed creates more severe voltage stability problems in the MV level, where undervoltages are present since 8 a.m until the end of the day. In the case of LV profiles, the demand peaks are still visible although more emphasized and lasting longer. However, despite the demand increase due to additional electrification and the integration of EVs and HPs, overvoltages are still present during the first hours of the day. This is because the new types of loads included in the network present the highest electricity consumption during the daytime, contributing to the deepening of the undervoltage problems during these hours.

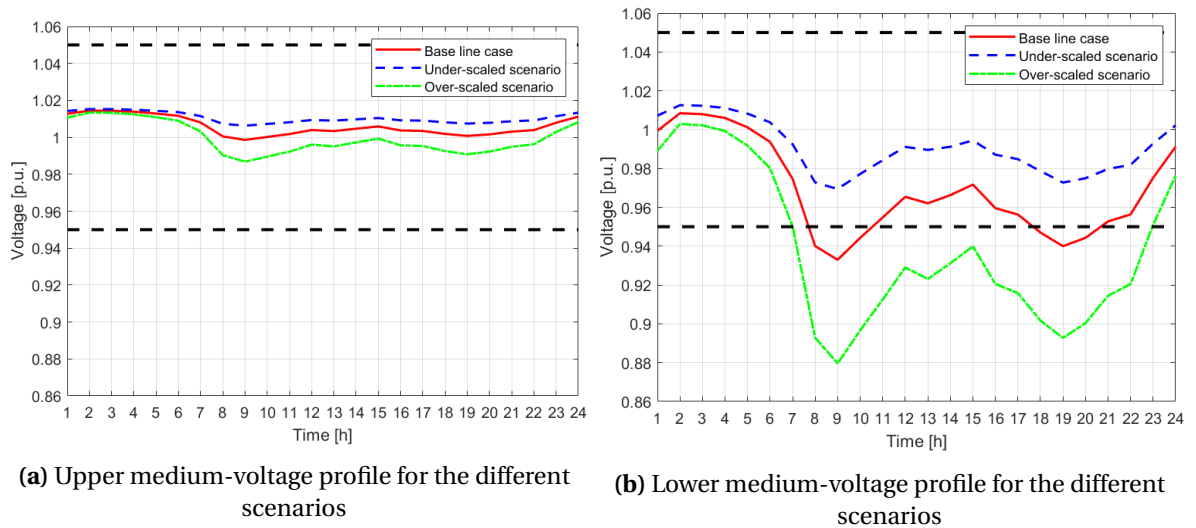


Figure 5.16: Comparison of the medium-voltage extreme profiles for the base line, under-scaled and over-scaled demand scenarios in summer

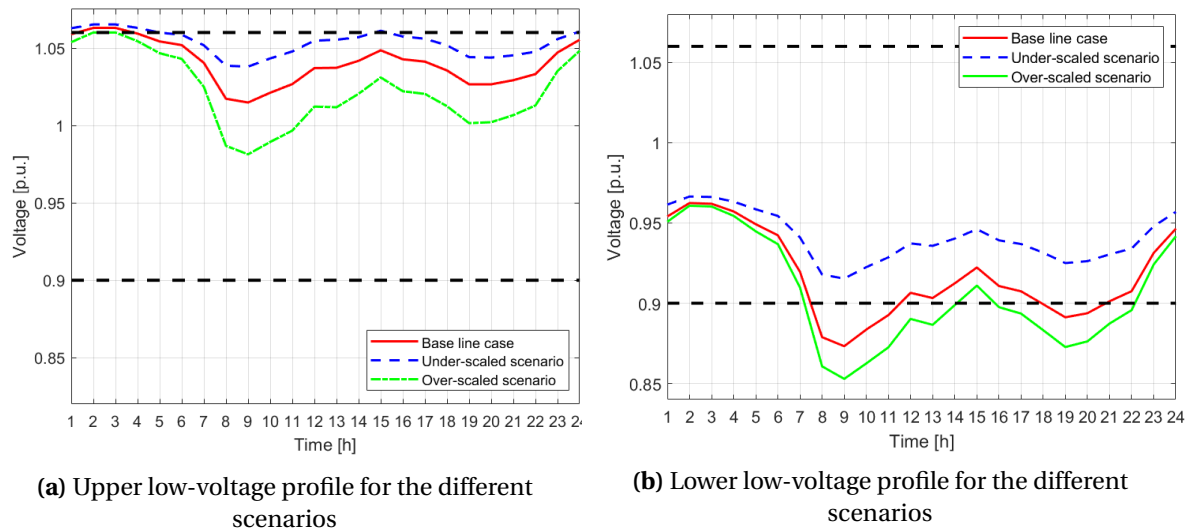


Figure 5.17: Comparison of the low-voltage extreme profiles for the baseline, under-scaled and over-scaled demand scenarios in summer

Considering the over-scaled case study, the voltage profiles present some differences if a summer or winter solar generation profile is simulated. Figure 5.18 illustrates the lower LV profile extreme for both daily generation profiles. The decrease of generation in the system also decreases the voltage profiles, but in this case the main factor of this voltage variation is the attributes of the seasonal demand. For the over-scaled scenario, the heat pumps present higher electricity consumption rates that influence the voltages to a larger extent. For instance, during winter there is no PV generation at 9 a.m, but the voltage profiles present some deviation due to the peak of consumption imposed by the heat pumps. However, the change is not highly noticeable network-wide since only a few loads present heat pumps or electric vehicles. Moreover, the final load addition of heat pumps represents a small percentage of the total additional electrification considered for 2030.

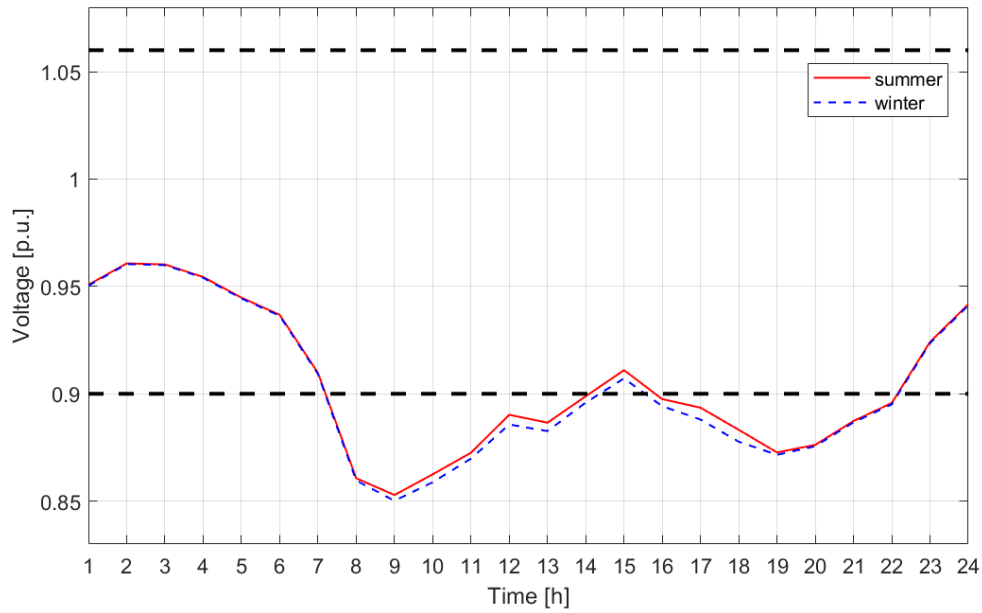


Figure 5.18: Voltage profile comparison with summer and winter PV generation conditions in the over-scaled scenario

Focusing on the impact of the flexibility sources, the combined control of flexible generation and demand is directly presented for the different case studies. Figure 5.19 represents the lower LV profile extreme for all the operational scenarios after the action of the combined control. As analysed for the base line case, the integration of flexibility regulates the undervoltage present in the evening peak, especially by means of power curtailment by demand response, and flattens the morning undervoltage peak. In the case of the under-scaled scenario, the control does not act since all the voltage profiles are already within the allowed range. Finally, the effect of the control on the over-scaled scenario is the most noticeable one.

In general, the control follows a similar pattern for the base line case study and the over-scaled one. The morning undervoltage peak is still present after the action of the control and it remains during more hours for the over-scaled scenario. This is due to the power curtailment limit imposed on the demand response control. In this way, with higher levels of demand in comparison with the base line case of the network, the control presents more limitations for regulating the voltage profiles. Taking as a reference hour 9 for the represented node, which experiences the highest voltage deviations, the control regulates the voltage until a value of 0.89 p.u. in the base line case, and 0.878 p.u. in the over-scaled case. However, the power has not been directly modified by the control, but the rest of the demand response loads influence this voltage value, getting it closer to the limits. Figure D.11 of the Appendix presents the same comparison after the effect of the combined control for the upper LV profile extreme.

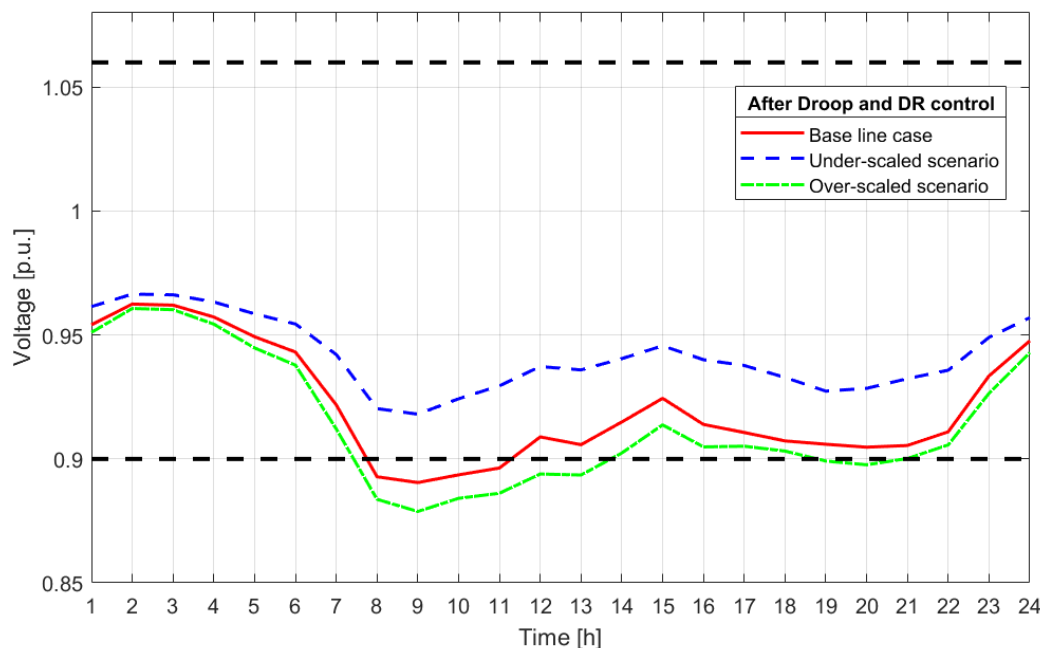


Figure 5.19: Lower LV profile extreme for all the scenarios after the action of the flexibility combined control

To conclude, the different rates of demand and generation in the network will directly influence the storage needs in the system. The storage capacity needed already presented in Table 5.2 showed the nodes that require a connected short-term flexible storage system in order to regulate the voltage profiles completely along the network. These results can be compared with the results obtained for the different case studies. The required storage locations and their respective capacities considering summer PV generation conditions for the different case studies are shown in Table 5.3. For winter generation conditions, the storage capacity required is shown in Table 5.4.

For this analysis, it is also assumed that the storage systems are applied after the effect of flexible generation and demand. The voltage results obtained for each case study after the control can be related to the storage needs stated in the tables. To begin with, overvoltages were found during the first hours of the day for all the case studies, leading to the need to connect batteries to the selected nodes. Moreover, the magnitude of the battery capacities for regulating overvoltage values are even 4 times higher for the under-scaled scenario due to the low levels of demands set.

In the same way, the over-scaled case study leads to the need of more storage capacity to cover undervoltage issues in several nodes. The higher the demand rates, the higher the capacity of the storage systems needed. In this case, the differences between the storage capacity needed in summer and winter also yield interesting results. The under-scaled case keeps the same capacity values since it only presents overvoltages during the night, when PV generation is not being produced. For the other two operational cases, the voltage decrease created by the lack of PV generation in winter increases the needs of storage capacity for the same nodes. The differences between summer and winter are highly noticeable for the over-scaled case, which presents a high increase of the needed capacity at each node.

These results represent the ideal storage capacities for achieving a complete voltage regulation in the operation conditions proposed. However, the connection of a battery system to a single node

with a capacity over 200 kWh would be too expensive and demanding from the technical point of view. Moreover, the space available for the installation of battery systems is limited in the Netherlands. In this context, short-term storage systems could be connected to the most critical nodes to cover unexpected voltage deviations created by peaks of demand. For both summer and winter, nodes 66, 88, 91 and 94 present a potential for the integration of batteries since they require additional flexibility actions in every operation situation.

	Node	Under-scaled case	Base line case	Over-scaled case
		Capacity [kWh]	Capacity [kWh]	Capacity [kWh]
Overvoltage	66	450	150	112,5
	67	250	-	-
	81	400	162	87,5
	85	125	-	-
Undervoltage	84	-	-	13,8
	86	-	-	3,8
	88	-	36	743,8
	91	-	-	407,5
	94	-	172	498,8

Table 5.3: Estimated battery capacity for voltage stability for the different case studies in summer

	Node	Under-scaled case	Base line case	Over-scaled case
		Capacity [kWh]	Capacity [kWh]	Capacity [kWh]
Overvoltage	66	450	150	100
	67	250	-	-
	81	400	162,5	75
	85	125	-	-
Undervoltage	84	-	-	106.3
	86	-	-	70
	88	-	98,8	998.8
	91	-	12,5	505
	94	-	197,5	492,5

Table 5.4: Estimated battery capacity for voltage stability for the different case studies in winter

This regional assessment for the test network developed shows that changes in load profiles will be considerably affected by the local adoption of PV distributed generators and new types of loads that contribute to higher demand rates, such as EVs and HPs. In this context, the distribution network loads are expected to become more volatile and load peaks could be more frequent in winter due to higher electrical heating and typically lower PV generation. DSOs will need to increase the flexibility levels of the distribution networks gradually in order to become more active in the coming years. Operational studies regarding voltage regulation and short-term congestion management should be performed in order to define the system flexibility needs and the available resources to meet this demand for flexibility.

6

Flexibility indicators

This research has shown that power systems will increasingly need flexibility in the coming years, mainly due to the integration of variable generation and changes in the demand patterns. Some of the consequences provoked by the presence of insufficient flexibility include the decrease of power reliability, damage of the system equipment, difficulties in increasing the presence of renewable energy sources or higher electricity prices [43]. In this context, system operators and regulators need to respond, requiring methods for making a quantitative operational flexibility assessment of the power system. The final goal will be to measure the level of flexibility required depending on the conditions of the system and the available resources. However, the transformation of the power systems and the emergence of the concept of operational flexibility lead to new challenges for the system operators. Firstly, assessing how much flexibility already exists in the system. Secondly, working out how much will be needed and at what time.

The previous chapter showed the results obtained after the integration of different flexibility controls in the test network, particularly in terms of voltages and branches loadings. As a final contribution of this research, this chapter proposes different short-term flexibility indicators that could be used by the system operator in order to determine the need and performance of different flexibility sources.

6.1. Flexibility metrics

The definition of the different flexibility indicators will depend mainly on the problems that are intended to be mitigated and the available network resources to carry this out. Firstly, it must be taken into account that these indicators would be directly related to the accessible data in Vision as well as the power flow results and flexibility simulations performed in Matpower.

Focusing on the main operational issues that can be detected in the network, the two investigated ones throughout this project have been voltage deviations and overloadings. On the other hand, the available resources that can be quantified and potentially fix these issues are active and reactive power, which were also regulated by the presented controls. These four aspects will be explored in the shape of different flexibility indicators and their value in the base line case will be compared before and after the combined flexibility control in order to obtain the desired conclusions about the network state.

Therefore, considering the accessible network input data and the power flow results obtained in the different simulations, four operational flexibility indicators have been proposed: the magnitude

of the voltage deviation, the presence of overloadings throughout the network, and the active and reactive power requirements for a complete voltage regulation at all the system nodes.

6.1.1. Voltage deviation

The deviation of the voltage profiles throughout the day and their regulation in order to be kept within the set limits have been the focus point of the different flexibility controls proposed. Therefore, an indicator that represents the severity of this deviation needs to be proposed as a measure of the network flexibility needs. In this context, Giménez [44] proposed several performance indexes for evaluating the dynamic security of a power system, among which the quasi-stationary voltage index (ICET) can be applied to this study. The calculation of this index is represented in Equation 6.1:

$$ICET = \min \left\{ 1, \max_{i=1..N} \left[\frac{|\Delta v_{i,pos}|}{|\Delta v_{i,max,adm}|} \right] \right\} \quad (6.1)$$

where:

$\Delta v_{i,pos}$ is the voltage variation with respect to the nominal value (V_N) at bus i .

$\Delta v_{i,max,adm}$ is the maximum allowable voltage deviation.

The voltage variation $\Delta v_{i,pos}$ can be directly obtained for each node and hour from the voltage results after the power flow calculations, the nominal voltage value for all nodes being $V_N=1$ p.u. On the other hand, $\Delta v_{i,max,adm}$ is represented by the fixed voltage limits that have been considered in the different controls. These values depend on the type of node (low-voltage or medium-voltage) and whether the deviation is over or below the nominal voltage. The maximum allowed voltage deviation that has been considered for the calculation of this indicator is shown in Table 6.1, as well as the set limits for the medium and low-voltage levels in the network.

	Voltage deviation limits [p.u.]		Maximum allowed voltage deviation [p.u.]	
	MV	LV	MV	LV
Overvoltage	1,05	1,06	0,05	0,06
Undervoltage	0,95	0,9	0,05	0,1

Table 6.1: Defined voltage limits and admissible voltage deviation ranges at medium and low-voltage levels

Following this logic, the voltage deviation indicators have been obtained for every node and every hour. However, the indicator limit has not been set at 1 as Equation 6.1 shows, since the severity of the deviation is necessary for comparing different network conditions in terms of voltage stability. Table 6.2 shows the maximum value of this voltage deviation indicator for each hour of the day. The hourly worst-case is extracted in order to detect the time periods with the risk of suffering voltage instability.

The non-flexible base line case is also compared with the results after the action of the combined control in order to evaluate the impact of flexibility on this particular indicator. Table 6.2 shows that the indicator is lower than the non-flexible case in practically all the hours due to the control regulation, and this decrease is more noticeable during the periods in which a violation of the voltage

limits occurs. These hours, coloured in red, present an indicator higher than 1 without flexibility. This would mean that at least the voltage of one node is not within the admissible voltage range, since the maximum indicator value for the whole network is considered for this analysis. As concluded in the previous chapter, the effect of the combined control regulates the voltage during the evening demand peak and only overvoltages in the first hours and undervoltages in the morning demand peak are still present. This voltage regulation can also be noticed in the table, since the value of the deviation decreases with the control and only these two time periods still present indicators higher than 1.

Hour	Voltage deviation indicator (base case)	Voltage deviation indicator (combined control)
1:00	0,982	0,982
2:00	1,050	1,050
3:00	1,050	1,050
4:00	1,024	1,024
5:00	0,983	0,984
6:00	0,940	0,942
7:00	0,801	0,816
8:00	1,200	1,071
9:00	1,302	1,091
10:00	1,153	1,074
11:00	1,069	1,017
12:00	0,936	0,882
13:00	0,971	0,911
14:00	0,874	0,824
15:00	0,828	0,909
16:00	0,908	0,858
17:00	0,928	0,873
18:00	1,064	0,913
19:00	1,184	0,967
20:00	1,096	0,953
21:00	0,979	0,946
22:00	0,919	0,890
23:00	0,785	0,813
24:00	0,922	0,925

Table 6.2: Worst-case voltage deviation indicator for each hour of the day in the base case and in the combined control scenario

However, the presented voltage deviation indicators do not show how many nodes have voltage problems during each hour. Figure 6.1 illustrates the voltage indicators for all nodes every hour for the base case. It can be observed that several nodes present a few voltage indicators greater than 1, or close to 1 during the same hour. This multiple violation of the voltage limits should also need to be considered when evaluating the general voltage deviation of the network. This could be added as a secondary voltage indicator which measures the severity of the deviation.

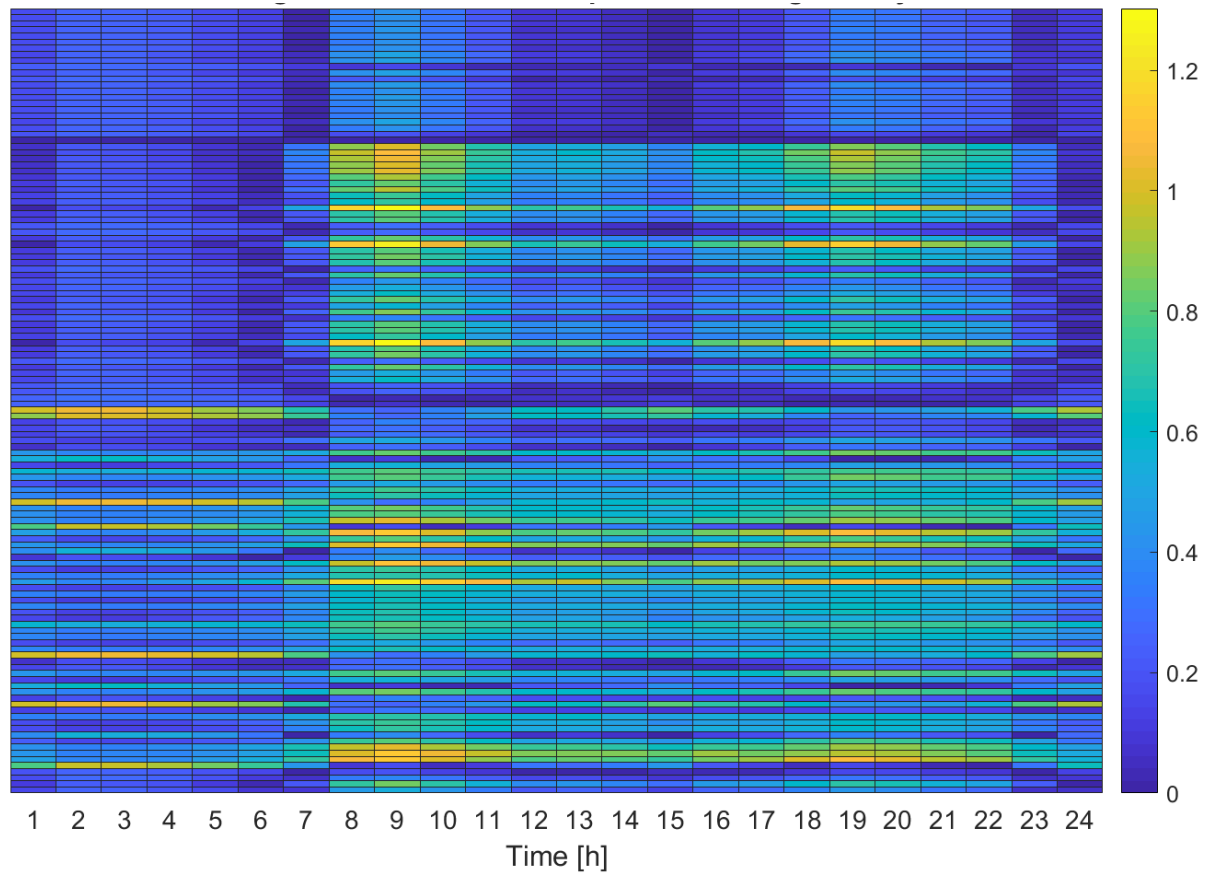


Figure 6.1: Heat map representing the magnitude of the voltage deviation for all the nodes and every hour of the day

6.1.2. Overloadings of the network elements

The second indicator that can evaluate the potential congestion issues refers to the overloadings present in the network. For this base line case study in particular, it was concluded that no overloadings occur throughout the different simulations, but the proximity to the 100% load rates can be stated as another interesting indicator to take into account.

In this way and similarly to the voltage deviation indicator, the obtained overloading indicator is presented in Table 6.3 as the worst-case result for each hour (greatest value) for the base case and the combined control scenario. In this case, the impact of the flexibility control is more noticeable during the morning and evening demand peaks, where the power decreased by demand response also decreases the load rates of the particular network branches.

Hour	Loading indicator (base case)	Loading indicator (combined control)
1:00	0,44	0,44
2:00	0,44	0,44
3:00	0,43	0,43
4:00	0,43	0,43
5:00	0,43	0,43
6:00	0,42	0,42
7:00	0,42	0,42
8:00	0,51	0,50
9:00	0,86	0,83
10:00	0,94	0,91
11:00	0,96	0,95
12:00	0,95	0,94
13:00	0,87	0,87
14:00	0,84	0,84
15:00	0,89	0,89
16:00	0,92	0,92
17:00	0,90	0,90
18:00	0,71	0,60
19:00	0,83	0,82
20:00	0,89	0,87
21:00	0,83	0,82
22:00	0,75	0,75
23:00	0,82	0,82
24:00	0,69	0,69

Table 6.3: Worst-case loading indicator for each hour of the day in the base case and in the combined control scenario

6.1.3. Reactive power requirements

Focusing now on the available network resources that might prevent the previous voltage and congestion problems, the regulation of reactive power performs a direct effect on the voltage profiles. Therefore, the quantification of the reactive power that needs to be decreased or increased by each node every hour would also inform about the network requirements throughout the day in order to obtain the desired voltage results. Figure 6.2 represents the amount of reactive power that needs to be increased or decreased each hour in order to bring the voltages within the allowed limits without changing the active power levels of the network. The higher need of reactive power is clearly distinguishable during the morning and evening demand peaks, although other nodes also present reactive power deficit almost all day.

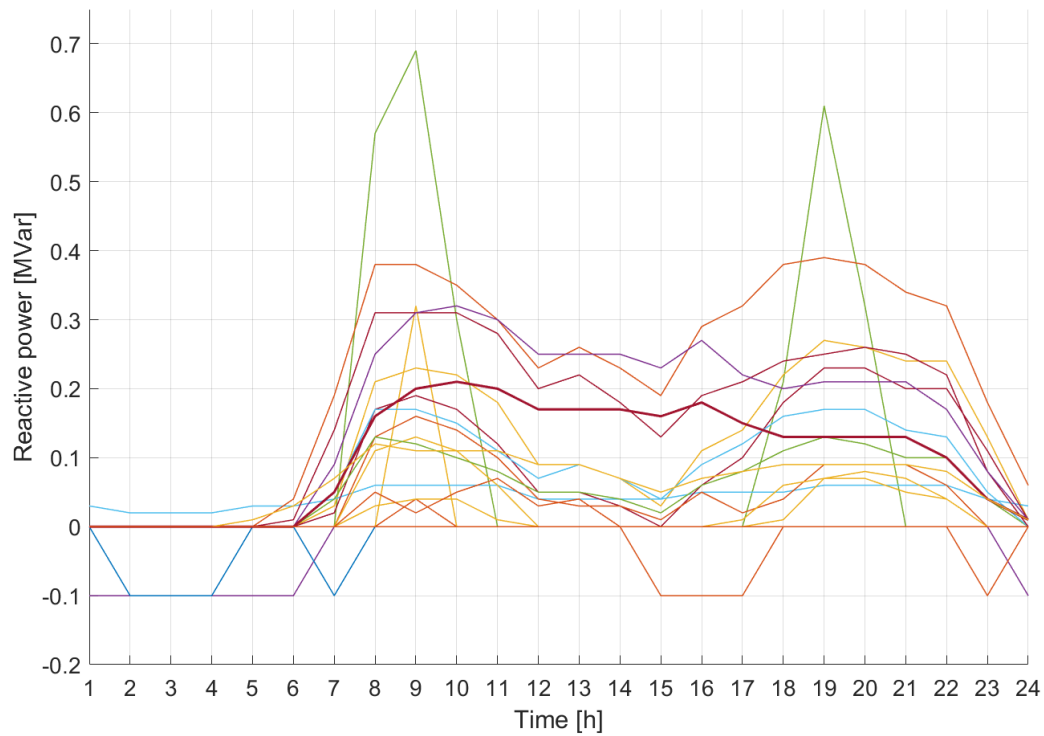


Figure 6.2: Amount of reactive power needed at the individual nodes throughout the day to respect voltage constraints in the base case

In order to have a network-wide overview of the reactive power needs for voltage stability, the comparison between the amount of available reactive power in the base case and the required value for each hour is presented in Figure 6.3. This comparison defines the reactive power indicator, calculated by dividing the extra reactive power needed each hour for keeping the voltages within the allowed range by the available amount for that hour. The indicator results represented in Table 6.4 show how the reactive power requirements are lower for the combined control scenario, especially during the demand peaks. This is because a reactive source is added by the droop control performed by the flexible generators, and demand response has already improved the voltage values by also decreasing the reactive power of the selected nodes. The worst-case indicator of each hour is represented in Table 6.4 as the maximum indicator among all the network nodes during that hour.

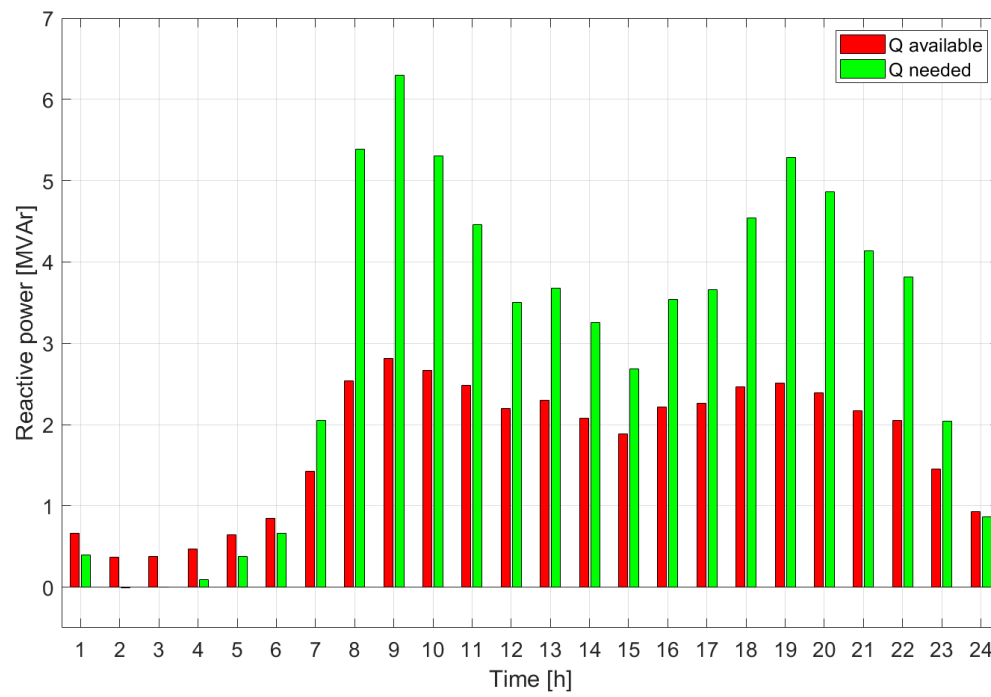


Figure 6.3: Comparison between the amount of reactive power needed each hour to respect voltage constraints and the available one in the network

Hour	Required Q indicator (base case)	Required Q indicator (combined control)
1:00	-0,405	-0,405
2:00	-1,022	-1,021
3:00	-0,998	-0,998
4:00	-0,811	-0,811
5:00	-0,405	-0,405
6:00	-0,224	-0,230
7:00	0,434	0,359
8:00	1,125	0,911
9:00	1,235	0,973
10:00	0,992	0,884
11:00	0,799	0,764
12:00	0,597	0,625
13:00	0,600	0,589
14:00	0,569	0,554
15:00	0,424	0,525
16:00	0,595	0,593
17:00	0,620	0,601
18:00	0,846	0,684
19:00	1,102	0,867
20:00	1,033	0,847
21:00	0,907	0,814
22:00	0,858	0,754
23:00	0,407	0,348
24:00	-0,065	-0,097

Table 6.4: Resulting reactive power indicator each hour in the base case and in the combined control scenario

6.1.4. Active power requirement

While reactive power directly affects voltage values, active power is directly related to the branches loadings. Therefore, it is presented as a flexibility resource with the potential of mitigating possible congestion periods. In a similar way to the reactive power indicator calculation, the voltage profiles are brought back within the limits by regulating the active power values of every node every hour and the amount needed for some particular nodes throughout the day in the base case is represented (Figure 6.4). As expected, a larger amount of active power needs to be decreased during the undervoltage periods and only extra P is required when overvoltage situations occur during the first hours of the day.

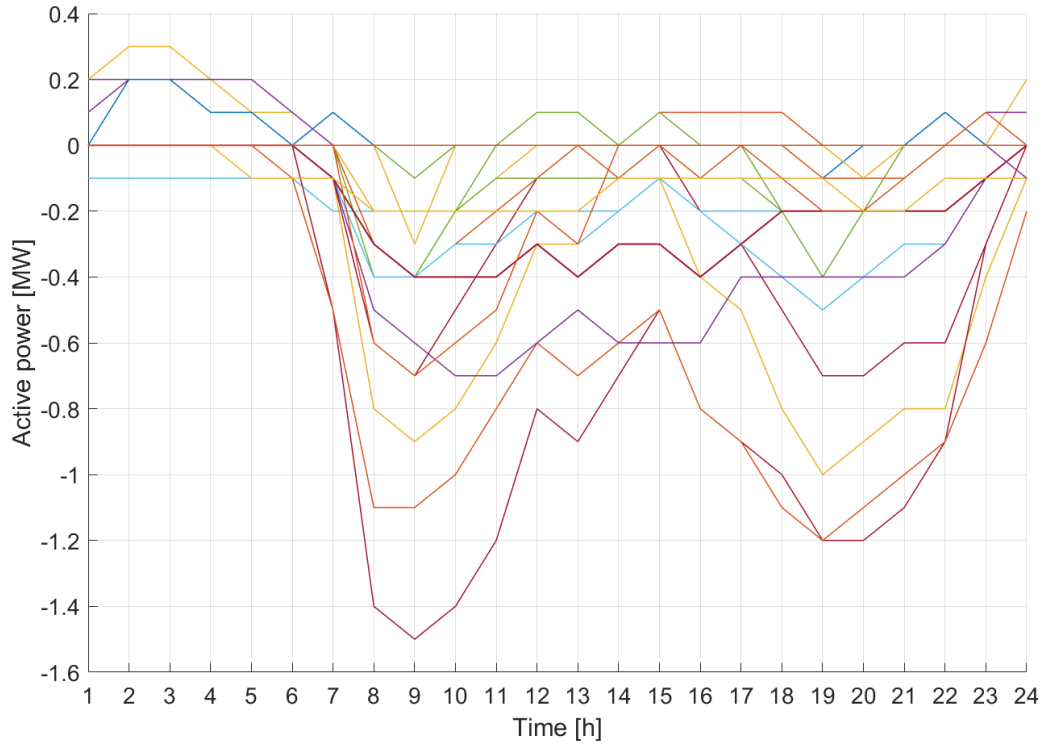


Figure 6.4: Amount of active power needed at the individual nodes throughout the day in the base case to respect voltage constraints

Finally, the total active power required each hour in the base case and after the action of the combined control is illustrated in Figure 6.5. In general, a large decrease is needed in order to keep the voltage and loading conditions. This fraction between the desirable amount of active power each hour and the available amount in the base case leads to the definition of the required active power indicator. Table 6.5 shows the maximum value for this indicator each hour of the day. In the same way as the reactive power indicators, this power change is smaller for the combined control scenario since demand response already curtailed the necessary active power during the critical time periods of the day.

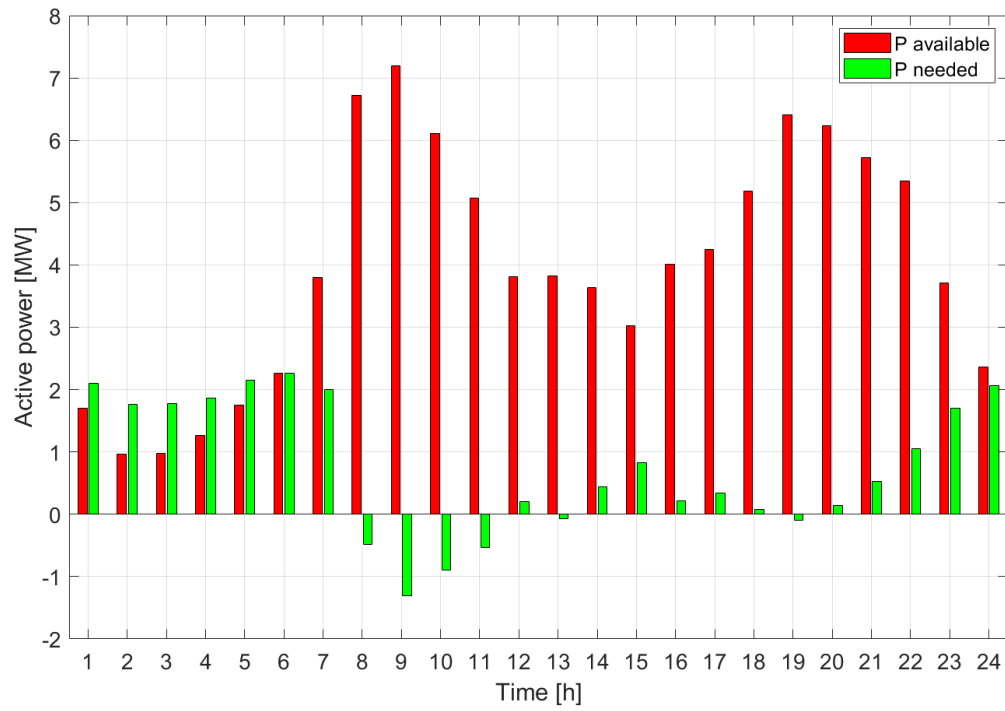


Figure 6.5: Comparison between the amount of active power needed each hour to respect voltage constraints and the available one in the network

Hour	Required P indicator (base case)	Required P indicator (combined control)
1:00	0,235	0,235
2:00	0,831	0,830
3:00	0,815	0,815
4:00	0,476	0,476
5:00	0,228	0,228
6:00	0,000	-0,019
7:00	-0,474	-0,426
8:00	-1,072	-0,908
9:00	-1,182	-1,000
10:00	-1,147	-0,940
11:00	-1,105	-0,860
12:00	-0,945	-0,660
13:00	-1,020	-0,667
14:00	-0,880	-0,549
15:00	-0,727	-0,505
16:00	-0,946	-0,667
17:00	-0,919	-0,642
18:00	-0,984	-0,783
19:00	-1,015	-0,871
20:00	-0,978	-0,837
21:00	-0,908	-0,812
22:00	-0,804	-0,732
23:00	-0,540	-0,491
24:00	-0,127	-0,109

Table 6.5: Resulting active power indicator each hour in the base case and in the combined control scenario

6.2. Conclusions for the case study

In this chapter, four different operational indicators have been proposed for the assessment of the network state in terms of voltage deviation and potential overloadings, and the required active and reactive power to mitigate these situations. Moreover, the non-flexible base case results have been compared with the scenario which includes flexible generators and demand response in order to evaluate the performance of the proposed flexibility controls.

The maximum indicators have been selected as the worst-case scenario for each hour in order to consider the extreme values during the day. These values for both network cases are represented in Table 6.6. On the other hand, a general indicator that shows an overview of the network state is also calculated as the average value of all the indicators of that particular hour. These average values can be observed in Table 6.7. Additionally, a graphical representation of these indicators results is provided in Figure 6.6.

In general, the indicators show lower values and, therefore, better results for the flexible network considering both the worst-case scenario and the average indicators for each hour. This especially the case of the active and reactive power required after the flexibility control, which decrease significantly compared to the base case, while the voltage profiles are also better regulated in the combined control, which is illustrated with a lower voltage deviation indicator. These indicators can

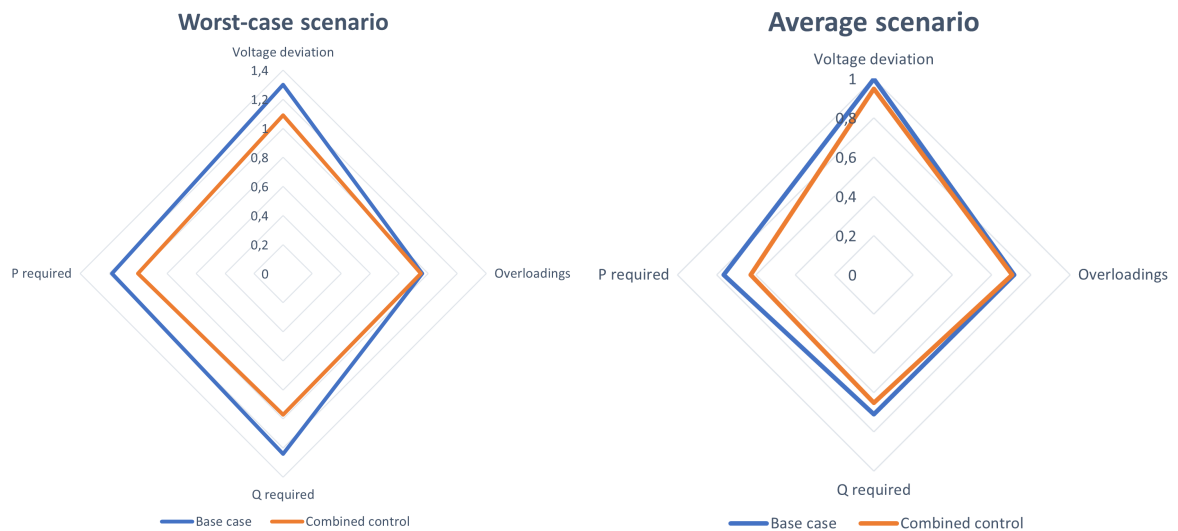
be applied to other network situations in order to follow a first approach of its operational performance, as well as for comparing different distribution networks and the urgency of the implementation of flexibility sources.

	Base case	Combined control
Voltage deviation	1,3	1,09
Overloadings	0,96	0,95
Q required	1,24	0,97
P required	1,18	1

Table 6.6: Indicator results for the worst-case scenario

	Base case	Combined control
Voltage deviation	0,998	0,948
Overloadings	0,715	0,705
Q required	0,711	0,652
P required	0,765	0,627

Table 6.7: Indicator results for the average scenario



(a) Radar chart comparing the worst-case indicators for the analysed case studies

(b) Radar chart comparing the average indicators for the analysed case studies

Figure 6.6: Flexibility indicators comparison between the base case and the combined control scenario, considering the daily worst-case and average indicator values

Conclusions and recommendations

The conclusions of the conducted study as well as some recommendations for future work are provided in this final chapter. The conclusions are presented by answering the two research questions that were proposed for this project, with the aim of achieving the main research objective proposed in this research. Section 7.1 presents the key research findings with regard to the research questions. Then, Section 7.2 proposes recommendations for future work.

7.1. Key research findings

In general, higher penetration rates of variable energy generation in the distribution grids, the emergence of prosumers or the addition of new types of loads such as heat pumps and electric vehicles impose operational challenges for the DSO in order to obtain the desirable real-time balance between production and demand. In this context, short-term flexibility has been pointed out as a potential solution to the fluctuations in demand and supply for the specific time horizon under analysis. For this purpose, traditional distribution grids should transform towards active distribution networks. This transformation would facilitate the control of the grid operation by the DSO. The general goal of this thesis has been to evaluate the performance of different flexibility sources and its short-term quantification in order to be assessed by the DSO in an active distribution network.

The research has focused on two main fields: Firstly, the development of a distribution test network based on Dutch standards for the subsequent power flow analysis and integration of flexibility controls. Secondly, the assessment of the performance of different flexibility resources in order to identify the operational challenges of the network under different demand and generation conditions. The results and conclusions obtained are used for the development of suitable short-term flexibility indicators, applied to the standard distribution network considered throughout this research.

These two sides of the research allow us to answer the research questions of this Master thesis:

1. How could a futuristic scenario of a Dutch distribution network be confidently modelled in an open-source tool for steady-state performance assessment of flexibility?

The first stage of this research was to model a typical Dutch distribution network for the subsequent simulation of flexibility controls under realistic scenarios. For this purpose, a real Dutch distribu-

tion network from the Netherlands was selected and adapted for this study. Since the test network was developed in the software *Vision Network Analysis*, used by energy companies and clients such as DSOs, an open-source tool also had to be developed for its application to subsequent research studies. Matpower was selected as a secondary tool for this analysis due to its similar procedure for performing steady-state power flow calculations and displaying the results.

Chapter 3 detailed the considerations and steps followed for the development of a Vision-Matpower converter in order to export the network data into the Matpower data matrix structure. With this converter, several distribution networks based on real data from the DSOs could be exported to a Matpower network file for performing additional simulations. Thus, the Matpower network file was used for the integration of flexibility sources into the network. Different controls were proposed in Chapter 4 for the simulation of flexibility actions from the supply, demand and storage sides, considering a complete day with 1-hour resolution. In the case of flexible distributed generation and demand response, a proportional droop control was applied with the aim of modifying the set values of active and reactive power and respond to voltage deviations along the network. Then, flexible storage was included in nodes that still presented high voltage deviations after the action of flexibility from the distributed generators and demand response. It was found that the mix of these flexibility sources, applied to the same active network in Matpower, can always bring voltage stability into different operating conditions. The main difference between the different cases will be the size of the storage capacity connected to the selected nodes.

2. What is a mathematical insightful method to assess flexibility from different sources in future Dutch distribution networks?

The need to better understand the impact of operational flexibility on the distribution networks and the requirements of more flexible resources lead to the necessity of quantifying their performance among different networks or scenarios. For this purpose, Chapter 5 applied the flexibility controls presented in Chapter 4 to the test network developed for this research. In order to detect the needs of flexibility in the network and its operational limits, three different levels of demand were included in the 24-hour load profile: an under-scaled scenario, a base line case scenario and an over-scaled demand scenario. Moreover, the influence of the presence of summer and winter PV generation conditions was also studied. In general, the base line case presented initial demand levels already set for the network, while the under-scaled case assumed a general 40% demand decrease throughout the day. Finally, the over-scaled scenario considers a demand increase, expected in 2030, with the addition of heat pumps and electric vehicles.

The impact of each flexibility control was assessed by looking at the variables changed, mainly active and reactive power, and its final effect by means of the regulation the hourly voltage values. For instance, it was shown that demand peaks lead to accentuated undervoltage periods that can only be solved by the combined action of demand response and the addition of storage systems, but with a 50% of the hourly total power set point drop in some cases, limit fixed in the control.

The comparative assessment of the impact of different flexibility sources under different network operation conditions performed in Chapter 5 focused on the control of P and Q for bringing back the voltage profiles back to the allowed voltage range. Moreover, the impact of these sources on the loading levels of the branches was analysed in order to assess their feasibility for short-term congestion management. Since these four factors (P, Q, voltages and loadings) are directly affected by the flexibility source applied, they are used for the formulation of operational flexibility indicators in the short term. Four indicators can be extracted from this analysis:

- Voltage deviation indicator, which measures the maximum voltage variation at every node with respect to the admissible allowable voltage deviation.
- Overloading indicator, which measures the proximity to a 100% loading level, or when it is exceeded.
- Reactive power requirements' indicator, which refers to the Q that needs to be added or extracted every hour for achieving voltage stability throughout the network.
- Active power requirements' indicator, which refers to the deficit or surplus of active power in the network for voltage stability and congestion management.

In general, the calculation of these short-term indicators for the base line case is able to show the impact of flexible sources in terms of voltage regulation, change of loadings and improvement in the active and reactive power required for a reliable network operation. However, their analysis can be extended to notice their impact per node and the magnitude of the changes of these indicators during the day.

The previous research questions aim to answer the main research objective of this project: **"To propose a systematic procedure to assess the impact of different sources of flexibility by a DSO in an active distribution network"**.

As presented in this section, the first stage of the research consisted in the modelling of a standard distribution grid in the Netherlands in an open-source tool. Then, the impact of different sources of flexibility was assessed by the control of certain network variables, and indicators were derived from the results. In general, the procedure that has been followed for the comparative assessment of flexibility sources has been as follows:

1. To export the distribution network values from Vision to the Matpower data matrix structure to carry out the steady-state power flow calculations. If the DSO does not use Vision, other tools could be developed for the transformation of the available data to the needed input data matrices in Matpower.
2. To analyse the power flow results without the integration of flexibility in order to identify the operational limits and needs of local flexibility.
3. To simulate the network in the chosen time horizon by applying the flexibility sources of interest. In this research, only droop control at flexible generators, demand response and short-term flexible battery systems have been investigated.
4. To identify the changes in the network variables due to the action of the flexibility sources. These changes can be quantified and translated into several indicators that inform the DSO about the flexibility needs of a particular network and how the flexibility sources would affect the network operation in terms of voltage stability and loadings of the branches.

7.2. Recommendations for future work

In the course of this project, several suggestions have been detected for the extension of this research and the expansion of the obtained results. The main recommendations for future investigations are listed below:

- Apart from focusing on the technical features linked to the flexibility sources, other non-technical aspects such as the market, regulatory and policy frameworks are needed for an

insightful flexibility assessment. A broader view of system flexibility will need to be developed, integrating the different market participants and the technical and non-technical characteristics of the network.

- The simulation of longer time periods such as a complete year would allow us to show the impact of seasonal generation conditions, as well as consumption patterns and load changes across the different months.
- The implementation of more sophisticated controls connected to the distributed generators should be included. The chosen controls will depend on the generator's size and network operating conditions, and they would be able to respond to unexpected fluctuations of the system variables. The performance of PV generators in comparison with other types of distributed generators such as wind turbines must be performed.
- The inclusion of a detailed assessment of the flexibility provided by heat pumps and electric vehicles from a regional point of view. For instance, smart charging controls can be integrated into the electric vehicles to have additional control elements in the network.
- The flexibility provided by demand response can be assessed by the integration of different demand response agreements and methodologies. Normally, demand response is activated by price signals and does not depend directly on the technical features of the network. Its economic viability taking into account the money incentives for the customers can also be added.
- Flexibility indicators in the planning context, more focused on the long term, can be formulated if enough probabilistic data are available. Although the focus of the DSO is on the quantification of the short-term operational flexibility, the considerations taken in the planning process are important for deciding the most urgent actions in terms of the integration of flexibility sources and their potential impact on the network operation.
- More detailed short-term operational flexibility indicators should be developed, considering the economic implications of the flexibility sources applied to the network and the technical characteristics of the elements included.

Bibliography

- [1] European Commission. EU Climate Action. Retrieved from: <https://ec.europa.eu/clima/citizens/eu>.
- [2] Philip Baker. Challenges facing distribution system operators in a decarbonised power system, 2020. Retrieved from: <https://www.raponline.org/wp-content/uploads/2020/05/rap-baker-dso-challenges-june-2020-final.pdf>.
- [3] Short-term flexibility in power systems: drivers and solutions. Technical report, Brochure 808, CIGRE, 2020.
- [4] IEA International Energy Agency. Status of power system transformation 2019. power system flexibility, 2019. Retrieved from: <https://www.iea.org/reports/status-of-power-system-transformation-2019>.
- [5] Sami Repo, Shengye Lu, Timo Pöhö, Davide Della Giustina, Guillermo Ravera, Josep M Selga, and Felipe Alvarez-Cuevas Figuerola. Active distribution network concept for distributed management of low voltage network. In *IEEE PES ISGT Europe 2013*, 1–5. IEEE, 2013.
- [6] Peng Li, Yuelong Wang, Haoran Ji, Jinli Zhao, Guanyu Song, Jianzhong Wu, and Chengshan Wang. Operational flexibility of active distribution networks: Definition, quantified calculation and application. *International Journal of Electrical Power & Energy Systems*, 119:105872, 2020.
- [7] Georgios Papaefthymiou, Edwin Haesen, and Thobias Sach. Power system flexibility tracker: Indicators to track flexibility progress towards high-RES systems. *Renewable energy*, 127:1026–1035, 2018.
- [8] Anjukan Kathirgamanathan, Thibault Péan, Kun Zhang, Mattia De Rosa, Jaume Salom, Michaël Kummert, and Donal P Finn. Towards standardising market-independent indicators for quantifying energy flexibility in buildings. *Energy and Buildings*, 220:110027, 2020.
- [9] Eamonn Lannoye, Damian Flynn, and Mark O’Malley. Evaluation of power system flexibility. *IEEE Transactions on Power Systems*, 27(2):922–931, 2012.
- [10] Yu Wen Huang, Noah Kittner, and Daniel M Kammen. ASEAN grid flexibility: Preparedness for grid integration of renewable energy. *Energy policy*, 128:711–726, 2019.
- [11] Francesco D’Ettorre, Mattia De Rosa, Paolo Conti, Daniele Testi, and Donal Finn. Mapping the energy flexibility potential of single buildings equipped with optimally-controlled heat pump, gas boilers and thermal storage. *Sustainable Cities and Society*, 50:101689, 2019.
- [12] N Menemenlis, M Huneault, and A Robitaille. Thoughts on power system flexibility quantification for the short-term horizon. In *2011 IEEE power and energy society general meeting*, 1–8. IEEE, 2011.
- [13] Andreas Ulbig and Göran Andersson. On operational flexibility in power systems. In *2012 IEEE Power and Energy Society General Meeting*, 1–8. IEEE, 2012.

- [14] Andreas Ulbig and Göran Andersson. On operational flexibility in power systems. In *2012 IEEE Power and Energy Society General Meeting*, 1–8. IEEE, 2012.
- [15] Mohammed Albadi. Power flow analysis. In *Computational Models in Engineering*. IntechOpen, 2019.
- [16] Serhat Berat EFE. Power flow analysis of a distribution system under fault conditions. *International Journal*, 1(1), 2016.
- [17] Hadi Saadat et al. *Power system analysis*, volume 2. McGraw-hill, 1999.
- [18] Reza Sirjani. Course: Power System Analysis I, Eaeatern Mediterranean University, 2019. Retrieved from: <https://faraday.emu.edu.tr/eeng457/>.
- [19] William Stevenson Jr and John Grainger. *Power system analysis*. McGraw-Hill Education, 1994.
- [20] Neel van Hoesel, JG Slootweg, WL Kling, TA Arentze, and AA Ishchenko. Computer-aided distribution network expansion planning using expert rules. , 2014.
- [21] Okwe Gerald Ibe and Akwukwaegbu Isdore Onyema. Concepts of reactive power control and voltage stability methods in power system network. *IOSR Journal of Computer Engineering*, 11(2):15–25, 2013.
- [22] Sandro Corsi. Relationship between voltage and active and reactive powers. In *Voltage Control and Protection in Electrical Power Systems*, 3–11. Springer, 2015.
- [23] Karel De Brabandere, Bruno Bolsens, Jeroen Van den Keybus, Achim Woyte, Johan Driesen, and Ronnie Belmans. A voltage and frequency droop control method for parallel inverters. *IEEE Transactions on power electronics*, 22(4):1107–1115, 2007.
- [24] Stefania Conti, R Nicolosi, SA Rizzo, and HH Zeineldin. Optimal dispatching of distributed generators and storage systems for MV islanded microgrids. *IEEE Transactions on Power Delivery*, 27(3):1243–1251, 2012.
- [25] Wenlei Bai and Kwang Lee. Distributed generation system control strategies in microgrid operation. *IFAC Proceedings Volumes*, 47(3):11938–11943, 2014.
- [26] Phase to Phase BV. Users manual Vision 8.15, 2020. Retrieved from: <https://phasetophase.nl/en/vision-network-analysis.html>.
- [27] Matpower 7.0. caseformat, 2020. Retrieved from: <https://matpower.org/docs/ref/matpower7.0/lib/caseformat.html>.
- [28] PS Meera and S Hemamalini. Optimal siting of distributed generators in a distribution network using artificial immune system. *International Journal of Electrical and Computer Engineering*, 7(2):641, 2017.
- [29] Russelectric. Load curtailment systems, 2020. Retrieved from: <https://www.russelectric.com>.
- [30] International Energy Agency. The who and how of power system flexibility, 2019. Retrieved from: <https://www.iea.org/commentaries/the-who-and-how-of-power-system-flexibility>.
- [31] Woosung Kim, Sungyoon Song, and Gilsoo Jang. Droop control strategy of utility-scale photovoltaic systems using adaptive dead band. *Applied Sciences*, 10(22):8032, 2020.

- [32] Anubrata Das, Ankul Gupta, Saurav Roy Choudhury, and Sandeep Anand. Adaptive reactive power injection by solar pv inverter to minimize tap changes and line losses. In *2016 National Power Systems Conference (NPSC)*, 1–6. IEEE, 2016.
- [33] JPM Sijm, J de Joode, P Gockel, W van Westering, and M Musterd. The demand for flexibility of the power system in the netherlands, 2015-2050. report of phase 1 of the flexnet project. , 2017.
- [34] U.S. Department of Energy. Demand response, 2020. Retrieved from: <https://www.energy.gov/oe/activities/technology-development/grid-modernization-and-smart-grid/demand-response>.
- [35] International Energy Agency. Buildings, a source of enormous untapped efficiency potential, 2020. Retrieved from: <https://www.iea.org/topics/buildings>.
- [36] European Commission. Energy use in buildings, 2020. Retrieved from: https://ec.europa.eu/energy/eu-buildings-factsheets-topics-tree/energy-use-buildings_en.
- [37] Junyong Liu, Hongjun Gao, Zhao Ma, and Yuanxi Li. Review and prospect of active distribution system planning. *Journal of Modern Power Systems and Clean Energy*, 3(4):457–467, 2015.
- [38] Woongchul Choi. A study on state of charge and state of health estimation in consideration of lithium-ion battery aging. *Sustainability*, 12(24):10451, 2020.
- [39] JPM Sijm, AJ van der Welle, P Gockel, and W van Westering. Demand and supply of flexibility in the power system of the Netherlands, 2015-2050. key messages. , 2017.
- [40] S Conti and SA Rizzo. Voltages sensitivity analysis in radial active distribution networks using novel closed-form approximate equations. *International Review of Electrical Engineering*, 6(6):2785–2795, 2011.
- [41] S Conti, AM Greco, and S Raiti. Voltage sensitivity analysis in mv distribution networks. In *Proceedings of the 6th WSEAS/IASME International Conference on Electric Power Systems, High Voltages, Electric Machines, Tenerife, Spain*, 16–18, 2006.
- [42] Nakisa Farrokhseresht, Arjen A van der Meer, José Rueda Torres, Mart AMM van der Meijden, and Peter Palensky. Increasing the share of wind power by sensitivity analysis based transient stability assessment. In *2019 2nd International Conference on Smart Grid and Renewable Energy (SGRE)*, 1–6. IEEE, 2019.
- [43] A Tuohy and E Lannoye. Metrics for quantifying flexibility in power system planning. Technical report, Technical Report, Electric Power Research Institute, 2014.
- [44] J Giménez. *Evaluación en línea de la seguridad dinámica de sistemas eléctricos*. PhD thesis, Tesis Doctoral, Universidad Nacional de San Juan, Argentina, 2006.

A

Data file format in Matpower

The Matpower case file forms a struct defines the *mpc* struct when loaded, which contains the input data of the network. The fields of this *mpc* struct includes the bus data (*mpc.bus*), branch data (*mpc.branch*) and generator data (*mpc.gen*). The different columns and their meaning, which are considered for the power flow calculations, are specified in Figure A.1, Figure A.2 and Figure A.3, respectively. Finally, Figure A.4 details the fields obtained in the resulting power flow results struct.

name	column	description
BUS_I	1	bus number (positive integer)
BUS_TYPE	2	bus type (1 = PQ, 2 = PV, 3 = ref, 4 = isolated)
PD	3	real power demand (MW)
QD	4	reactive power demand (MVar)
GS	5	shunt conductance (MW demanded at $V = 1.0$ p.u.)
BS	6	shunt susceptance (MVar injected at $V = 1.0$ p.u.)
BUS_AREA	7	area number (positive integer)
VM	8	voltage magnitude (p.u.)
VA	9	voltage angle (degrees)
BASE_KV	10	base voltage (kV)
ZONE	11	loss zone (positive integer)
VMAX	12	maximum voltage magnitude (p.u.)
VMIN	13	minimum voltage magnitude (p.u.)
LAM_P	14	Lagrange multiplier on real power mismatch (u /MW)
LAM_Q	15	Lagrange multiplier on reactive power mismatch (u /MVar)
MU_VMAX	16	Kuhn-Tucker multiplier on upper voltage limit (u /p.u.)
MU_VMIN	17	Kuhn-Tucker multiplier on lower voltage limit (u /p.u.)

Figure A.1: Bus data (*mpc.bus*) structure in MatPower [27]

name	column	description
F_BUS	1	"from" bus number
T_BUS	2	"to" bus number
BR_R	3	resistance (p.u.)
BR_X	4	reactance (p.u.)
BR_B	5	total line charging susceptance (p.u.)
RATE_A	6	MVA rating A (long term rating), set to 0 for unlimited
RATE_B	7	MVA rating B (short term rating), set to 0 for unlimited
RATE_C	8	MVA rating C (emergency rating), set to 0 for unlimited
TAP	9	transformer off nominal turns ratio, if non-zero (taps at "from" bus, impedance at "to" bus, i.e. if $r = x = b = 0$, $tap = \frac{ V_f }{ V_t }$; $tap = 0$ used to indicate transmission line rather than transformer, i.e. mathematically equivalent to transformer with $tap = 1$)
SHIFT	10	transformer phase shift angle (degrees), positive \Rightarrow delay
BR_STATUS	11	initial branch status, 1 = in-service, 0 = out-of-service
ANGMIN	12	minimum angle difference, $\theta_f - \theta_t$ (degrees)
ANGMAX	13	maximum angle difference, $\theta_f - \theta_t$ (degrees)
PF	14	real power injected at "from" bus end (MW)
QF	15	reactive power injected at "from" bus end (MVar)
PT	16	real power injected at "to" bus end (MW)
QT	17	reactive power injected at "to" bus end (MVar)
MU_SF	18	Kuhn-Tucker multiplier on MVA limit at "from" bus (u/MVA)
MU_ST	19	Kuhn-Tucker multiplier on MVA limit at "to" bus (u/MVA)
MU_ANGMIN	20	Kuhn-Tucker multiplier lower angle difference limit ($u/degree$)
MU_ANGMAX	21	Kuhn-Tucker multiplier upper angle difference limit ($u/degree$)

Figure A.2: Bus data (mpc.branch) structure in MatPower [27]

name	column	description
GEN_BUS	1	bus number
PG	2	real power output (MW)
QG	3	reactive power output (MVar)
QMAX	4	maximum reactive power output (MVar)
QMIN	5	minimum reactive power output (MVar)
VG	6	voltage magnitude setpoint (p.u.)
MBASE	7	total MVA base of machine, defaults to <code>baseMVA</code>
GEN_STATUS	8	machine status, > 0 = machine in-service, ≤ 0 = machine out-of-service
PMAX	9	maximum real power output (MW)
PMIN	10	minimum real power output (MW)
PC1	11	lower real power output of PQ capability curve (MW)
PC2	12	upper real power output of PQ capability curve (MW)
QC1MIN	13	minimum reactive power output at PC1 (MVar)
QC1MAX	14	maximum reactive power output at PC1 (MVar)
QC2MIN	15	minimum reactive power output at PC2 (MVar)
QC2MAX	16	maximum reactive power output at PC2 (MVar)
RAMP_AGC	17	ramp rate for load following/AGC (MW/min)
RAMP_10	18	ramp rate for 10 minute reserves (MW)
RAMP_30	19	ramp rate for 30 minute reserves (MW)
RAMP_Q	20	ramp rate for reactive power (2 sec timescale) (MVar/min)
APF	21	area participation factor
MU_PMAX	22	Kuhn-Tucker multiplier on upper P_g limit (u/MW)
MU_PMIN	23	Kuhn-Tucker multiplier on lower P_g limit (u/MW)
MU_QMAX	24	Kuhn-Tucker multiplier on upper Q_g limit ($u/MVar$)
MU_QMIN	25	Kuhn-Tucker multiplier on lower Q_g limit ($u/MVar$)

Figure A.3: Generator data (mpc.gen) structure in MatPower [27]

name	column	description
GEN_BUS	1	bus number
PG	2	real power output (MW)
QG	3	reactive power output (MVar)
QMAX	4	maximum reactive power output (MVar)
QMIN	5	minimum reactive power output (MVar)
VG	6	voltage magnitude setpoint (p.u.)
MBASE	7	total MVA base of machine, defaults to <code>baseMVA</code>
GEN_STATUS	8	machine status, > 0 = machine in-service ≤ 0 = machine out-of-service
PMAX	9	maximum real power output (MW)
PMIN	10	minimum real power output (MW)
PC1	11	lower real power output of PQ capability curve (MW)
PC2	12	upper real power output of PQ capability curve (MW)
QC1MIN	13	minimum reactive power output at PC1 (MVar)
QC1MAX	14	maximum reactive power output at PC1 (MVar)
QC2MIN	15	minimum reactive power output at PC2 (MVar)
QC2MAX	16	maximum reactive power output at PC2 (MVar)
RAMP_AGC	17	ramp rate for load following/AGC (MW/min)
RAMP_10	18	ramp rate for 10 minute reserves (MW)
RAMP_30	19	ramp rate for 30 minute reserves (MW)
RAMP_Q	20	ramp rate for reactive power (2 sec timescale) (MVar/min)
APF	21	area participation factor
MU_PMAX	22	Kuhn-Tucker multiplier on upper P_g limit (u /MW)
MU_PMIN	23	Kuhn-Tucker multiplier on lower P_g limit (u /MW)
MU_QMAX	24	Kuhn-Tucker multiplier on upper Q_g limit (u /MVar)
MU_QMIN	25	Kuhn-Tucker multiplier on lower Q_g limit (u /MVar)

Figure A.4: Power flow results in Matpower [27]

B

Visualisation of the Vision-Matpower converter

First, the network that will be converted is loaded, appearing at the bottom, as shown in Figure B.1. In this case, the IEEE distribution network of 33 buses was loaded ('case33bw'). Then, the conversion to Matpower format can be selected.

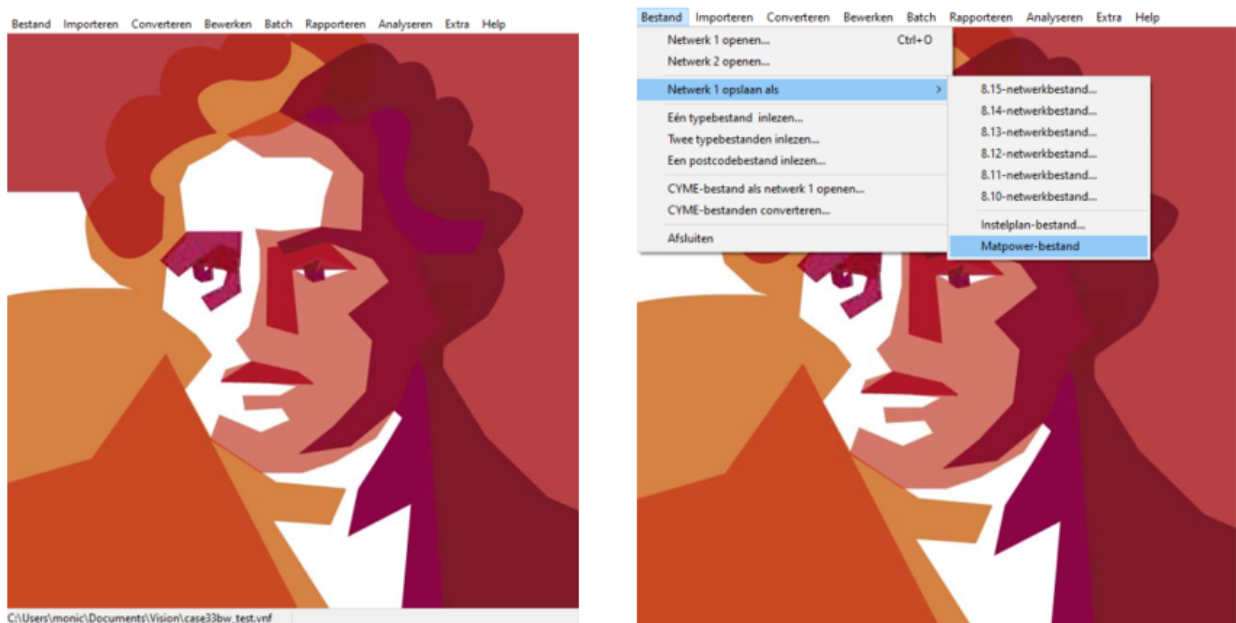









Figure B.1: The developed converter Vision-Matpower

After the S_{base} and frequency of the system have been set, the output of the conversion can be extracted. As noticed in Figure B.2, the different variables are presented in the data matrices format of Matpower. Loads are directly expressed in MV or MV and resistances, reactances and conductances of the branches are expressed in p.u. and not in Ohms, since different voltage levels might be present in the network and then different impedances have to be scaled differently.

 Output

Bestand Bewerken Lettertype

      | A⁺ A⁻ |

```
function mpc = case33bw_test
%% Imported from Vision network file: C:\Users\monic\Documents\Vision\case33bw_test.vnf

%% MATPOWER Case Format : Version 2
mpc.version = '2';

%%----- Power Flow Data -----%%
%% system MVA base
mpc.baseMVA = 100;

%% bus data
% bus_i type Pd Qd Gs Bs area Vm Va baseKV zone Vmax Vmin
mpc.bus = [%% (Pd and Qd are specified in MW & MVar)
1 3 0.000 0.000 0 0 1 1.000 0.000 12.660 1 1.2 0.8
2 1 0.100 0.060 0 0 1 1.000 0.000 12.660 1 1.2 0.8
3 1 0.090 0.040 0 0 1 1.000 0.000 12.660 1 1.2 0.8
4 1 0.120 0.080 0 0 1 1.000 0.000 12.660 1 1.2 0.8
5 1 0.060 0.030 0 0 1 1.000 0.000 12.660 1 1.2 0.8
6 1 0.060 0.020 0 0 1 1.000 0.000 12.660 1 1.2 0.8
7 1 0.200 0.100 0 0 1 1.000 0.000 12.660 1 1.2 0.8
8 1 0.200 0.100 0 0 1 1.000 0.000 12.660 1 1.2 0.8
9 1 0.060 0.020 0 0 1 1.000 0.000 12.660 1 1.2 0.8
10 1 0.060 0.020 0 0 1 1.000 0.000 12.660 1 1.2 0.8
11 1 0.045 0.030 0 0 1 1.000 0.000 12.660 1 1.2 0.8
12 1 0.060 0.035 0 0 1 1.000 0.000 12.660 1 1.2 0.8
13 1 0.060 0.035 0 0 1 1.000 0.000 12.660 1 1.2 0.8
14 1 0.120 0.080 0 0 1 1.000 0.000 12.660 1 1.2 0.8
15 1 0.060 0.010 0 0 1 1.000 0.000 12.660 1 1.2 0.8
16 1 0.060 0.020 0 0 1 1.000 0.000 12.660 1 1.2 0.8
17 1 0.060 0.020 0 0 1 1.000 0.000 12.660 1 1.2 0.8
18 1 0.090 0.040 0 0 1 1.000 0.000 12.660 1 1.2 0.8
19 1 0.090 0.040 0 0 1 1.000 0.000 12.660 1 1.2 0.8
20 1 0.090 0.040 0 0 1 1.000 0.000 12.660 1 1.2 0.8
21 1 0.090 0.040 0 0 1 1.000 0.000 12.660 1 1.2 0.8
22 1 0.090 0.040 0 0 1 1.000 0.000 12.660 1 1.2 0.8
23 1 0.090 0.050 0 0 1 1.000 0.000 12.660 1 1.2 0.8
24 1 0.420 0.200 0 0 1 1.000 0.000 12.660 1 1.2 0.8
25 1 0.420 0.200 0 0 1 1.000 0.000 12.660 1 1.2 0.8
26 1 0.060 0.025 0 0 1 1.000 0.000 12.660 1 1.2 0.8
27 1 0.060 0.025 0 0 1 1.000 0.000 12.660 1 1.2 0.8
```

Figure B.2: The results from the converter in Matpower format

C

Validation of the coupling between Vision and Matpower

Section 3.3 explained the validation process followed for the Vision-Matpower converter. Table C.1 and Table C.2 detail the comparison of the power flow results obtained by Vision and Matpower for the nodes, loads and branches of the test network (IEEE 33-bus distribution grid).

N	Nodes		Loads			
	V_m (pu)		P (MW)		Q (Mvar)	
	Vision	Matpower	Vision	Matpower	Vision	Matpower
1	1	1	3,917	0	2,434	0
2	0,997	0,99703	0,1	0,1000	0,06	0,060
3	0,983	0,98294	0,09	0,0900	0,04	0,040
4	0,975	0,97546	0,12	0,1200	0,08	0,080
5	0,968	0,96806	0,06	0,0600	0,03	0,030
6	0,95	0,94966	0,06	0,0600	0,02	0,020
7	0,946	0,94617	0,2	0,2000	0,1	0,100
8	0,941	0,94133	0,2	0,2000	0,1	0,100
9	0,935	0,93506	0,06	0,0600	0,02	0,020
10	0,929	0,92924	0,06	0,0600	0,02	0,020
11	0,928	0,92838	0,045	0,0450	0,03	0,030
12	0,927	0,92688	0,06	0,0600	0,035	0,035
13	0,921	0,92077	0,06	0,0600	0,035	0,035
14	0,919	0,91850	0,12	0,1200	0,08	0,080
15	0,917	0,91709	0,06	0,0600	0,01	0,010
16	0,916	0,91572	0,06	0,0600	0,02	0,020
17	0,914	0,91370	0,06	0,0600	0,02	0,020
18	0,913	0,91309	0,09	0,0900	0,04	0,040
19	0,997	0,99650	0,09	0,0900	0,04	0,040
20	0,993	0,99293	0,09	0,0900	0,04	0,040
21	0,992	0,99222	0,09	0,0900	0,04	0,040
22	0,992	0,99158	0,09	0,0900	0,04	0,040
23	0,979	0,97935	0,09	0,0900	0,05	0,050
24	0,973	0,97268	0,42	0,4200	0,2	0,200
25	0,969	0,96936	0,42	0,4200	0,2	0,200
26	0,948	0,94773	0,06	0,0600	0,025	0,025
27	0,945	0,94517	0,06	0,0600	0,025	0,025
28	0,934	0,93373	0,06	0,0600	0,02	0,020
29	0,926	0,92551	0,12	0,1200	0,07	0,070
30	0,922	0,92195	0,2	0,2000	0,6	0,600
31	0,918	0,91779	0,15	0,1500	0,07	0,070
32	0,917	0,91687	0,21	0,2100	0,1	0,100
33	0,917	0,91659	0,06	0,0600	0,04	0,040

Table C.1: Comparison of the IEEE-33 bus power flow results for the network nodes and loads obtained by Vision and Matpower

For Table C.2, P_1 , Q_1 and P_2 , Q_2 represent the active and reactive power injected at the beginning ('from') and at the end ('to') of the branch, respectively.

Branches									
From	To	P1 (MW)		Q1 (Mvar)		P2 (MW)		Q2 (Mvar)	
		Vision	Mp	Vision	Mp	Vision	Mp	Vision	Mp
1	2	3,917	3,91768	2,434	2,43514	-3,904	-3,90544	-2,428	-2,42890
2	3	3,443	3,44430	2,207	2,20782	-3,392	-3,39251	-2,181	-2,18144
3	4	2,362	2,36290	1,683	1,68420	-2,342	-2,34299	-1,673	-1,67407
4	5	2,222	2,22299	1,593	1,59407	-2,203	-2,20430	-1,584	-1,58454
5	6	2,143	2,14430	1,554	1,55454	-2,105	-2,10605	-1,521	-1,52152
6	7	1,094	1,09527	0,528	0,52789	-1,093	-1,09335	-0,521	-0,52156
7	8	0,893	0,89335	0,421	0,42156	-0,888	-0,88851	-0,42	-0,41996
8	9	0,688	0,68851	0,32	0,31996	-0,684	-0,68433	-0,317	-0,31696
9	10	0,624	0,62433	0,297	0,29696	-0,62	-0,62077	-0,294	-0,29443
10	11	0,561	0,56077	0,274	0,27443	-0,56	-0,56022	-0,274	-0,27425
11	12	0,515	0,51522	0,244	0,24425	-0,514	-0,51434	-0,244	-0,24396
12	13	0,454	0,45434	0,209	0,20896	-0,451	-0,45167	-0,207	-0,20686
13	14	0,391	0,39167	0,172	0,17186	-0,391	-0,39094	-0,171	-0,17090
14	15	0,271	0,27094	0,0909	0,09090	-0,27	-0,27059	-0,0906	-0,09058
15	16	0,21	0,21059	0,0806	0,08058	-0,21	-0,21030	-0,0804	-0,08038
16	17	0,15	0,15030	0,0604	0,06038	-0,15	-0,15005	-0,0601	-0,06004
17	18	0,09	0,09005	0,04	0,04004	-0,09	-0,09000	-0,04	-0,04000
2	19	0,361	0,36114	0,161	0,16108	-0,361	-0,36098	-0,161	-0,16093
19	20	0,271	0,27098	0,121	0,12093	-0,27	-0,27014	-0,12	-0,12018
20	21	0,18	0,18014	0,0802	0,08018	-0,18	-0,18004	-0,0801	-0,08006
21	22	0,09	0,09004	0,0401	0,04006	-0,09	-0,09000	-0,04	-0,04000
3	23	0,94	0,93961	0,457	0,45724	-0,936	-0,93643	-0,455	-0,45507
23	24	0,846	0,84643	0,405	0,40507	-0,841	-0,84129	-0,401	-0,40101
24	25	0,421	0,42129	0,201	0,20101	-0,42	-0,42000	-0,2	-0,20000
6	26	0,95	0,95078	0,973	0,97364	-0,948	-0,94818	-0,972	-0,97231
26	27	0,888	0,88818	0,947	0,94731	-0,885	-0,88485	-0,945	-0,94562
27	28	0,825	0,82485	0,92	0,92062	-0,813	-0,81355	-0,91	-0,91065
28	29	0,753	0,75355	0,89	0,89065	-0,745	-0,74572	-0,883	-0,88383
29	30	0,626	0,62572	0,813	0,81383	-0,622	-0,62182	-0,811	-0,81184
30	31	0,422	0,42182	0,212	0,21184	-0,42	-0,42023	-0,21	-0,21027
31	32	0,27	0,27023	0,14	0,14027	-0,27	-0,27001	-0,14	-0,14002
32	33	0,06	0,06001	0,04	0,04002	-0,06	-0,06000	-0,04	-0,04000

Table C.2: Comparison of the IEEE-33 power flow results obtained for the network branches by Vision and Matpower

D

Supplementary results figures

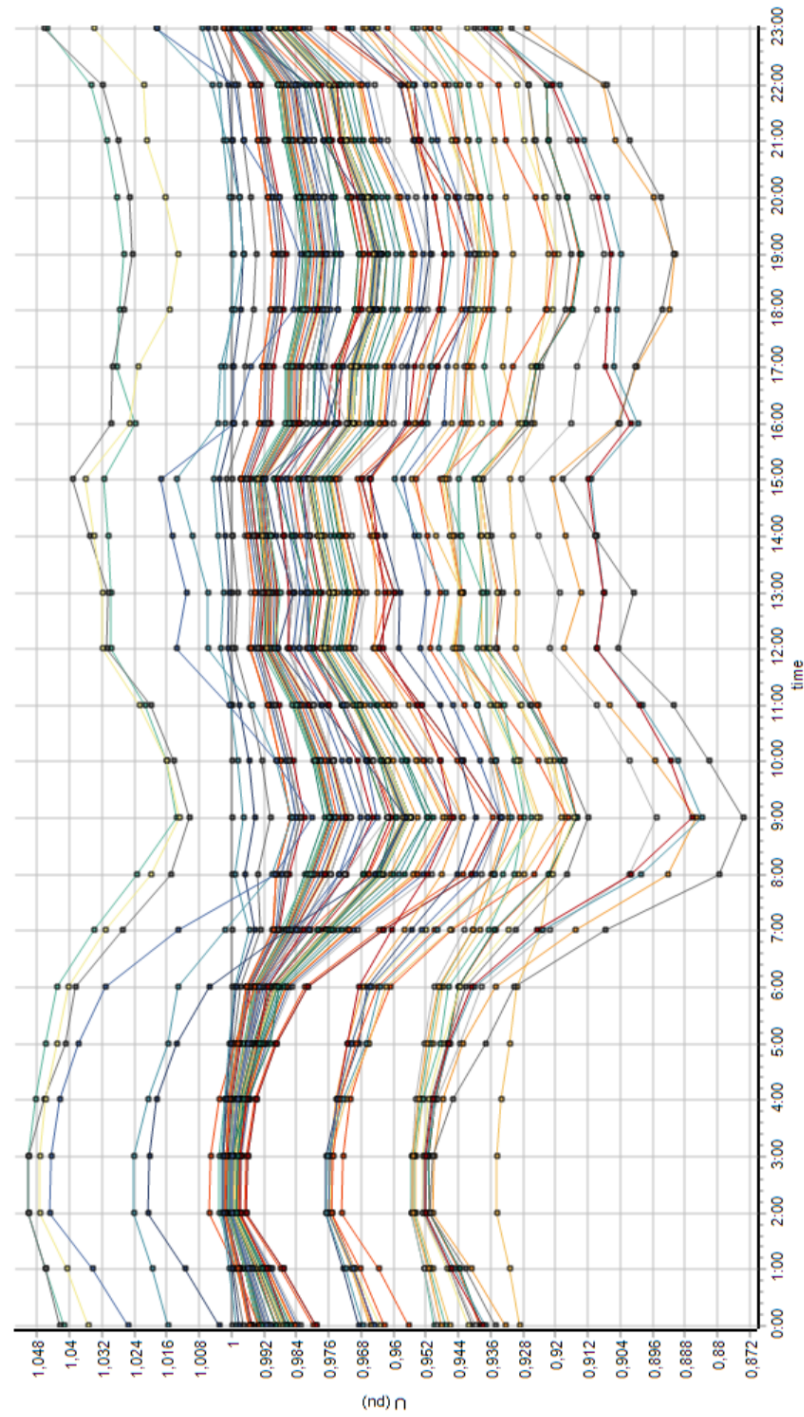


Figure D.1: Landscape view of the voltage profiles throughout the day obtained in Vision for the network without flexibility

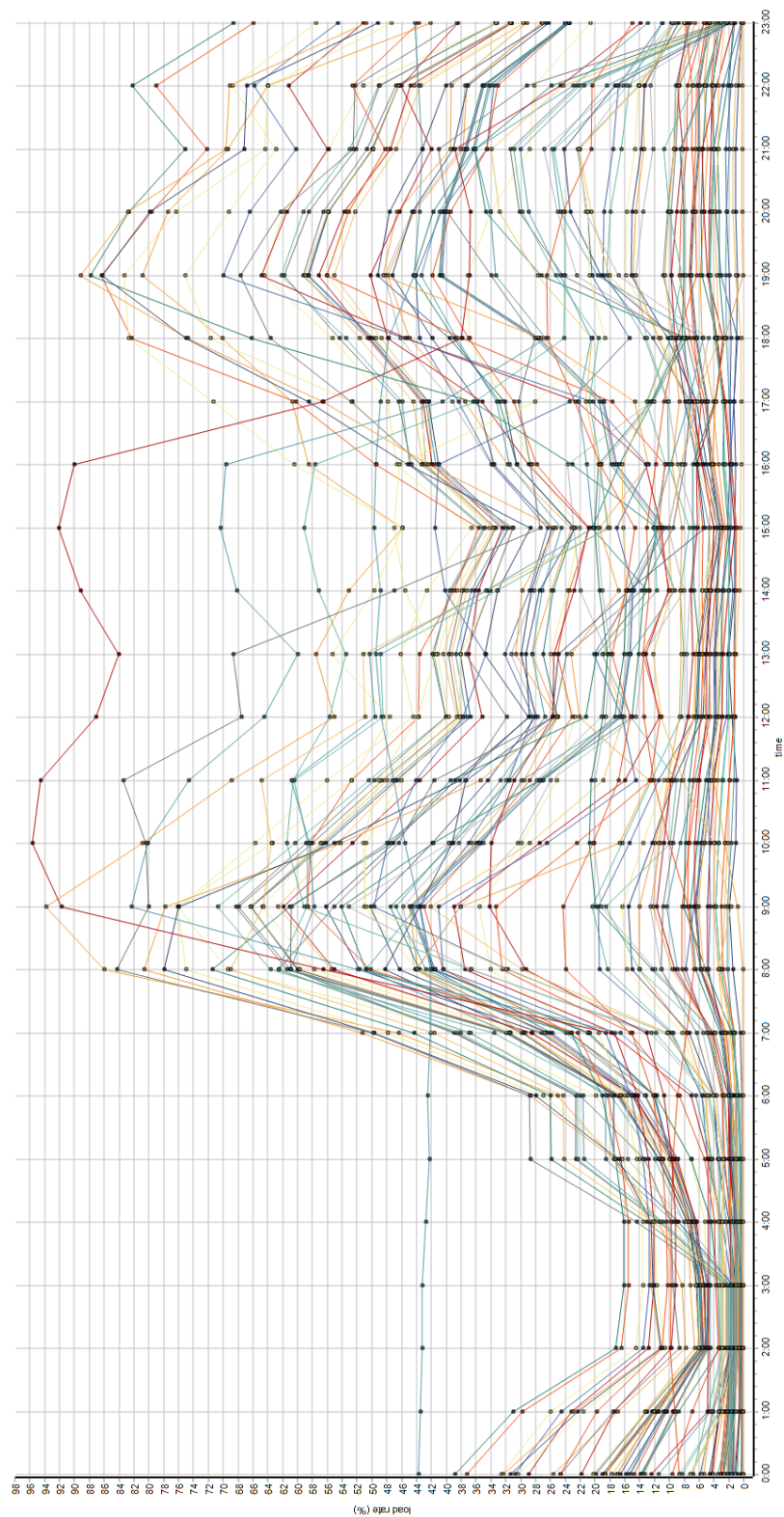


Figure D.2: Load rates of the network branches obtained with Vision for the network without flexibility

D.1. Sensitivity analysis

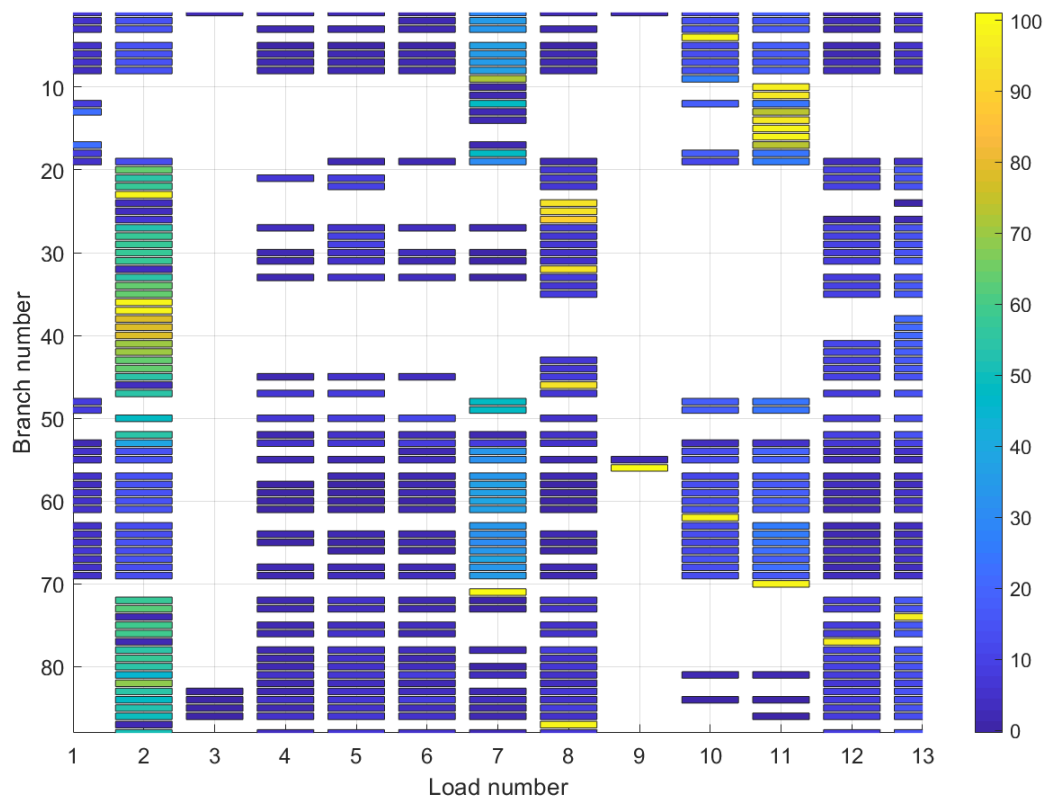


Figure D.3: View of the relative loading sensitivity factor magnitude per load and branch

D.2. Assessment of the flexibility sources

D.2.1. Network voltage profiles without flexibility:

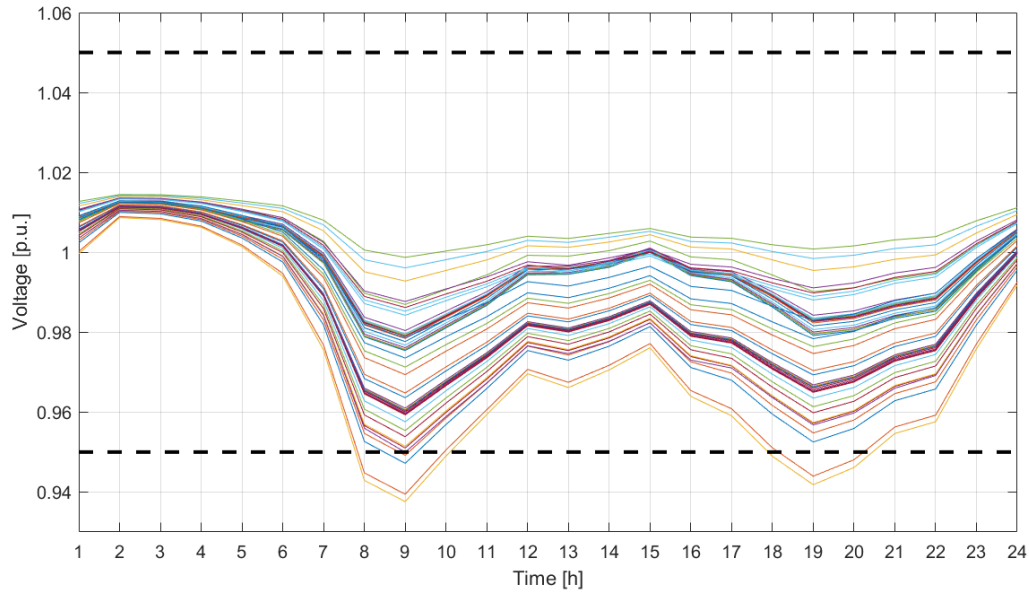


Figure D.4: Medium-voltage profiles in the network for the base line case

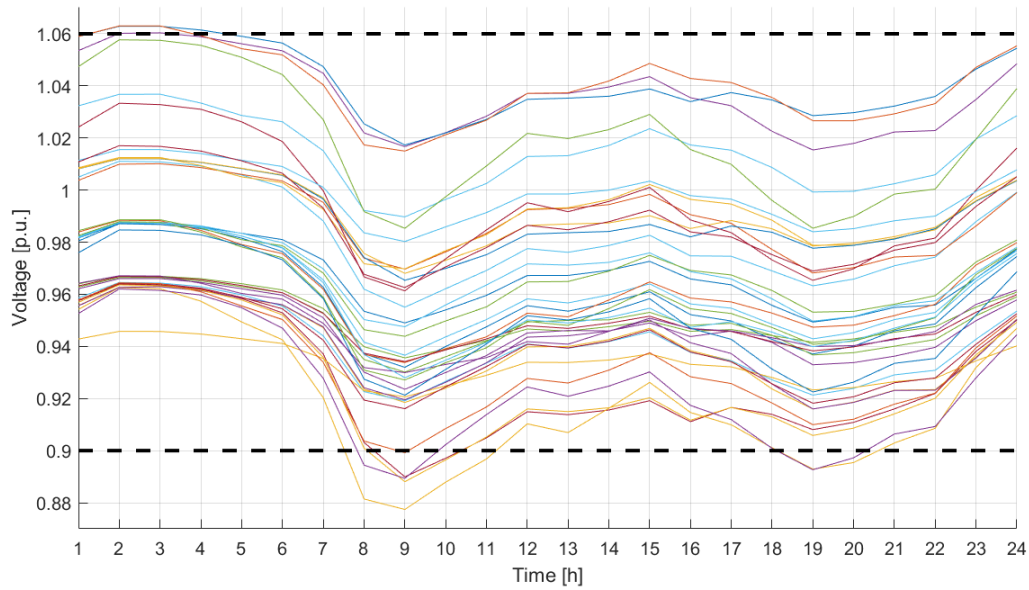


Figure D.5: Low-voltage profiles in the network for the base line case

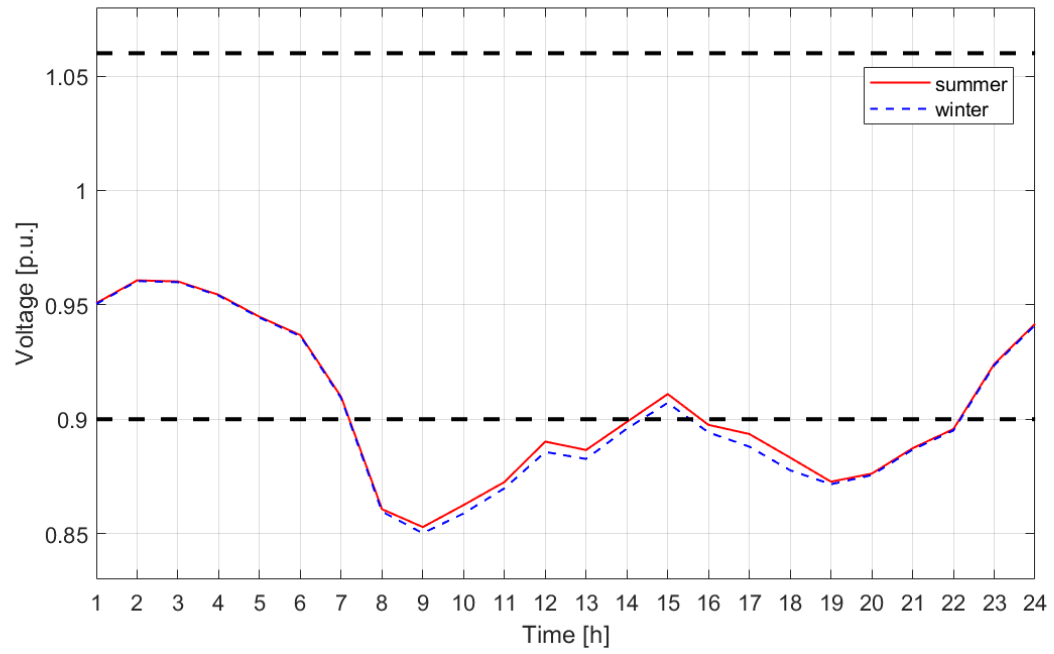


Figure D.6: Lower extreme voltage profile for the over-scaled case in summer and winter

D.2.2. Effect of the droop control characteristic on voltage regulation:

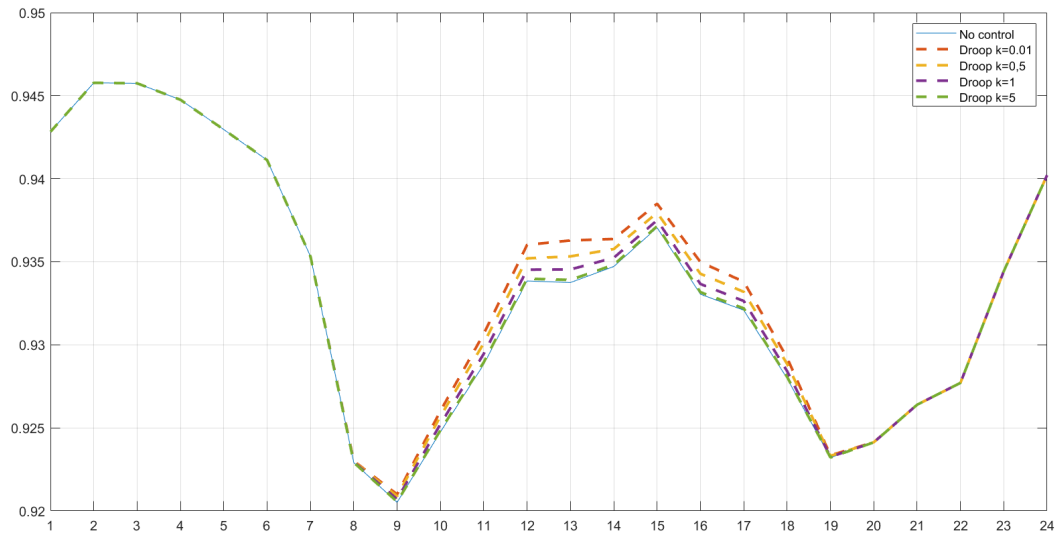


Figure D.7: Droop control voltage regulation with different k values

D.2.3. Network voltage profiles after demand response control:

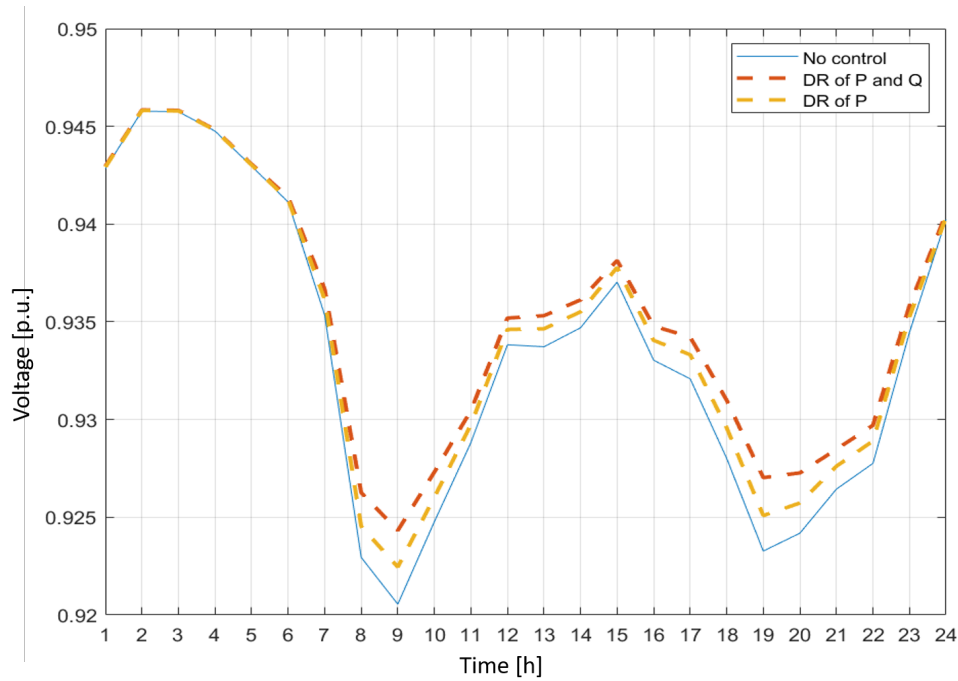


Figure D.8: Difference of demand response control of P-Q and only P

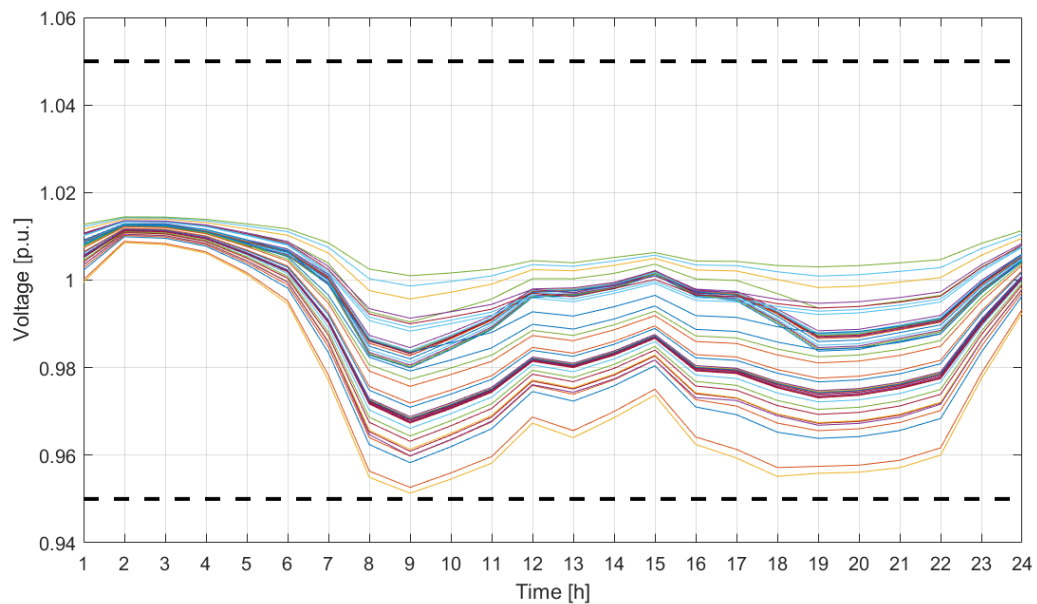


Figure D.9: Medium-voltage profiles in the network after the effect of the combined control of flexible generation and demand

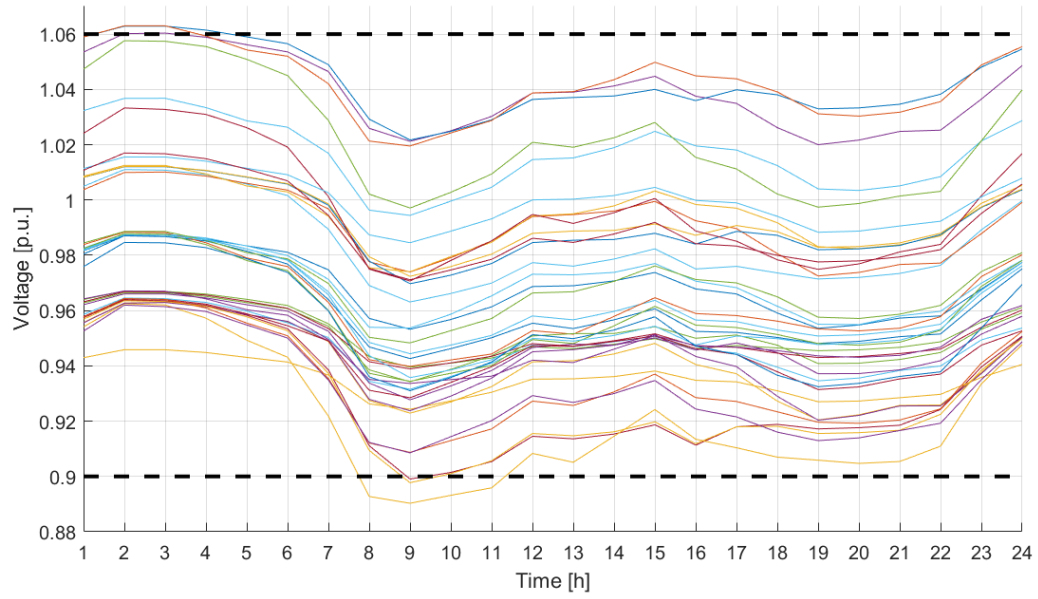


Figure D.10: Low-voltage profiles in the network after the effect of the combined control of flexible generation and demand

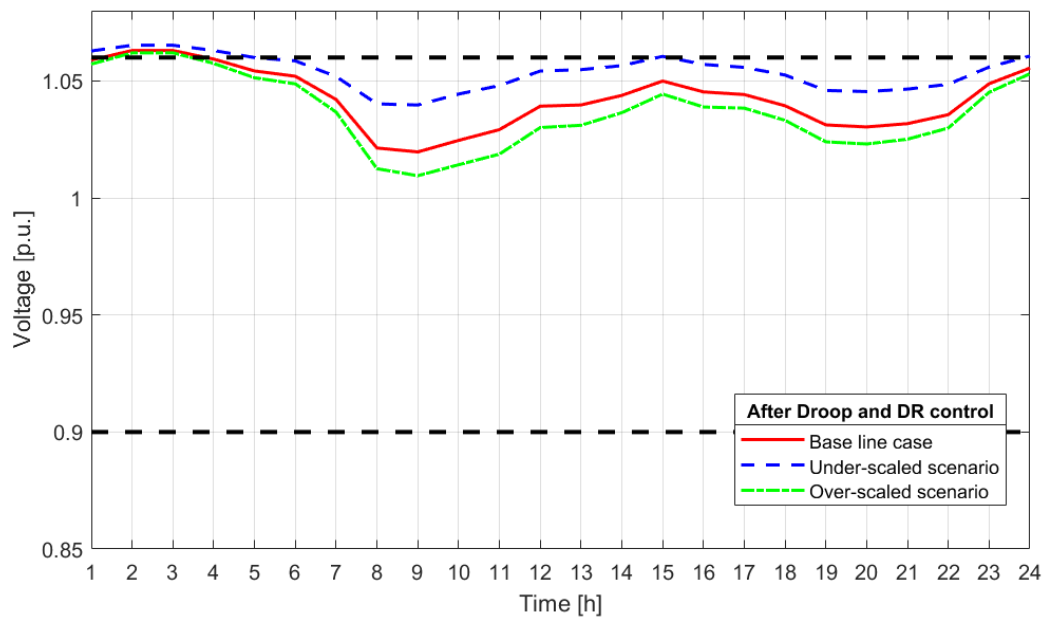


Figure D.11: Upper extreme voltage profile for all the scenarios after the action of the combined control (droop and DR)

D.2.4. Integration of battery systems in the network:

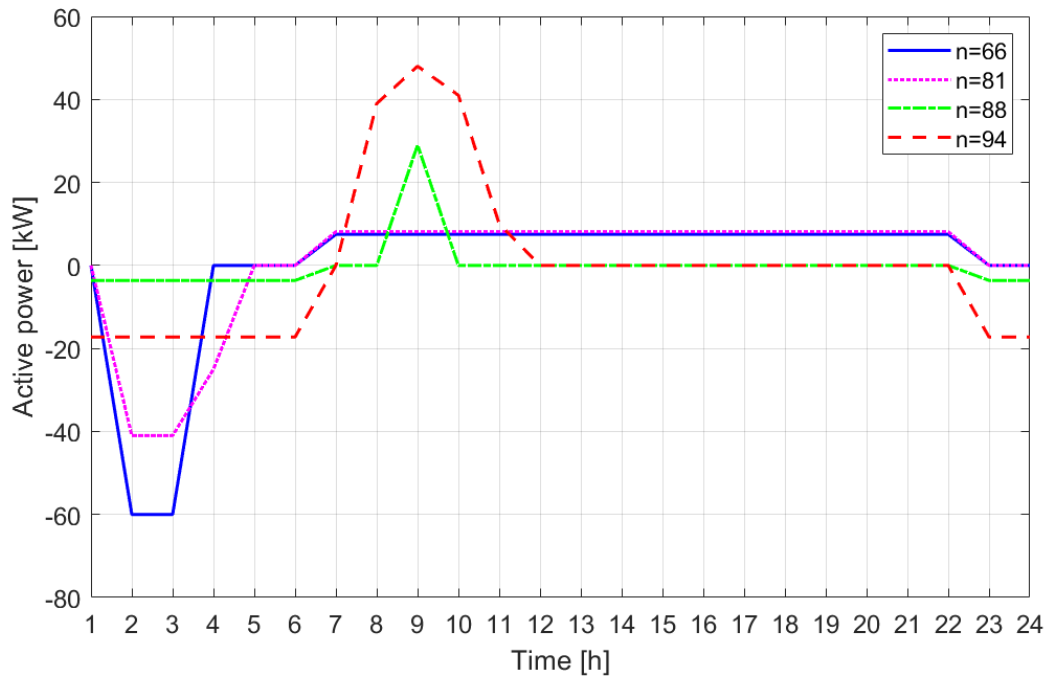


Figure D.12: Power charged and discharged by each battery throughout the day

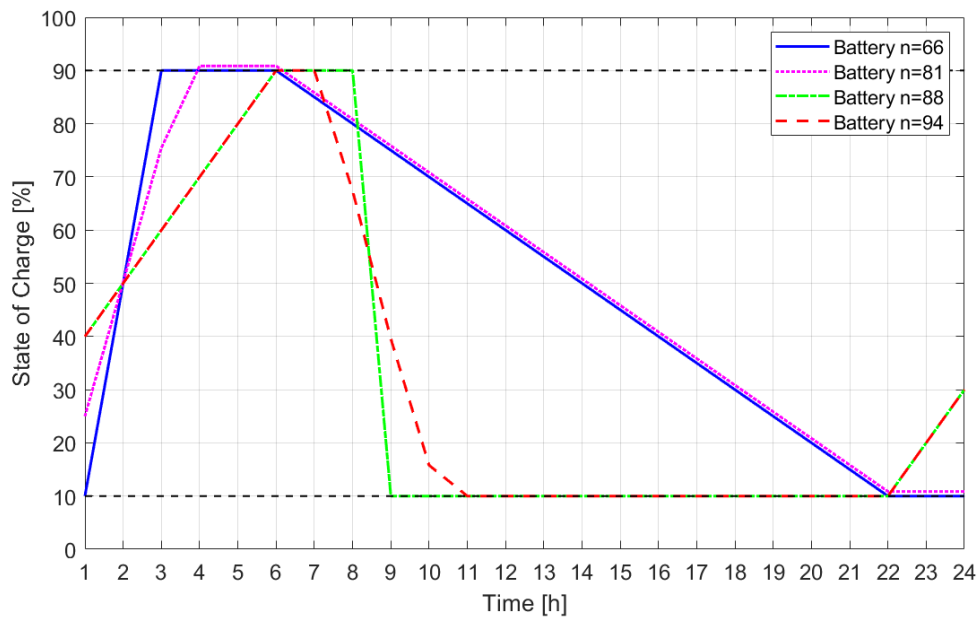


Figure D.13: State of Charge of the batteries considered during the day

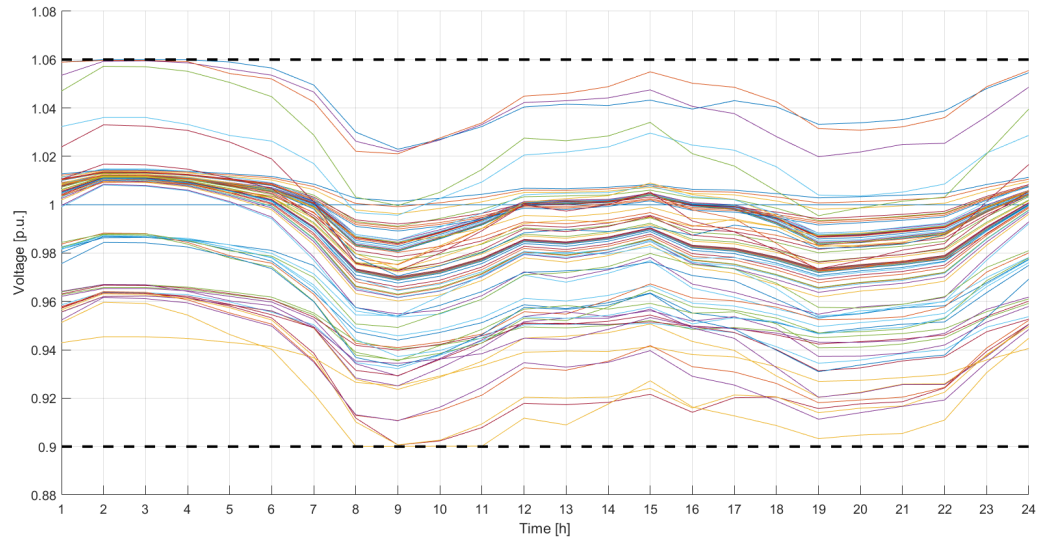


Figure D.14: Controlled voltage profiles within the allowed limits after the integration of short-term flexible storage